# Power Stabilizer for Dynamic Wireless Charging Applications

## A Drive Towards a Sustainable Future

Master Thesis

Namo Rauf

TU Delft

# Power Stabilizer for Dynamic Wireless Charging Applications

## A Drive Towards a Sustainable Future

by

Namo Rauf

to obtain the degree of Master of Science at the Delft University of Technology
to be defended publicly on 27 November, 2025 at 10:00

| | |
|---|---|
| Thesis committee: | Daily Supervisor: Dr. ir. W. Shi |
| | Chair, Supervisor: Prof. dr. ir. P. Bauer |
| | External Examiner: Dr. ir. F. Muñoz |
| Project Duration: | December, 2024 - November, 2025 |
| Faculty: | Faculty of EEMCS, Delft |
| Student number: | 4662636 |



TU Delft

# Preface

Use what is gifted to you to serve mankind. When I began my bachelor in Electrical Engineering, my goal extended beyond obtaining a degree, pursuing a career and securing a stable future. I also wanted to gain knowledge that could be used to serve humanity. This aspiration guided my academic path and inspired me to pursue further studies beyond my bachelor. After completing my bachelor's program, I decided to do so by starting a master's program in Sustainable Energy Technology.

For a long time, I have been fascinated by wireless power transfer. While I was searching for a thesis topic I came across this project, which immediately captured my interest. I was looking for a project that was innovative, and dynamic wireless charging for electric vehicles is an emerging and exciting area of research. Moreover, dynamic wireless charging has the potential to make the usage of electric vehicles more attractive, which will contribute to a cleaner and more sustainable world. Through this project, I hope to contribute making our planet cleaner and more sustainable.

These two years were not only an educational journey but also an era of new friendships, growth and gaining experiences. Two years ago, when I graduated from my bachelor's program, I could not have foreseen that my master's program would create such amazing memories that I will cherish for life.

During this master thesis I faced several challenges. However, having Dr. ir. Wenli Shi as my supervisor eased the process. I would like to express my sincere gratitude to him for his valuable support during this thesis. Furthermore, I would like to thank Prof. dr. ir. Pavol Bauer and Dr. ir. Fabio Muñoz for taking the time and effort to be part of my thesis committee. I am deeply grateful to my family, especially my parents, for their encouragement and support throughout my academic journey. Finally, I would like to thank my friends for their support and the wonderful memories we made during these two years.

*Namo Rauf*
*Delft, November 2025*

# Summary

With the rise of greenhouse gasses, increasing environmental concerns and pollution, solutions to a cleaner and more sustainable world are demanded. This thesis contributes to a step towards a cleaner and more sustainable planet Earth. Road transportation has a relatively high contribution to greenhouse gas emissions. A promising approach to lower these emissions is to use electric vehicles(EVs) instead of traditional combustion engine vehicles for road transport.

However, EVs come with their challenges. In general, they have long charging time, introduce range anxiety and have a higher initial cost compared to combustion engine vehicles. By introducing dynamic wireless charging(DWC), these challenges will be eliminated/mitigated. In a scenario in which an EV is charged by using DWC, the EV can continue its journey on the road while its charging. However, due to the dynamic behavior of the mutual inductance, between the transmitting and receiving coil, the output power will not be constant, while for charging a battery a stable output power is required. Therefore, it is necessary to stabilize the power.

There are several methods to stabilize the power. This thesis will provide a comparative analysis of three methods to stabilize power which are, stabilizing the power by using a buck converter, an inverter or an active rectifier. Three different models are constructed in MATLAB Simulink in which each model contains the dynamic wireless power transfer (DWPT) circuit and one of the mentioned circuits to stabilize the output power. The circuits are compared based on five characteristics, namely, voltage ripple, space efficiency, voltage regulation, modulation complexity and start-up time. According to the results the active rectifier is the most suitable circuit to stabilize the output power of a DWC system.

# Contents

# Nomenclature

## Abbreviations

| Abbreviation | Definition |
|---|---|
| WPT | Wireless Power Transfer |
| DWPT | Dynamic Wireless Power Transfer |
| SS | Series-Series |
| DLCC | Double-sided LCC |
| EV | Electric Vehicle |
| Tx | Transmitter |
| Rx | Receiver |
| PI | Proportional Integral |
| PSM | Phase Shift Modulation |
| UN | United Nations |
| COP | Conference of the Parties |
| EU | European Union |
| CCM | Continous Conduction Mode |
| DCM | Discontinous Conduction Mode |
| MPC | Model Predictive Control |
| DSMC | Dynamic Sliding Mode Control |
| MOSFET | Metal-Oxide-Semiconductor Field-Effect Transistor |

# List of Figures

# List of Tables

# 1

# Introduction

A decade ago, 195 parties gathered in Paris for the United Nations(UN) Climate Change Conference in which a historic agreement to combat climate change was signed. One of the key points agreed upon is to keep the rise of global average temperature below 2 °C above the pre-industrial level. After COP21, world leaders began to address their concerns and decided to signify the urge to lower global temperature by calling to limit global warming to 1.5 °C by the end of this century. Furthermore, the UN's Intergovernmental Panel on Climate Change warned that reaching beyond the 1.5 °C increases the change of more extreme climate change impacts, such as, more and harsher heatwaves, heavy rainfall and droughts[1].

In 2023, the transport sector was the largest greenhouse gas emission contributor in the European Union(EU). It accounted for 22.68% of total greenhouse gas emissions. Among these 22.68%, around 75% were originating from road vehicles. To emphasize on the contribution of cars to this part, 60% of emission by road vehicles are from cars[2][3]. To reduce the amount of these emissions, electric vehicles(EVs) were becoming more attractive as an alternative to combustion engine vehicles. Utilizing EVs to combat emission is a valid option towards a more sustainable form of transport, however, they also come with limitations. For instance, long charging time, range anxiety, heavy batteries which leads to higher initial costs and more energy consumption. As a result, these drawbacks form a barrier to the adoption of EVs on a large scale. Currently in the Netherlands, on average, the charging time for an EV is four to ten hours depending on the type of charger, state of the battery and the specifications of the EV. In case fast charging is used, it takes on average 30 minutes to charge from 20% to 80%, however, these type of charges are not easily accessible and are higher in cost. Furthermore, 60% of Europeans consider purchasing an EV if the minimum driving range is 500 km on one charge[4][5].

There is an innovative solution to address these limitations. Currently, EVs are primarily charged through stationary methods, typically a plug-in connection to a charging post. This method not only requires the vehicle to remain immobile during the charging process but also leads to time inefficiency and user inconvenience. Furthermore, in order to extend the driving range of EVs, they are equipped with large battery packs. However, these battery packs lead to an increases of the vehicle's total mass, demands higher production costs and leads to an increase of energy consumption of the EV[4][6][7].
The solution to these limitations is dynamic wireless charging(DWC). In DWC the EV can continue its journey on the road while being charged, which results in a reduced charging time. Furthermore, since the vehicle is being charged on the road it reduces the amount of energy it has to store in its battery. Therefore, a smaller battery pack can be used. To indicate the reduction of battery size, in the USA, if 3% of the total roadways were optimally deployed for DWC the EV battery capacity could be downsized by up to 48%, compared to the non-DWC scenarios[5][8].

Like, charging by plug, this method has its limitations. One of these limitations is the variability of

output power. A wireless power transfer(WPT) circuit, as illustrated in Figure 3.1, consists of two parts, namely, a transmitting side and a receiving side. In static WPT the coils that transmit and receive power are optimally aligned, which means that the maximum power possible is received by the secondary side of the WPT circuit. A device that uses static WPT is a smartphone when it is charged wirelessly. In DWPT for EVs, the primary side of the WPT circuit is embedded in the road and the secondary side is located on the EV, as illustrated in Figure 1.1. Due to the relative movement of the vehicle to the road, the coils are not optimally aligned. This results in an output power that is not constant, more about this will follow. In order to provide a constant output power, the power needs to be stabilized. There are several approaches to stabilize the power output, namely, by using a buck converter, an inverter or an active rectifier, integrated with a control strategy. The question arises, which of these methods is the most suitable to be used in DWC.

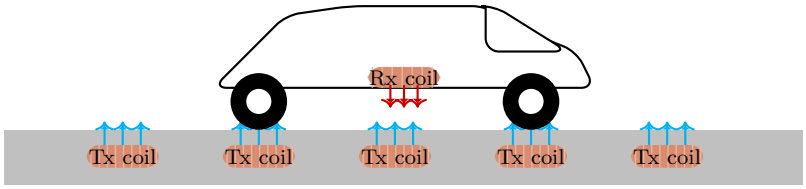


**Figure 1.1:** An overview of dynamic wireless charging for an electric vehicle.

## 1.1 Problem Definition

One of the most important aspects of dynamic wireless power transfer(DWPT) for EVs is the stabilization of the output power. Figure 1.2 illustrates how the mutual inductance between the transmitting and receiving side varies depending on the position of the vehicle. Like it is shown, when the Rx and Tx coils are completely aligned, the mutual inductance is at its peak, and when the coils are far from being aligned, the mutual inductance is zero. In Figure 1.3, a graph is shown where the impact of a changing mutual inductance on the output voltage of a DWPT circuit is presented. As it is observed, the amplitude of the sine wave voltage increases or decreases depending on the magnitude of the mutual inductance.

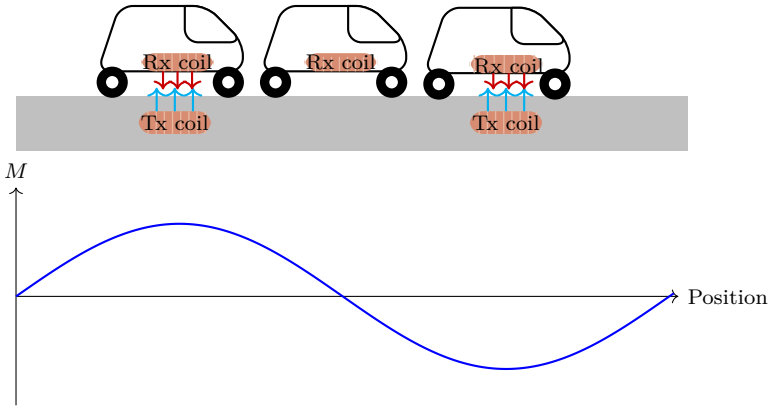


**Figure 1.2:** Mutual inductance variation due to the vehicles position.

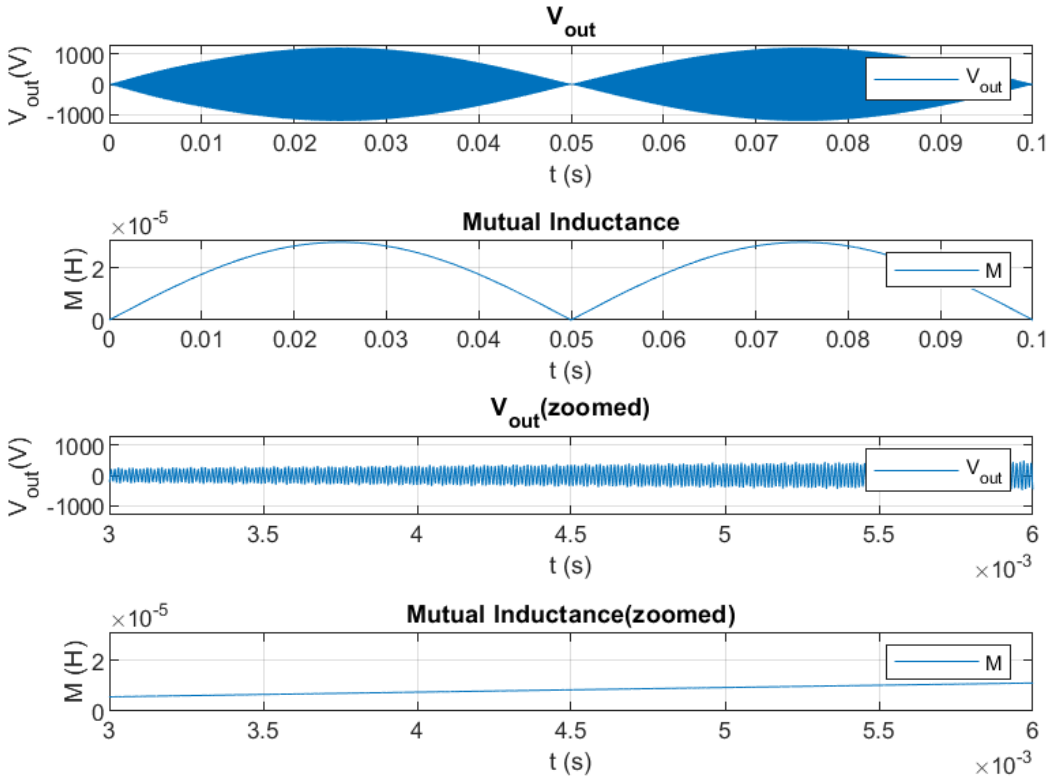


**Figure 1.3:** Impact of a varying mutual inductance on the output voltage.

There are several methods to stabilize the voltage, including inverter, active rectifier and buck converter. Each of these methods differs in voltage ripple, voltage regulation, space efficiency, modulation complexity and start-up time. To fairly compare these metrics to one another, for each individual method, the test has to be conducted under identical conditions. Currently, there are numerous of studies in which power is stabilized by using a buck converter, inverter or an active rectifier. However, they are implemented under different conditions, used for different case studies and/or different objectives. This lacks a fair comparison between these three to select which circuit suits best for stable power delivery. This thesis addresses this gap by providing a comparative analysis between these three methods to stabilize the power under the same input/output power, load condition and component values, ensuring an accurate comparison for future designers to select one of the methods. Furthermore, there does not exist detailed literature on how to develop a complete DWC model in which the power is stabilized by one of the above mentioned methods. This thesis report provides a detailed step-by-step approach to construct a Simulink model for DWPT integrated with the power stabilization methods. In addition, the model is adaptable such that component values and voltage levels could be modified to implement it for different purposes.

## 1.2 Research Objective

This thesis report will focus on the comparison of three different methods to stabilize the power for dynamic wireless charging of electric vehicles. These methods are buck converter, inverter and active rectifier. The outcome will be an elaborated analysis on which of the three methods is the most suitable in terms of voltage ripple, voltage regulation, space efficiency, start-up time and modulation complexity. Therefore, this thesis answers the following research question:

***"Which method of power stabilization for dynamic wireless charging of electric vehicles is the most suitable in terms of voltage ripple, space efficiency, voltage regulation, modulation complexity and start-up time?"***

## 1.3 Thesis Outline

This thesis consists of eight chapters, a brief introduction on the content of each chapter is presented below:

- **Chapter 1: Introduction**
  In the introduction a brief explanation on the topic, its relevance to the current global warming challenges and the problem definition will be provided.
- **Chapter 2: Socio-economical Impact**
  In this chapter, the impact of dynamic wireless charging of EVs on the social well being and economics will be presented.
- **Chapter 3: Fundamentals of Wireless Power Transfer**
  This chapter provides a brief but profound explanation of the working principle of wireless power transfer.
- **Chapter 4: Power Stabilization Methods**
  This chapter introduces the three methods to stabilize the power in dynamic wireless charging. It provides the circuit schematics, the necessary formulas to design it and the working principles of it.
- **Chapter 5: Control Strategy and Modulation**
  In this chapter, the PI control and phase shift modulation will be introduced along with the modulation approach necessary to apply it to each individual power stabilization method.
- **Chapter 6: Simulink Model Design**
  This chapter presents the design methodology and functional validation of the following circuits: SS and DLCC compensation, rectifier, buck converter, inverter and active rectifier. In addition, it provides a brief comparison between the SS and DLCC compensation circuit that provides the technical justification to select DLCC compensation to be used in this project.
- **Chapter 7: Results**
  This chapter provides a comparative analysis of the five characteristics, which are, voltage ripple, space efficiency, voltage regulation, modulation complexity and start-up time, to select which method of power stabilization is the best among the three.
- **Chapter 8: Conclusion and Future Work**
  In this chapter, one of the three methods is selected to be the best option to stabilize the power in a DWC system. In addition, a few suggestions for future research are provided.

# 2

# Socio-economical Impact

The stabilization of power in dynamic wireless charging leads to significant developments in the electric vehicle's industry. This innovation promotes social inclusivity, leads to environmental benefits and enhances economic growth.

- **Economic Opportunity:** The implementation of dynamic wireless charging enables the EV to charge while it is driving. This eliminates the necessity for a large battery. As a result, the size of the battery will be relatively smaller, which will lead to lower initial cost of the vehicle. For an average EV, the battery capacity is 71.1 kWh. The price of 1 kWh battery capacity was on average in 2024 115 USD/kWh. Assuming, that due to DWC of EVs, the battery capacity will decrease by 25% to 50%, it will safe 2000 USD to 4000 USD. This reduction in costs causes a decrease in the purchase price of an EV. As a result, it becomes more affordable by potential buyers, and manufactures will sell more units. Therefore, it benefits both producer and consumer[9][10][11].
- **Social Well-being:** A lower manufacturing and purchase cost of EVs promotes social inclusivity by making it possible for a broader range of income levels throughout the population to be able to purchase an EV. In addition, dynamic wireless charging eliminates two other concerns from potential buyers, namely, range anxiety and charge inconvenient. Due to the ability of the vehicle to charge while driving on the road, it will solve range anxiety concerns, and there will be no unnecessary time consumption for long stops to charge the vehicle while on a journey. This creates a user friendly and convenient experience with EVs.
- **Environmental Benefits:** Due to the decrease in charging time and purchasing cost, there will be a decrease in greenhouse gas emissions. Due to a lower purchase price for these vehicles, EVs will become more affordable to a wider section of the population. This encourages them to consider buying an EV over a traditional combustion engine car. Similarly, eliminating the concerns of long charging time and range anxiety, people will be encouraged to buy an EV. As a result, there will be less greenhouse gas emissions, paving the way towards a cleaner environment.

# 3

# Fundamentals of Wireless Power Transfer

Many of us have used wireless charging, for instance, to charge a smartphone, a smartwatch or a toothbrush. However, few are familiar with the working principles of wireless power transfer(WPT). In this section, the history and theory behind WPT is presented.

WPT commenced with a prediction by the famous physicist and mathematician, James Clerk Maxwell. Maxwell invented a set of equations, the Maxwell equations. These equations predicted that one day power could be transmitted between two points in space without any physical wiring between them. Then the physicist Heinrich Hertz experimentally validated Maxwell's equations in the time period 1885-1889. After that, the genius engineer and inventor Nikola Tesla experimented with and demonstrated WPT. Today, WPT is widely used throughout the world. However, how does it work?[12][13].
In Figure 3.1, a schematic is shown of a simple WPT circuit to provide a visual insight of it. This will aid in understanding the explanation on WPT that will follow. A WPT circuit consists of two sub-circuits that do not have any physical connection in common. These two sub-circuits are referred to as the primary side and the secondary side. The primary side is where the power is transmitted from, and the secondary side is the sub-circuit that receives the transmitted power from the primary side.
According to Ampere's circuital law, when a current passes through a conductive wire a magnetic field will be generated. In Figure 3.1, the WPT schematic consists of a source and inductor on the primary side, and an inductor and load on the secondary side. Due to the current, $i_1(t)$, flowing through the inductor $L_1$, it creates magnetic field lines indicated by the magnetic fluxes $\phi_{11}$ and $\phi_{12}$. The magnetic flux is the total amount of magnetic field lines that pass through a surface. $\phi_{12}$ are the field lines that reach the inductor $L_2$ and pass through the coil, which according to Faraday's law induces a voltage that is proportional to the number of turns of the coil and the rate of change of the flux $\phi_{12}$. This relationship is expressed as $V_{ind}=N\ \frac{d\phi_{12}}{dt}$. Since $\phi_{12}$ is caused by the current $i_1(t)$, $V_{ind}$ can be re-written as $V_{ind}=N_2\ \frac{d\phi_{12}}{di_1}\ \frac{di_1}{dt}$, where $N_2\ \frac{d\phi_{12}}{di_1}$ is called the mutual inductance. The final expression is: $V_{ind}=M\ \frac{di_1}{dt}$. The induced voltage, $V_{ind}$, will power the secondary part of the circuit. Therefore, power is transferred from the primary to the secondary side without the necessity for physical wiring between the two circuits. Hence, wireless power transfer is established[14][15][16][17].

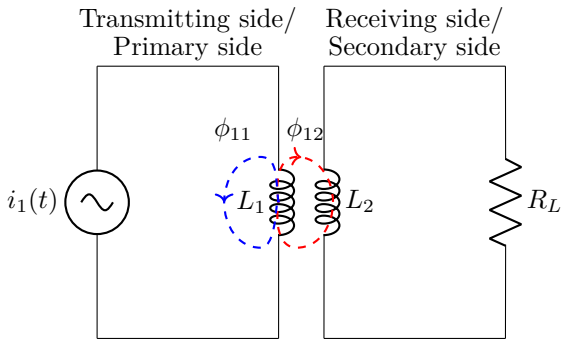


**Figure 3.1:** Circuit to illustrate WPT.

## 3.1 Compensation

A WPT circuit, like the one shown in Figure 3.1, will have a lower power output than expected. The reason for such lower power output is the reactive element introduced by the inductor. There are two types of power, real power(P) and reactive power(Q), Q corresponds to the power of the reactive elements in the circuit. The sum of these two power types is called apparent power(S). Translating this into an equation: S=P+jQ. In practice, only the real power is consumable. The reactive power leads to increased current to achieve the rated power. This increased current will introduce additional ohmic losses, $P_{loss}$=$I^2$·R. The equation for the real power is: P=I·V, in case reactive power is present in the circuit, it introduces another parameter into the equation which is the power factor(PF). The equation adapts to P=I·V·PF. PF is the ratio of P to S, which indicates that if the reactive power is a non-zero value, the PF will be below unity, and this leads to a decrease in magnitude of the real power. This decrease is undesirable. To solve this, the effect of the reactive power on the circuit has to be nullified. As a result, the PF will be equal to unity, which leads to no power losses by the reactive element(s).
To cancel out the reactive power of the inductors, capacitors are inserted into the circuit. The value of the capacitor should be selected such that it satisfy $X_C$=$X_L$, where $X_C$ is the reactance of the capacitor and $X_L$ is the reactance of the inductor. This condition in which $X_C$=$X_L$ is called resonance condition, it happens at a fixed frequency called the resonance frequency. Due to practical reasons, the value of the inductor is determined first and then the value of the capacitor since the value of the capacitor is less complicated to tune compared to that of the inductor.
The derivation of the formula used to determine the capacitance at resonance is shown in the Equation series 3.1.

$$\begin{aligned} & X_L = X_C \\ & \Rightarrow 2\pi f_r L = \frac{1}{2\pi f_r C} \\ & \Rightarrow (2\pi f_r L \cdot 2\pi f_r C) = 1 \\ & \Rightarrow C = \frac{1}{4\pi^2 f_r^2 L}(\mathrm{F}) \end{aligned} \tag{3.1}$$

To construct the WPT circuit in Simulink, two topologies are considered, namely, series series compensation, abbreviated as SS compensation, illustrated in Figure 3.2, and double sided LCC compensation, abbreviated as DLCC compensation, shown in Figure 3.3. These two circuits have two main functions, namely, facilitating WPT between the primary and secondary sides and compensating the reactive impedance of the primary and secondary coil. The latter function is referred to as compensation.

In the following sections/chapters, the DLCC compensation circuit and the SS compensation circuit are discussed in detail and compared. Eventually, one of the topologies is selected to be used in this thesis[18][19].

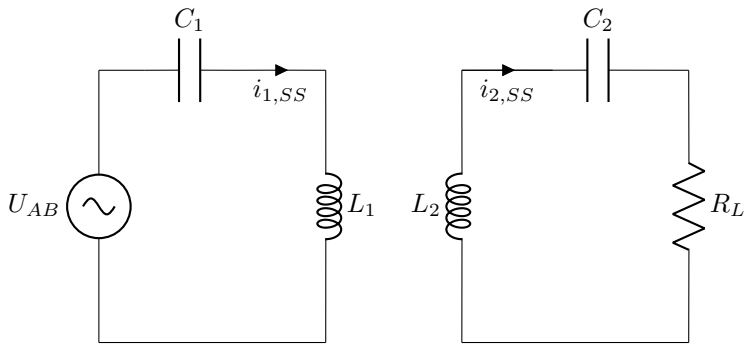


**Figure 3.2:** SS compensation circuit.

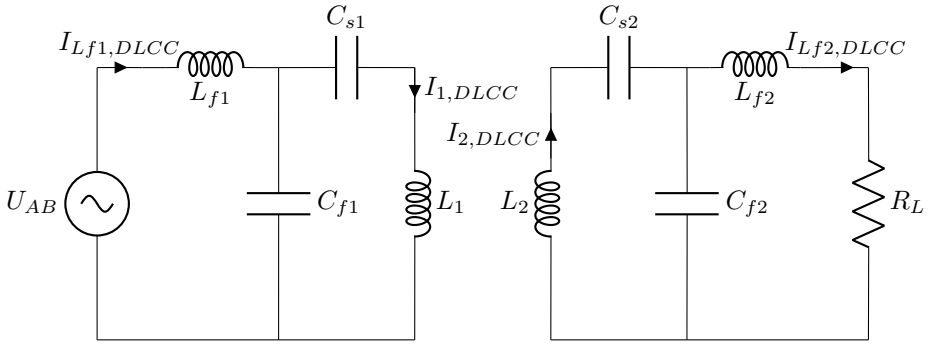


**Figure 3.3:** DLCC compensation circuit.

## 3.2 Current Derivation in SS Compensation Circuit

This section is dedicated to the derivation of the primary current($I_{1,SS}$), secondary current($I_{2,SS}$) and the output current($I_0$) of the SS compensation circuit shown in Figure 3.4. The derived expressions of these currents will be used to verify the results attained from the Simulink model, and will be used to decide whether the SS or DLCC compensation will be used as the DWPT circuit for this thesis project. To derive $I_{1,SS}$, $I_{2,SS}$ and $I_0$, Kirchoff's Voltage Law(KVL) is used. Note that in this circuit $I_{2,SS}$ and $I_0$ will be identical due to the series positioning of component $C_2$ and $R_L$. The derivation of $I_{1,SS}$ and $I_{2,SS}(I_0)$ is shown in Equation series 3.2 to 3.9.

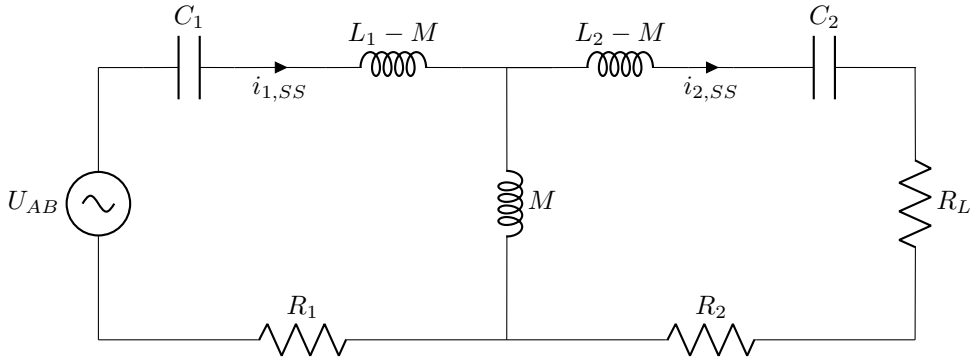


**Figure 3.4:** SS compensation circuit used for current derivation.

For the current loop in the left-hand-side of the circuit the following equation is established:

$$\begin{aligned} &- U_{AB} + \frac{1}{j\omega C_1} I_{1,SS} + j\omega \left(L_1 - M\right) I_{1,SS} + \left(I_{1,SS} - I_{2,SS}\right) j\omega M \\ &+ I_{1,SS} R_1 = 0 \end{aligned} \tag{3.2}$$

To achieve resonance state, the following expression is used for $C_1$:

$$C_1 = \frac{1}{\omega_s^2 L_1} \tag{3.3}$$

Then by substituting Equation 3.3 into Equation 3.2 the expression for $I_{1,SS}$ can be derived. As is shown below:

$$\begin{aligned} &-U_{AB} - j\omega_s L_1 I_{1,SS} + j\omega_s L_1 I_{1,SS} - j\omega_s M I_{1,SS} + j\omega_s M I_{1,SS} - j\omega_s M I_{2,SS} + I_{1,SS} R_1 = 0 \\ &\Rightarrow -U_{AB} - j\omega_s M I_{2,SS} + I_{1,SS} R_1 = 0 \\ &\Rightarrow I_{1,SS} = \frac{U_{AB} + j\omega_s M I_{2,SS}}{R_1} \end{aligned} \tag{3.4}$$

Now KVL is applied on the right-hand-side of the circuit. This results in:

$$j\omega_s M \left(I_{2,SS} - I_{1,SS}\right) + j\omega_s \left(L_2 - M\right) I_{2,SS} + \frac{1}{j\omega_s C_2} I_{2,SS} + I_{2,SS} R_L + I_{2,SS} R_2 = 0 \tag{3.5}$$

Again, to achieve resonance state, the following expression is used for $C_2$:

$$C_2 = \frac{1}{\omega_s^2 L_2} \tag{3.6}$$

Then by substituting Equation 3.6 into Equation 3.5 the expression for $I_{2,SS}$ can be derived. As is shown below:

$$\begin{aligned} &j\omega_s M I_{2,SS} - j\omega_s M I_{1,SS} + j\omega_s I_{2,SS} L_2 - j\omega_s M I_{2,SS} - j\omega_s L_2 I_{2,SS} + I_{2,SS} R_L + I_{2,SS} R_2 = 0 \\ &\Rightarrow -jM I_{1,SS} + I_{2,SS} \left(R_L + R_2\right) = 0 \\ &\Rightarrow I_{2,SS} = \frac{j\omega_s M I_{1,SS}}{R_L + R_2} \end{aligned} \tag{3.7}$$

To find $I_{1,SS}$, the expression for $I_{2,SS}$ is substituted into Equation 3.4.

$$\begin{aligned} I_{1,SS} &= \frac{U_{AB} + j\omega_s M \frac{j\omega_s M I_{1,SS}}{R_2 + R_L}}{R_1} \\ &\Rightarrow I_{1,SS} R_1 = \frac{U_{AB}(R_2 + R_L) + \omega_s^2 M^2 I_{1,SS}}{R_2 + R_L} \\ &\Rightarrow I_{1,SS} R_1 (R_2 + R_L) = U_{AB}(R_2 + R_L) - \omega_s^2 M^2 I_{1,SS} \\ &\Rightarrow I_{1,SS} R_1 (R_2 + R_L) + \omega_s^2 M^2 I_{1,SS} = U_{AB}(R_2 + R_L) \\ &\Rightarrow I_{1,SS} \left[R_1 (R_2 + R_L) + \omega_s^2 M^2\right] = U_{AB}(R_2 + R_L) \\ &\Rightarrow I_{1,SS} = \frac{U_{AB}(R_2 + R_L)}{R_1 (R_2 + R_L) + \omega_s^2 M^2} \end{aligned} \tag{3.8}$$

To find $I_{2,SS}$, the final expression for $I_{1,SS}$ in Equations series 3.8, is substituted in 3.7.

$$\begin{aligned} I_{2,SS} &= \frac{j\omega_s M}{R_2 + R_L} \cdot \frac{\left(U_{AB} + j\omega_s M I_{2,SS}\right)}{R_1} \\ &\Rightarrow I_{2,SS} \left(R_2 + R_L\right) R_1 + \omega_s^2 M^2 I_{2,SS} = j\omega_s M U_{AB} \\ &\Rightarrow I_{2,SS} = \frac{j\omega_s M U_{AB}}{R_1 \left(R_2 + R_L\right) + \omega_s^2 M^2} \end{aligned} \tag{3.9}$$

Since $R_1$ and $R_2$ are much smaller than $\omega_s^2 \cdot M$, Equation 3.8 and 3.9 can be further simplified to:

$$I_{1,SS} = \frac{U_{AB} R_L}{\omega_s^2 M^2} \tag{3.10}$$

$$I_{2,SS} = \frac{j\omega_s M U_{AB}}{\omega_s^2 M^2} \tag{3.11}$$

## 3.3 Current Derivation in DLCC Compensation Circuit Using T-type Circuit

To derive the winding currents and the output current of the DLCC compensation circuit, shown in Figure 3.8, the T-type circuit is used. This type of circuit is used since it makes it simple to study the impedances, currents and voltages of a WPT circuit, the T-type circuit is shown in Figure 3.5. An expression for the input impedance($Z_{in}$) and the output current ($I_0$) of the T-type circuit will be derived first and then it will be applied to the DLCC compensation circuit at a later stage in this section.

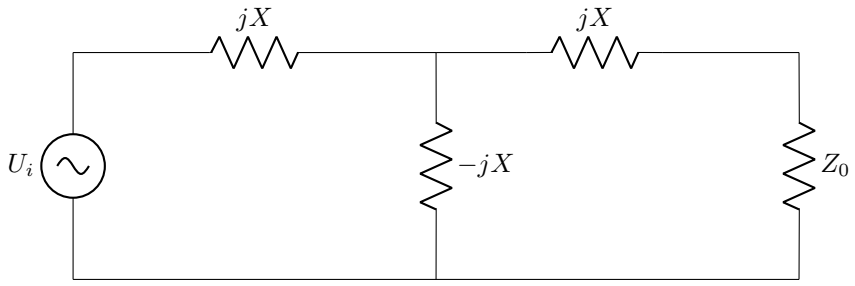


**Figure 3.5:** Schematic of T-type circuit.

First, $Z_{in}$ is determined, which is necessary to derive the output current of the T-type circuit. The derivation for $Z_{in}$ is given in Appendix B.1, which shows that the expression for $Z_{in}$ is $\frac{X^2}{Z_0}$. To derive the output current, the circuit in Figure 3.5 is simplified to the circuit shown in Figure 3.6. The reason for this simplification is that in the latter one the voltage over $Z_0$+jX and -jX is identical due to their parallel relationship, and due to this relationship the expression for the output current($I_0$), shown in Equation 3.12, is derived.

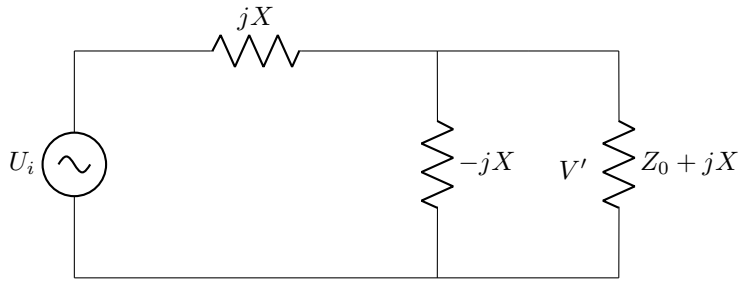


**Figure 3.6:** T-type circuit simplified.

$$\begin{aligned} I_0 &= \frac{V'}{Z_0 + jX} \\ I_0 &= \frac{\mathrm{I_{in}}\,(Z_0 + jX) \,\|(-jX)}{Z_0 + jX} \end{aligned} \tag{3.12}$$

Note that in the expression shown in Equation 3.12, the parameter $I_{in}$, the input current, is an unknown variable. To find an expression for $I_{in}$ the circuit is further simplified to the one shown in Figure 3.7.

In this simplified version of the T-type circuit, the current that flows through the electrical components is similar. By using Ohm law, $I_{in}$ could be replaced by $U_{in}/Z_{in}$, and $Z_{in}$ was derived to be $X^2/Z_0$. Substituting the expression for $I_{in}$ and $Z_{in}$ in Equation 3.12, and simplifying the terms will result in $I_o = \frac{U_{in}}{jX}$. The step-by-step derivation is shown in Appendix B.2.

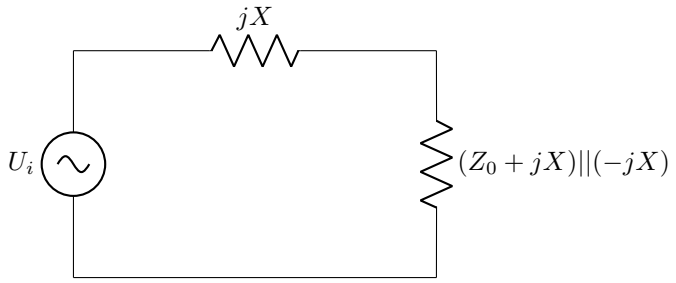


**Figure 3.7:** T-type circuit simplified.

The next step is to geographically compare the impedances, the source and the load of the non-simplified T-type circuit, shown in Figure 3.5, to specifically selected source/components in the DLCC compensation circuit, shown in Figure 3.3. In the DLCC compensation circuit, to find the output current($I_{Lf2,DLCC}$) and the secondary winding current($I_{2,DLCC}$), $U_i$ is considered to be $= \frac{MU_{AB}}{L_{f1}}$, $R_L$ to be $Z_0$ and $L_{f2}$ to be $= jX$. Substituting these parameters into Equation 3.13 gives the expression for the DLCC output current shown in Equation 3.14.

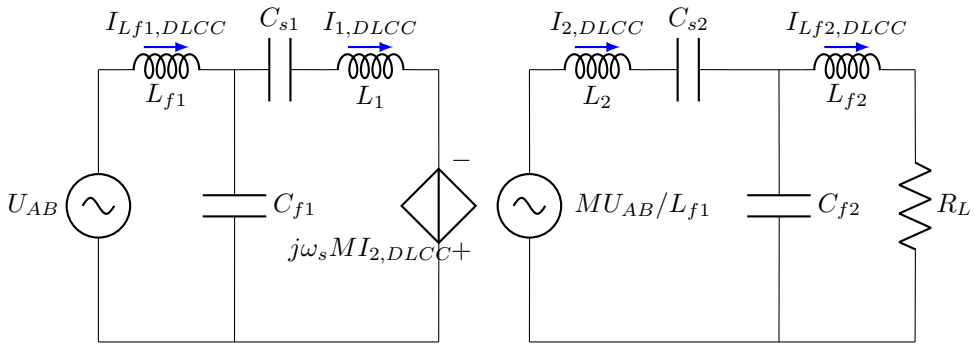


**Figure 3.8:** DLCC compensation circuit used for current derivation.

$$I_0 = \frac{U_i}{jX} \tag{3.13}$$

$$I_0 = \frac{U_i}{j\omega_s L_{f_2}} = \frac{\mathrm{MU}_{AB}}{j\omega_s L_{f_2} L_{f1}} \tag{3.14}$$

To find the secondary current, $I_{2,DLCC}$, $I_0$ is multiplied by $R_L$ which results in $\frac{MU_{AB}R_L}{j\omega L_{f2} Lf1}$. This is the voltage at the output of the secondary side and can be seen as a voltage source. The T-type circuit is compared to this adapted circuit, whereby this time $U_i = \frac{MU_{AB}R_L}{j\omega L_{f2} Lf1}$ and $j\omega X = j\omega\ L_2 + \frac{1}{j\omega C_{s2}}$. Substituting these parameters in Equation 3.13 results in the following expression for the secondary winding current($I_{2,DLCC}$):

$$I_{2,DLCC} = \frac{\frac{MU_{AB}R_L}{j\omega L_{f2} Lf1}}{j\omega L_2 + \frac{1}{j\omega C_{s2}}} \tag{3.15}$$

However, this equation can be simplified further. The DLCC circuit will operate under resonant condition. To achieve resonant condition the following must hold for $C_{s2}$:

$$C_{s2} = \frac{1}{\omega_s^2(L_2 - L_{f2})} \tag{3.16}$$

Substituting this expression for $C_{s2}$ into Equation 3.15 results in the following final expression for the secondary winding current:

$$I_{2,DLCC} = \frac{MU_{AB}R_L}{\omega_s^2 L_{f1} L_{f2}^2} \tag{3.17}$$

To find the primary winding current, $I_{DLCC}$, $U_{in}$ is set to be $U_{AB}$ and jX is set to $\frac{1}{j\omega_s C_{s1}}$+j$\omega_s L_1$. Once again, these parameters are substituted in Equation 3.13 and by taking the resonance condition into account, the expression shown in Equation 3.18 is derived for the primary winding current[18][20].

$$I_{1,DLCC} = \frac{U_{AB}}{j\omega_s L_{f_1}} \tag{3.18}$$

A step-by-step derivation is provided in Appendix B.3.

# 4

# Power Stabilization Methods

In this chapter, the buck converter, the inverter and the active rectifier that will be used to stabilize the output power will be introduced. To provide an overview, the three different schematics of the Dynamic Wireless charging(DWC) system are shown in Figures 4.1, 4.3 and 4.2. Each system includes the DLCC compensation circuit discussed in the previous chapter and one of the power stabilization methods that will be discussed in this chapter. In Figure 4.1 and Figure 4.2, the input of the system is labeled as inverter. This is to indicate that an inverter should be implemented to convert the frequency from the mains to 85 kHz. The input voltage of the DWC system is 800V.

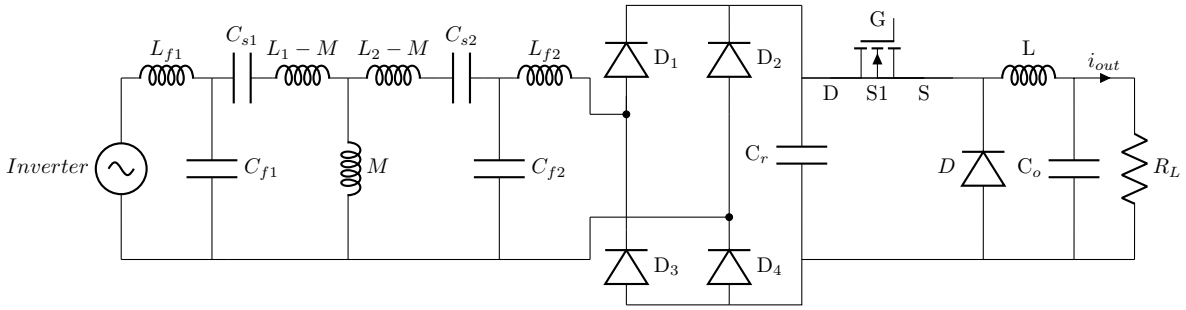


**Figure 4.1:** DWC system using the buck converter.

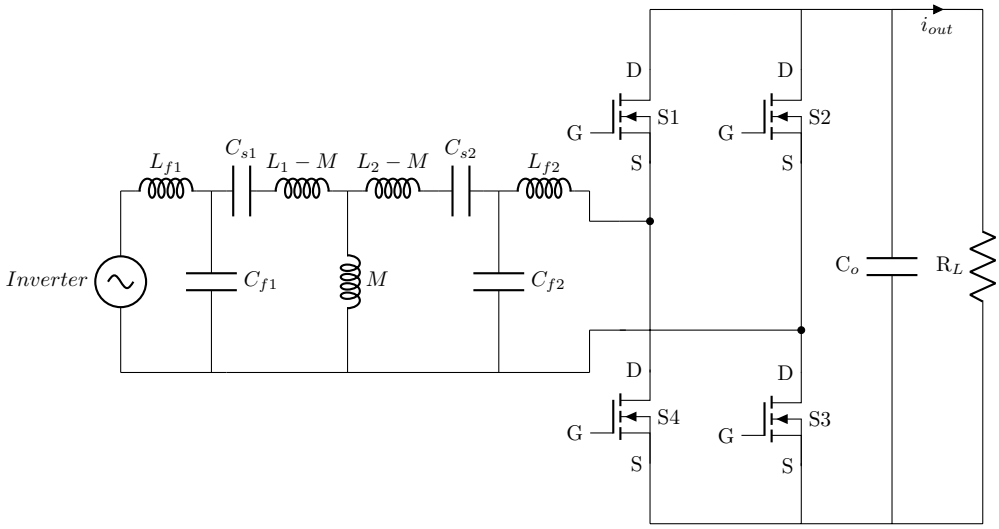


**Figure 4.2:** DWC system using the active rectifier.

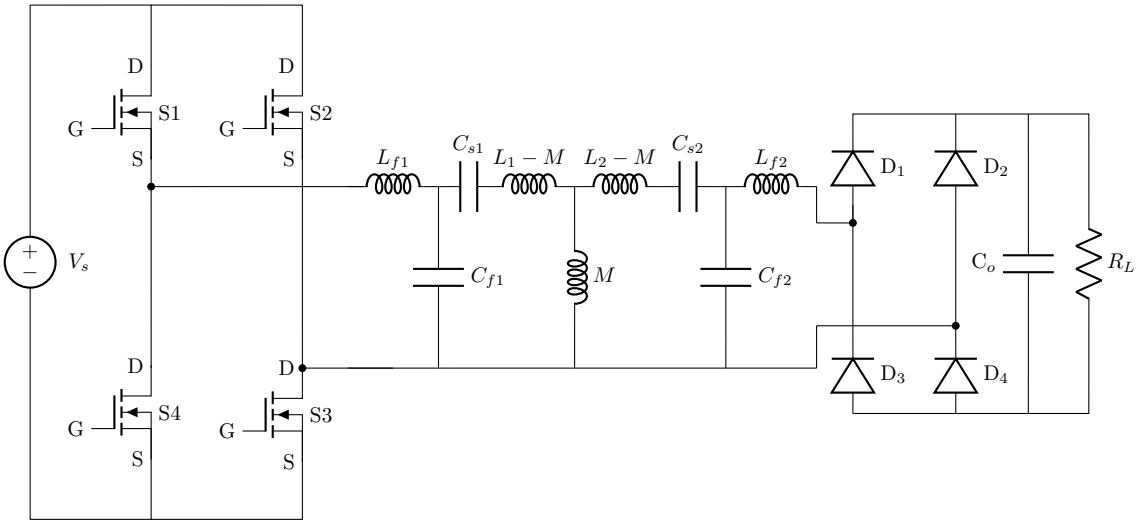


**Figure 4.3:** DWC system using the inverter.

## 4.1 Buck Converter

The buck converter is a widely used circuit for power stabilization. It is a DC-DC converter that is capable of reducing the voltage at its input to a desired voltage at its output. In Figure 4.4, the circuit of a buck converter is shown which consists of a switch(MOSFET), inductor, diode and a capacitor. The magnitude of the output voltage is regulated by controlling the time duration for which the switch is on or off. The ratio of the on-time of the switch to the total switching period is defined as the duty cycle. The signal that controls the switching of the MOSFET is known as Pulse-Wide Modulation(PWM). PWM is a square wave with a constant frequency referred to as the switching frequency. The duty cycle controls the amount of time that the square wave has a high or low value. For instance, if the duty cycle is set to 75%, the square wave will have a high value for 75% of the time period and a low value for 25% of the time period.

The duty cycle will determine the proportion of the input voltage present at the output voltage. To achieve a better understanding, if the input voltage is 100 V and the duty cycle is 50%, then the output voltage will be 50 V, assuming Continous Conduction Mode(CCM). The buck-converter has two modes of operation, namely, CCM and Discontinous Conduction Mode(DCM). In CCM, the inductor current will stay non-zero for the entire switching cycle, while, in contrast to CCM, in DCM the inductor current

will decrease to zero. These two operating modes differ not only in their inductor current range but also in the equations used for the design of the buck converter. The preferred conduction mode for this thesis will be selected during the design stage of this project.

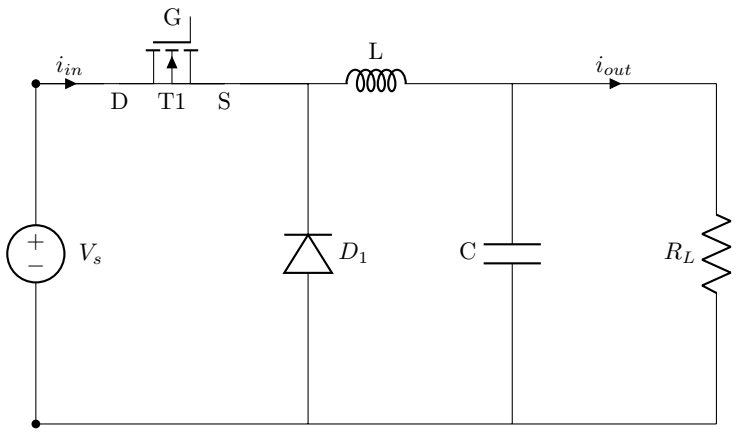


**Figure 4.4:** Schematic of the buck converter.

How does the buck converter work? When the switch is closed, the capacitor, C, and inductor, L, start charging. Due to the nature of the inductor, the current can not increase instantly but will increase linearly. Energy will be stored as a magnetic field in the inductor. Current will flow through the switch, the inductor, the capacitor and the load. This stage of operation is depicted in 4.5.

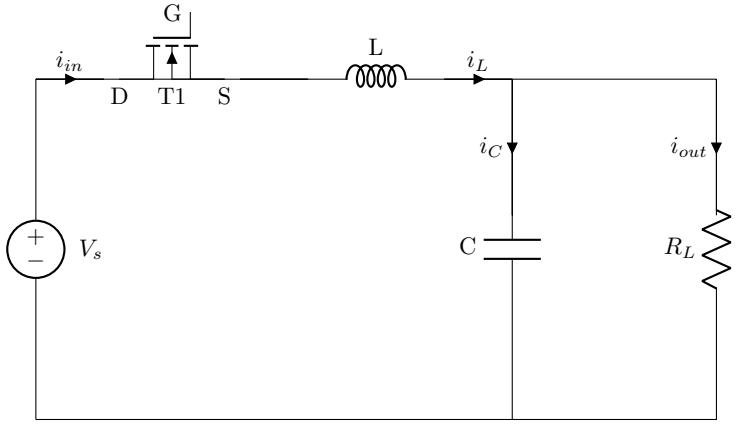


**Figure 4.5:** Schematic of the buck converter when switch is "on".

Once the switch turns off, the energy stored as a magnetic field in the inductor is delivered back to the circuit, and it provides current to $R_L$. The inductor voltage is reverse biased at this stage. The circuit of this stage of operation is depicted in Figure 4.6. In this stage of operation, the current can not decrease at an instant due to the nature of the inductor. Hence, it will decrease linearly.

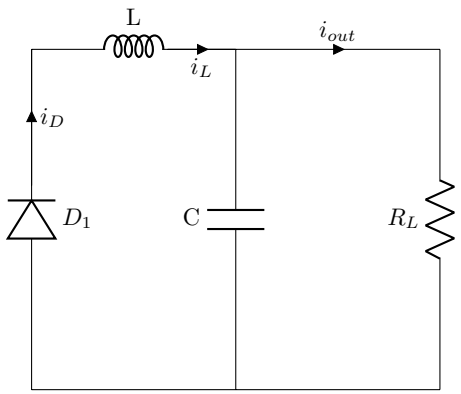


**Figure 4.6:** Schematic of the buck converter when switch is "off".

Now the question is, how does a buck converter lower the voltage? Like mentioned before, the inductor can not change at an instant, it will cause the current to increase or decrease linearly. When the switch turns on, instead of jumping from 0 V to the maximum value of the input voltage, it will linearly increase trying to reach the maximum voltage. However, when the switch turns off, it will stop increasing and provide energy back to the circuit. Instead of rushing the current into the circuit, decreasing from its current value to 0 V, it will decrease linearly until the switch turns on and the cycle repeats. This will result in a sawtooth wave like shown in Figure 4.7. By using a capacitor in parallel with the load, like shown in Figure 4.6, this relatively high ripple voltage can be turned into a constant DC voltage in which the ripple is equal to or less than 1% of the output voltage[21][22][23][24].

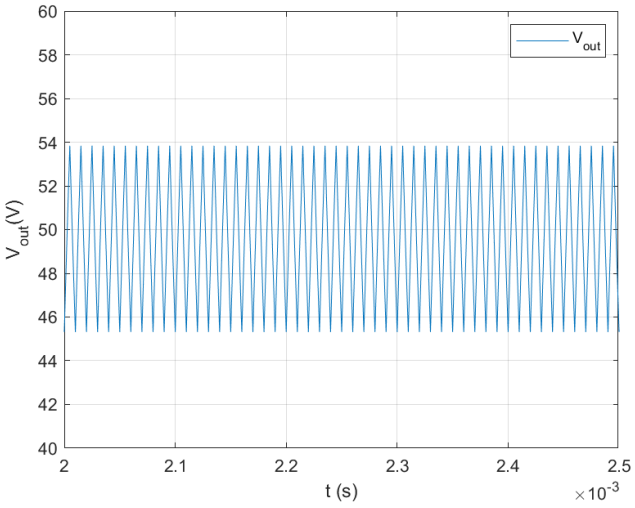


**Figure 4.7:** $V_{out}$ of buck converter without smoothing capacitor.

The diode present in the circuit is to provide a path for the inductor current when the switch is turned off. This prevents the current from causing damage to the switch[25].
When the input voltage is a constant, a fixed duty cycle is used to generate a constant output voltage of interest. However, when the input voltage is dynamic, using a fixed duty cycle will cause the output voltage to vary with respect to the dynamic input voltage. To prevent this, closed loop feedback should be used to make the duty cycle dynamic. This will be elaborated on in Chapter 5.

The equations to determine the duty cycle for the operating modes CCM and DCM are shown in Equation 4.1 and 4.2, respectively. In addition, the equation to calculate the inductance and capacitance is presented in Equation 4.3 and 4.4, respectively[22][26].

$$D = \frac{V_{\text{out}}}{V_{\text{in}}} \tag{4.1}$$

$$D = \frac{V_{\text{out}}}{V_{\text{in}}} \cdot \sqrt{\frac{I_{out/I_{LB.max}}}{1 - V_{out}/V_{in}}} \tag{4.2}$$

$$L = \frac{V_{\text{out}} \cdot (1 - D) \cdot T_s}{\Delta I_L} \tag{4.3}$$

$$C = \frac{V_{\text{out}} \cdot (1 - D) \cdot T_s^2}{8 \cdot \Delta V_{\text{out}} \cdot L} \tag{4.4}$$

Where:

- $C$ is the smoothing capacitance
- $L$ is the inductance
- $D$ is the duty cycle
- $T_s$ is the switching period ($T_s = 1/f_s$)
- $\Delta I_L$ is the inductor ripple current
- $\Delta V_{\text{out}}$ is the output voltage ripple
- $V_{\text{in}}$ is the input voltage
- $I_{\text{out}}$ is the output current
- $\Delta I_{\text{LB,max}}$ is the maximum inductor boundary current

## 4.2 Inverter

An inverter is a circuit that converts a DC input voltage to an AC output voltage. The circuit consists of four switches in which a control signal is used to turn-on or turn-off the switches at the correct time moment to convert a signal from DC to AC. Figure 4.8 shows the schematic of the inverter. For simplicity, engineers use the term "leg" to refer to two switches that are located on the same vertical side with respect to each other. During the converting process, two switches, each on opposite legs, have to conduct at the same time to power the output while the other two switches must be non-conducting; two switches on the same leg must not conduct at the same time. The guiding of this switching process is carried out by a PWM signal. At each individual switch gate, a unique PWM signal will be provided. The PWM signal will be a square wave with a frequency of interest for the output voltage because the frequency of the PWM signal will translate to the frequency of the output voltage. Besides converting an AC voltage to a DC voltage, the inverter can also be utilized for power stabilization. In an inverter, two switches, each on different legs, have to conduct to deliver the desired AC output voltage. When the turn-on time of one of the switches is delayed, it results in a decrease in the proportion of the time period, in which the output voltage is non-zero. This results in a lower average output voltage. The method used to insert the delay is called Phase Shift Modulation(PSM) and will be discussed in Section 5.3 [27].

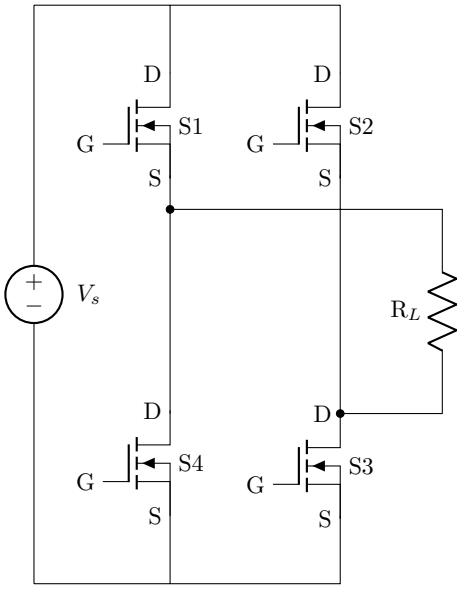


**Figure 4.8:** Schematic of the inverter.

## 4.3 Full Bridge Rectifier

To connect the DLCC compensation circuit to the buck converter, a full bridge rectifier has to be placed between them to convert the AC output voltage of the DLCC circuit to a DC input voltage for the buck converter. Also, in case the inverter is used, the rectifier has to be used to convert the AC output voltage of the DLCC circuit to a DC output voltage to charge the battery. In Figure 4.9, the schematic of the rectifier used in this project is shown. The rectifier consists of a voltage source, four diodes and a capacitor to smoothen the output voltage.

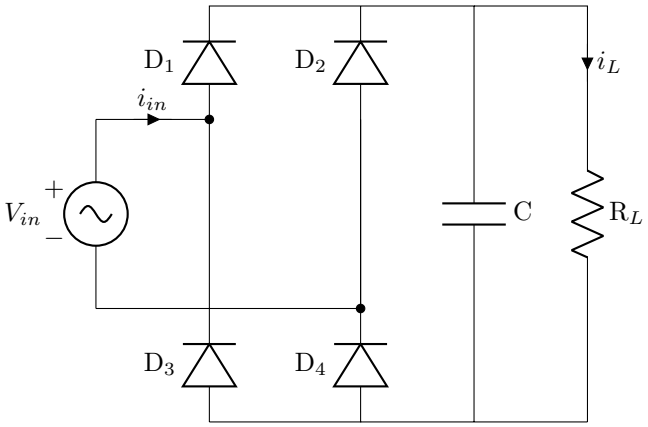


**Figure 4.9:** Schematic of the full bridge rectifier.

Having established the circuit topology, the operations of the rectifier will be explained. The rectifier will have a sinusoidal voltage at its input. When the sinusoid wave is at its positive half-cycle, diode D1 and D4 will conduct and the circuit outputs a positive voltage like shown in Figure 4.10b. To show the path of the current an adapted version of the full bridge circuit is shown in Figure 4.10a. After half of the time period has passed, the wave will switch to its negative half-cycle for the remaining time period. During this half-cycle, diodes D2 and D3 will conduct, see Figure 4.11a for the current path. The output voltage during this half-cycle will be a positive voltage like illustrated in Figure 4.11b. In each of the current path shaped by these two modes, the current flows through the load in the same direction during both half-cycles. As a result, a positive voltage is present across the load.

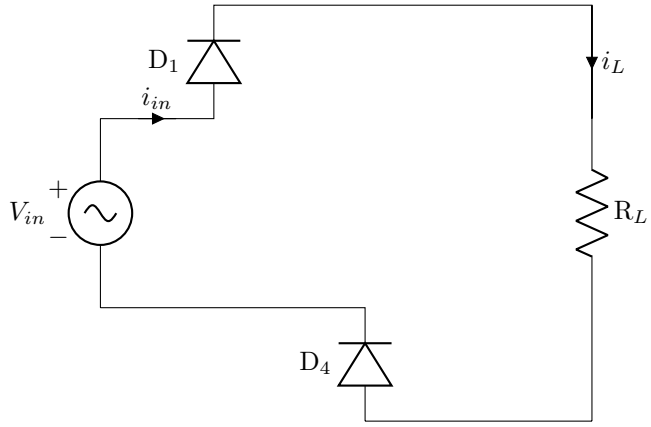


**(a)** Schematic when D1 and D4 are conducting.

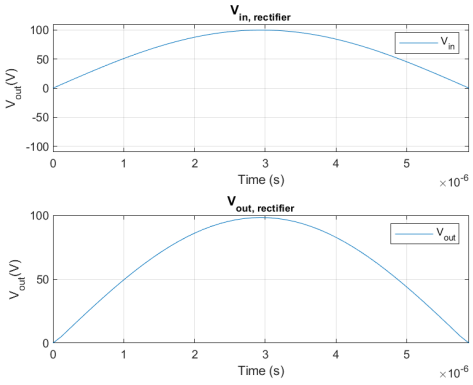


**(b)** Input and output voltage waveforms.

**Figure 4.10:** Full bridge rectifier when only $D_1$ and $D_4$ are conducting.

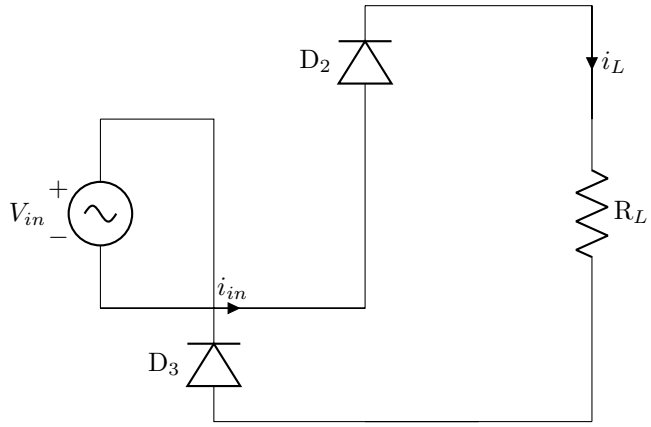


**(a)** Schematic when D2 and D3 are conducting.

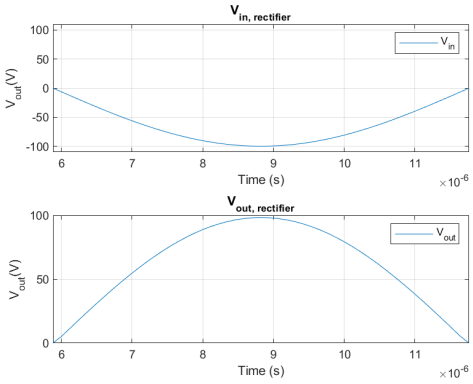


**(b)** Input and output voltage waveforms.

**Figure 4.11:** Full bridge rectifier when only $D_2$ and $D_3$ are conducting.

The output voltage is positive during the complete time period, however, it is not DC. In order to turn this into a DC output voltage, the smoothing capacitor will be used. The capacitor saves energy and returns it to the circuit when the voltage drops below 100 V. Figure 4.12 shows the graph of the output voltage with the smoothing capacitor present in the circuit. The reason why it is not exactly 100 V and that there is a ripple will be explained later in this thesis.

The expression displayed in Equation 4.5 will be used to calculate the value of the capacitance $C_{out}$. $I_{out}$ will be determined by using Ohm's Law, $I_{out} = V_{out}R_L$. Like shown in the previous paragraph, $V_{out}$ will roughly be the input voltage. The resistance $R_L$, input voltage and the ripple voltage would be determined later on during the design of the circuit[28].

$$C_{out} = \frac{I_{out}}{2f \cdot V_{ripple}} \tag{4.5}$$

Where:

- $f$ frequency of the input voltage(V)
- $I_{out}$ is the output current(A)(current flowing through $R_L$)
- $V_{ripple}$ is the ripple output voltage(V)

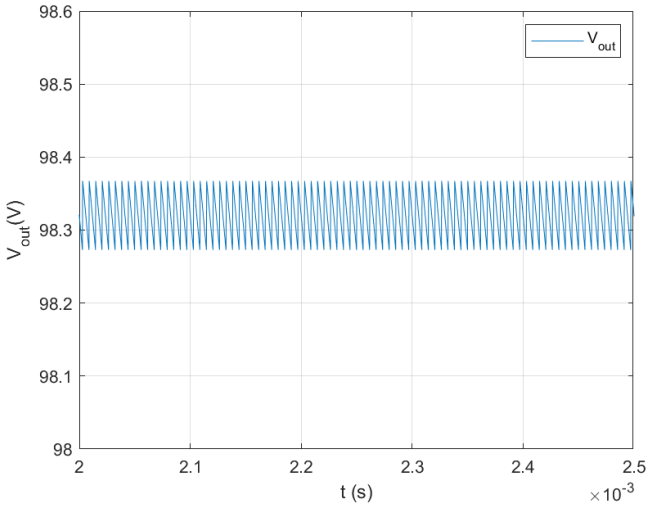


**Figure 4.12:** $V_{out}$ of the rectifier with DC-link capacitor.

## 4.4 Active Rectifier

The third method used in this thesis to stabilize the power is by using an active rectifier. The active rectifier converts an AC signal to a DC signal. In addition, it is capable of controlling the magnitude of the DC signal. A schematic of this circuit is shown in Figure 4.13. Likewise with the inverter, each switch needs a unique PWM signal to control its gate. In case the aim is to only rectify the input signal, when a PWM signal with a duty cycle of 50% can be used for the switches. Keep in mind that switches on the same leg can not conduct at the same time. For this reason, an inverted version of the PWM signal used to drive gate S1, is used for S4, and an inverted version of the PWM signal used to drive gate S2 is used for gate S3.

In case it is necessary to decrease the output voltage, the duty cycle can be adapted. However, if the input voltage is dynamic in magnitude, using a constant duty cycle will not result in a constant output voltage of interest. To achieve a constant pre-determined output voltage, when having an input voltage that varies in magnitude, the switching signals need to be adapted. This is achieved by making a closed loop feedback system in which PSM is used to vary the PWM signal. In Chapter 5, more about PSM and the control strategy will be shared[16][29].

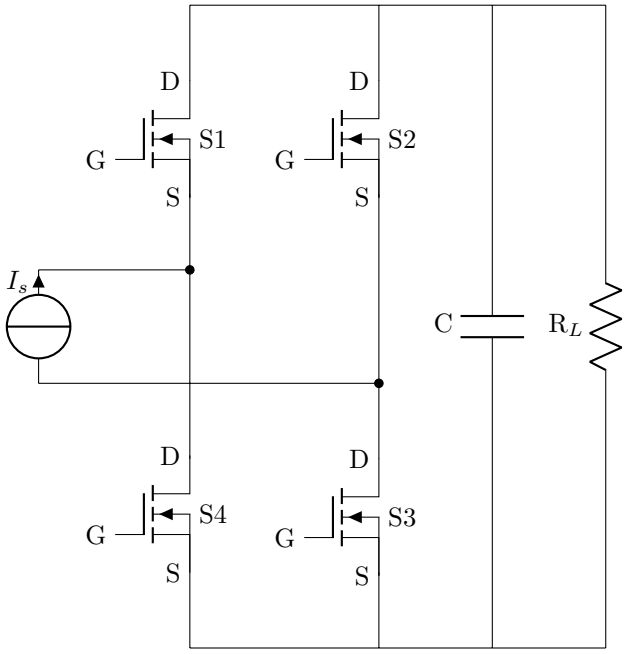


**Figure 4.13:** Schematic of active rectifier.

# 5

# Control Strategy and Modulation

In this chapter, the control strategy and modulation for all three power stabilization methods will be explained and discussed.

## 5.1 PI Control

Like discussed in the previous section, in a dynamic environment, a constant duty cycle is incapable of maintaining a constant output voltage. Since the input is changing, the duty cycle should change accordingly to maintain a preferred constant output voltage. To achieve this, a control strategy will be implemented in the DWC system. There are several controlling strategies to achieve a stable output voltage, namely PI, Model Predictive Control(MPC) and Dynamic Sliding Mode Control(DSMC). A brief comparison of these three strategies will be made to decide which method is the most suitable to be selected for implementation in the DWC system.

Depending on the conditions under which the control strategy is implemented and the preference of the designer, in general, DSMC and MPC have the potential to achieve better results. MPC has a faster response time compared to PI control and DSMC is more robust and has a better dynamic performance compared to PI control. However, both are relatively complex to implement when having limited time. Meanwhile, by using PI control the desired result can also be achieved[30][31].

PI control is a type of feedback control that uses two variables, namely, the proportional gain, $K_p$, and the integral gain, $K_i$, to tune the output of a system towards a reference value of interest called the set point. The process of tuning the output towards the set point starts by comparing the simultaneous output to the set point. The difference of these two is the error signal(e(t)). $K_p$ is then multiplied by the error signal and $K_i$ is multiplied by the integral of the error signal. The sum of these make up the control signal. The equation of the control signal is shown in Equation 5.1[32].

$$u(t) = K_p\, e(t) + K_i \int_0^t e(\tau)\, d\tau \tag{5.1}$$

In this project, the PI output signal determines the on or off time for the switch(es) in the buck converter, inverter and active rectifier. In each of these circuits the PI signal needs to be modulated to be a suitable PWM. In the sections that follow, an elaboration is given on the modulation process for each of the power stabilization methods. In order to achieve the set point as output, the gain parameters of the PI control needs to be tuned. There are different methods used for this purpose, such as Ziegler-Nicholas and trail-and-error method. Ziegler-Nicholas method proved to be unsuccessful in practice. Therefore, the most suitable of the two methods would be trail-and-error. In trail-and-error method, first, $K_i$ is set to zero and $K_p$ is increased from zero until a gain value is achieved for which

the output is marginally stable and $K_p$ can not be increased further without giving overshoot. In this case, $K_p$ is not further adapted. However, a relatively small difference between the actual output value and the reference point will be observed, called the steady-state error. To eliminate this small error $K_i$ is increased from zero while $K_p$ is kept constant. This process continues until the output value is equal to the reference point. There are cases in which the output signal of the circuit shows an overshoot while increasing $K_i$. When this happens, the overshoot can be solved by slightly decreasing $K_p$[32][33].

There are two approaches in Simulink to implement the PI controller. The first approach involves using a built-in PI control block available in the Simulink library. The approach is relatively simple to implement, however, it also comes with its limitations in terms of transparency of the internal behavior of the block for the user. The second approach entails the construction of the PI controller manually by using fundamental Simulink blocks. Although this approach requires more effort and a deeper understanding of control theory and the controller's functionality, it provides a greater insight into the controller's internal operation. As a result, it becomes relatively less difficult to trace the generation of the control signal, which makes debugging, analyzing and adjusting the control signal relatively easier. For these reasons, the second approach is selected to be implemented. In Figure 5.1 the diagram of the PI controller is illustrated[24][34][35].

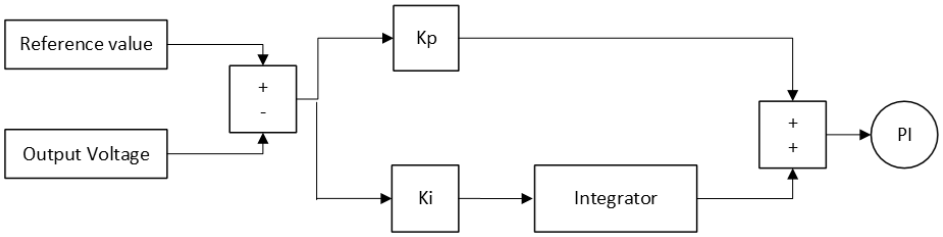


**Figure 5.1:** Block diagram of the PI controller.

## 5.2 Control Signal Modulation for the Buck Converter

Like stated previously, the PI output signal needs to undergo modulation such that it transforms into a suitable PWM signal for the input of the MOSFET switch of the buck converter. To turn-on the MOSFET, and keep it on, it should receive a continuous input signal higher than its threshold voltage which is 0.8 V. Therefore, the signal needs to be larger than 0.8 V for a larger amount of time in case the switch needs to be on. A PWM signal is a square wave with either zero or one as a value. Hence, it is capable of keeping the switch on or off as necessary. To achieve the above discussed wave-type, the PI controller signal will be compared via a comparator block from Simulink library with a sawtooth signal that varies between zero and one with a frequency of 100 kHz. Typically, the switching frequency of a buck converter is in the range of 100 kHz to a few MHz. Although a higher switching frequency allows the use of smaller inductor(s) and capacitor(s), it introduces more losses due to more frequent switching. Therefore, a switching frequency of 100 kHz was selected. When the control signal is equal to or higher than the sawtooth signal, the comparator will output the value one, and when the control signal is lower than the sawtooth signal, the comparator block will output the value zero. As a result, a 100 kHz square wave signal that is either one or zero will be generated to drive the switch, see Figure 5.2 for the block diagram[36][37].

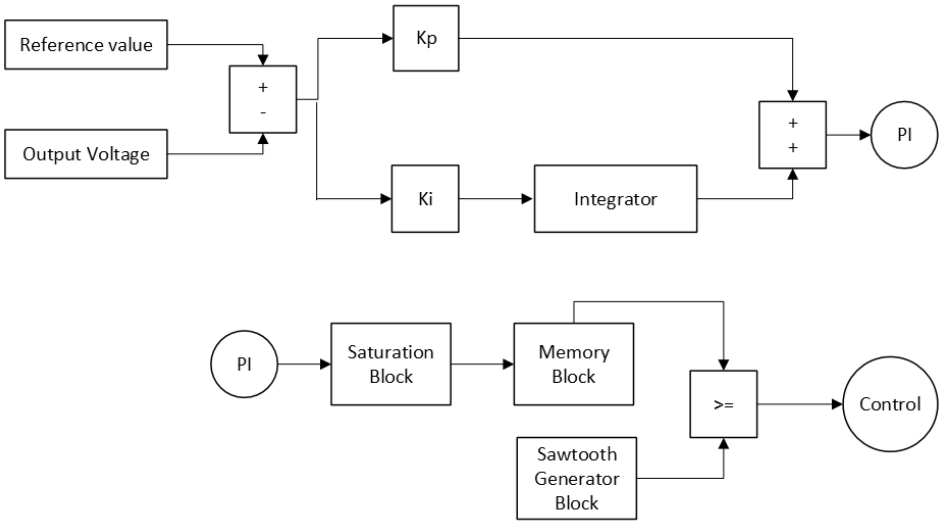


**Figure 5.2:** Block diagram of control and modulation for the buck converter.

## 5.3 Phase Shift Modulation

In PSM, a phase shift is introduced to a signal which will translate to a time delay in that signal. In order to have a profound understanding of PSM, the switching behavior is studied in detail. For this, the inverter circuit is used as an example to apply the PSM on. Before moving on, there are three criteria that should be satisfied for PSM:

- All PWM signals should have 50% duty cycle.
- Frequency of each of the PWM signals should be identical to the fundamental frequency of the system.
- Switches located on the same leg should be complementary to each other.

In Figure 5.3, the schematic of the inverter is illustrated. In this schematic, switch S1 and S3 are a conducting pair, and S2 and S4 are another conducting pair. Like mentioned above, two switches on the same leg should not conduct simultaneously since it will cause a short circuit. In order to prevent this, the control signal that is used for a switch is used for the other switch on the same leg, but the control signal is inverted. In the schematic shown in Figure 5.3, the control signal of S1 will be inverted and used for S4, and the control signal of S3 will be inverted and used for S2. Moreover, the phase shift is applied to switch S3. As a result, switch S3 will have a time delay relative to switch S1.

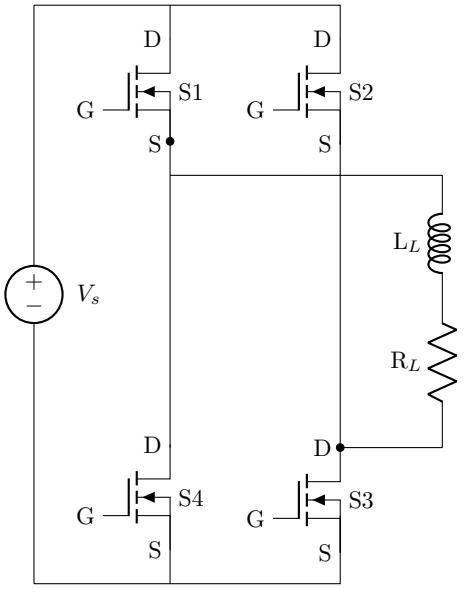


**Figure 5.3:** Schematic of the inverter.

There are four conduction modes, namely, S1-S2, S1-S3, S3-S4 and S2-S4. For each mode, the corresponding circuit and a graphical visualization of the switching signal will be provided. Each time duration of the conduction mode is indicated by a unique line color in Figure 5.4. The first mode of conduction is between 0 s and the vertical red line, the second is between the red line and orange line, the third between the orange line and green line and the last mode is between the green and blue line. The first mode is when switch S1 and S2 are on. From the graph in Figure 5.4 it is observed that the output voltage is zero. This due to that there is no closed circuit involving the voltage source. Due to the inductive property of the load, the load will provide energy to the circuit and there will be no load present in the circuit; it loses its function as a load. Therefore, the output voltage will be zero since there is no voltage drop. The schematic of this circuit is shown in 5.5a. When switch S2 turns off, switch S3 turns on. The circuit changes to the one shown in Figure 5.5b. Switch S3 is the switch to which the phase shift is given to. The phase shift used in this example is 90°, which translates to a time delay of a quarter of the time period. Observing the graph in Figure 5.4, only half of the positive half-cycle is present at the output. This is due to the 90°phase shift given to S3. In this way, the magnitude of the average output voltage can be controlled. Then S1 turns off and S4 turns on, while S3 remains switched on. The schematic of the corresponding circuit is shown in Figure 5.6a. From the graph, it is observed that the output voltage is zero. Like the first mode of conduction, there is no closed circuit involving the voltage source, the load will act as a source due to its inductive property. Therefore, the output voltage will be zero since there is no voltage drop. Then, S3 turns off and the last mode is initiated in which S2 and S4 are both on. The circuit is adjusted to the schematic illustrated in Figure 5.6b. The graph shows that the output voltage is negative and equal in magnitude to the input voltage. Due to the current path the switches have created, the current is flowing through the load in the opposite direction compared to the mode when S1 and S3 were on. Therefore, the output voltage for this mode will have a negative polarity. After this mode, S4 turns off and S1 turns on and the cycle discussed above will repeat itself[38].

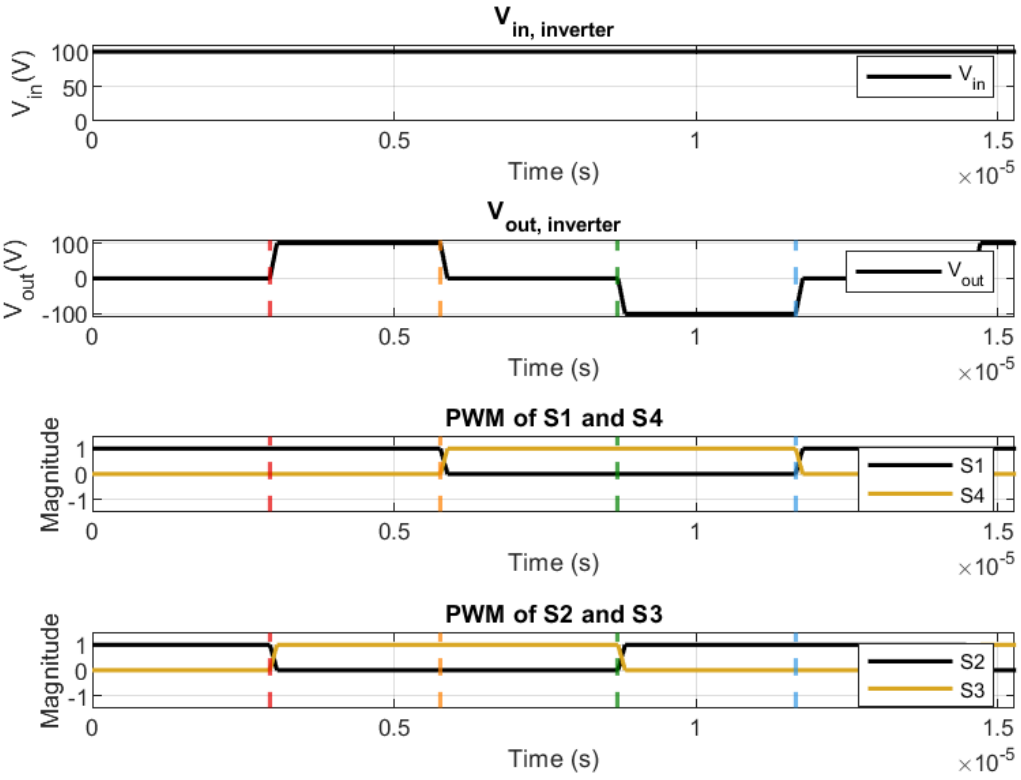


**Figure 5.4:** Inverter output voltage and switching signals when using a phase shift of 90°.

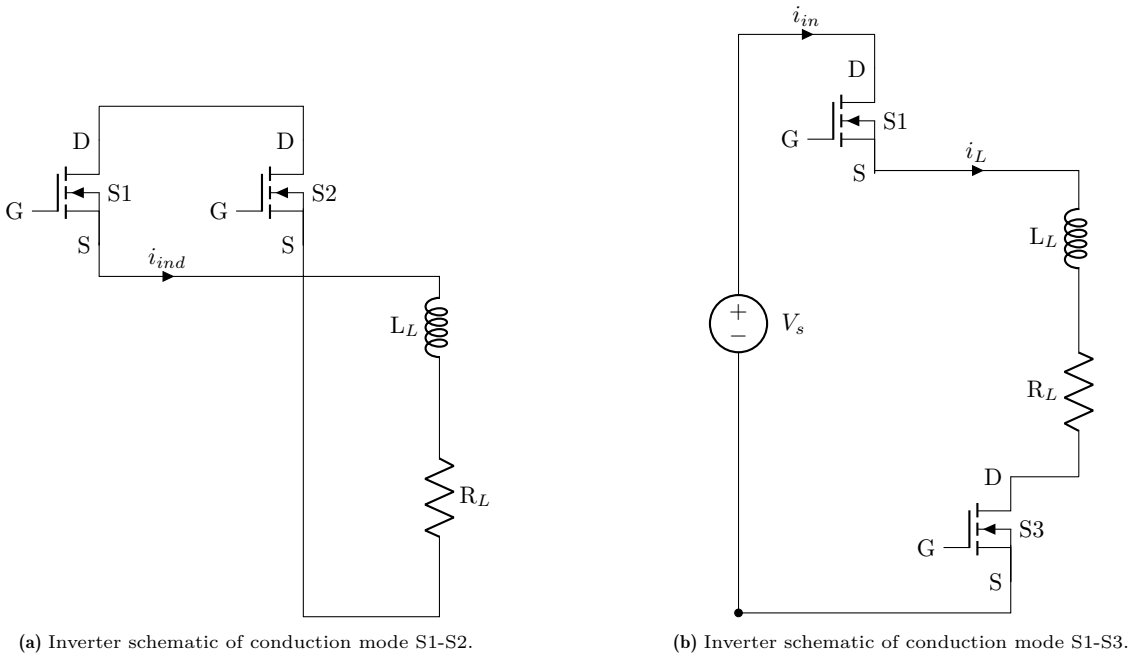


**(a)** Inverter schematic of conduction mode S1-S2.

**(b)** Inverter schematic of conduction mode S1-S3.

**Figure 5.5:** Schematics of the inverter conduction modes when using PSM.

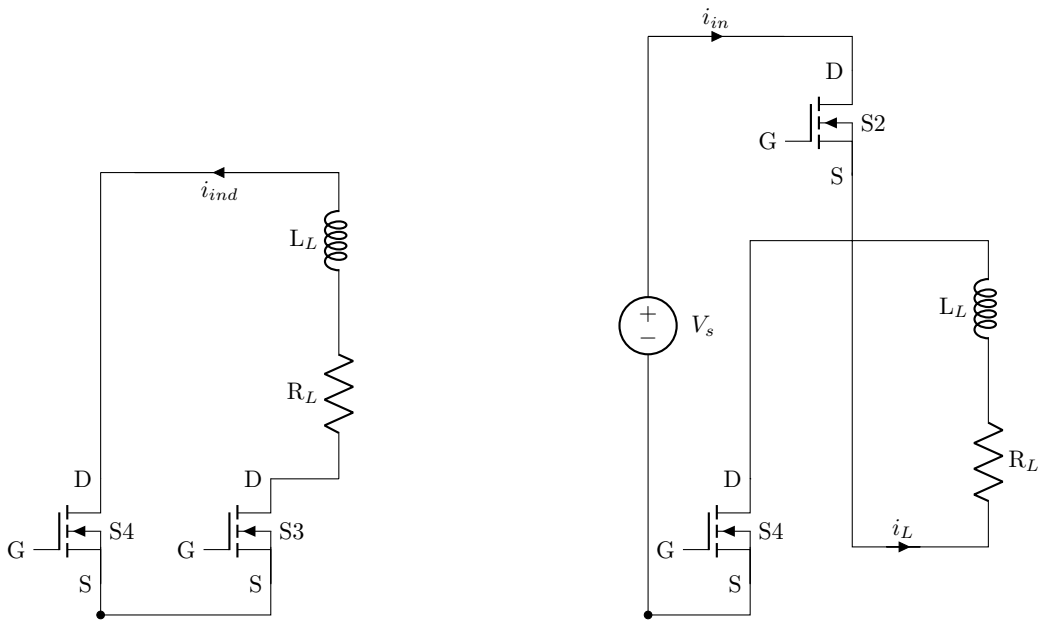


**(a)** Inverter schematic of conduction mode S3-S4.

**(b)** Inverter schematic of conduction mode S2-S4.

**Figure 5.6:** Schematics of the inverter conduction modes when using PSM.

The phase shift in both the inverter and active rectifier will be determined by the PI output signal. The PI output signal will undergo modulation to make it suitable as a switching signal. The modulation strategy for the inverter as well for the active rectifier are different. In the following two sections this strategies will be introduced.

## 5.4 Control Signal Modulation for Inverter

Like mentioned above, the PI output signal will determine the delay of the switching signals S2 and S3. The base signal used for the switches is a square wave with a frequency of 85 kHz, which translates to a time period of 11.765 µs. The PI output will have a much larger order of magnitude. If this raw signal is used, switch S2 will remain on since the delay given to switch S3 will be much longer than the time period. Which means that it keeps delaying it with a time value larger than the time period. To solve this issue, the PI output signal needs to be a value in the time period of the circuit. Therefore, first a saturation block will be used to keep the PI output between zero and one, and then the signal is multiplied to 11.765 µs. However, due to that the output signal can hold a value for a maximum time duration of half the time period, the maximum amount of delay that can be given will be half of the time period. Which means that the PI output signal will be multiplied by half of the time period; 0.5·11.765. In Figure 5.7, the block diagram of this modulation is illustrated.

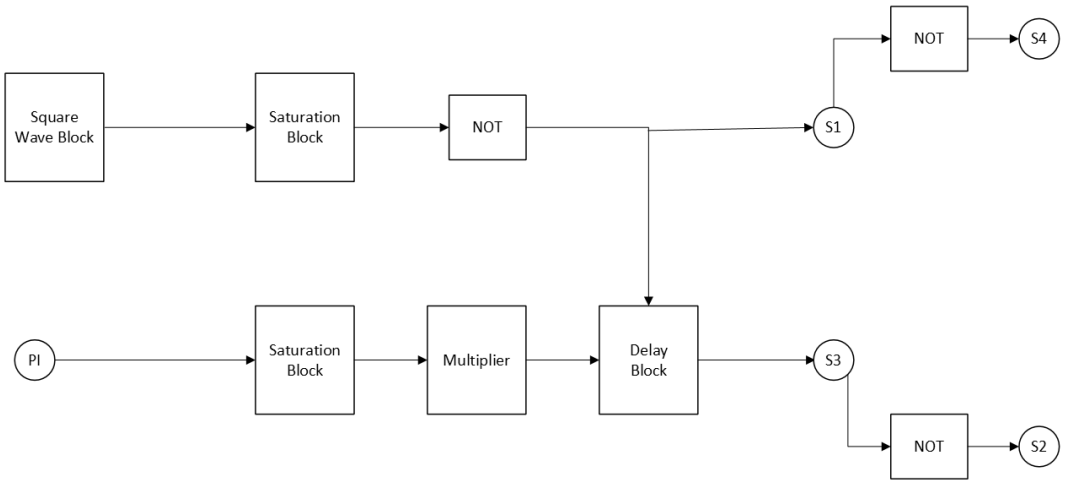


**Figure 5.7:** Block diagram of the modulation used for the switching signals of the inverter switches.

## 5.5 Control Signal Modulation for Active Rectifier

For the modulation of the active rectifier, the input current and input voltage of the rectifier, which are the output of the DLCC circuit, should be in phase. To do so, a square wave is used as the base signal for the switches. This square wave should be in phase with the input current of the active rectifier. To achieve this a sign detection block is used which will output a positive one or a negative one, alternately, whenever the AC current crosses zero. However, during the simulation the phase difference between the square wave and input current changes. Therefore, it needs be tuned. Furthermore, the PSM should be applied to achieve an output voltage of interest. To keep the input current and output voltage in phase and obtain a desired output voltage, a closed loop feedback is used with PI controller. The PI output signal is used to determine the duty cycle. From this two angles, $\alpha$ and $\beta$, will be determined. $\alpha$ will be used to phase shift the switching signal of S2 to achieve the desired output voltage. $\beta$ will be used to phase shift the square wave to keep the input current and input voltage of the active rectifier in phase. The angles will be determined by the following two equations:

$$\alpha = d * 180 \tag{5.2}$$

$$\beta = 90 - d * 90 \tag{5.3}$$

Where:

- $d$ is the duty cycle

This angles are converted to time by using the following equation:

$$t = \frac{\theta}{360} * T \tag{5.4}$$

Where:

- $t$ is time in seconds
- $\theta$ is the angle($\alpha$ or $\beta$) in degrees
- $T$ is the switching time period in seconds

Due to the delays in the switching signal the output voltage showed spikes. These delays were caused by the ramp up of the signal. To solve this issue, each signal passes through an AND gate in which it only let the signal pass if the switching signal is one. The modulation diagram is shown in Figure 5.8.

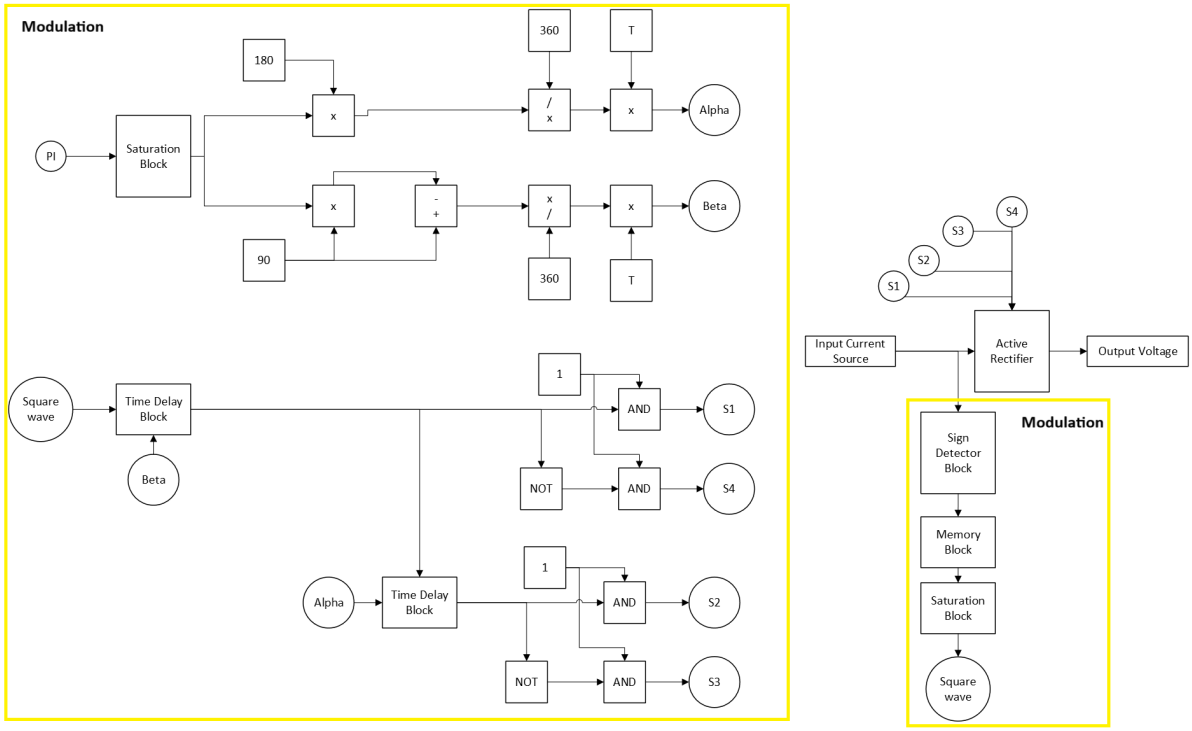


**Figure 5.8:** Modulation diagram used for the switching signals of the active rectifier switches.

# 6

# Simulink Model Design

This chapter is dedicated to the design of the DWC system using either the buck converter, the inverter or the active rectifier for power stabilization, and the construction of it in MATLAB Simulink. First, the necessary parts are constructed and verified for their proper functioning, and then the parts are combined to form the complete system. The parts being designed or/and constructed are: SS compensation and DLCC compensation circuit in static and dynamic mode, buck converter, rectifier, inverter, active rectifier, modulation and control. In addition, a comparison between SS compensation and DLCC compensation will be provided.

## 6.1 SS Compensation Circuit: Static Model

In this section, the SS compensation circuit is build in Simulink. The simulation results are compared to the analytically obtained results to verify the correctness of the Simulink model.

In Figure 6.1, the schematic of the static SS compensation circuit is illustrated. The value of the components used in this model, which are listed in Table 6.1, are obtained from the book *Dynamic Wireless Charging of Electric Vehicles* by Dr. W. Shi[18]. Since the main purpose of this thesis is to determine which power stabilization method is relatively the best, for the sake of time, and since these values are proven to be suitable for such circuit, the same values are used. The values of $\omega_s$, $C_1$ and $C_2$ were determined using the formula displayed in the table in order to achieve a high level of accuracy. The approximate values are included in the table as well.

**Table 6.1:** Electrical component values used for SS compensation circuit.

| Parameter | Value | Unit |
|---|---|---|
| $U_{AB}$ | 800 | V |
| $f_s$ | 85 | kHz |
| $\omega_s$ | $2\pi f_s$=53 | Mrad/s |
| $L_1$ | 292.77 | µH |
| $L_2$ | 199.18 | µH |
| $M$ | 17.21 | µH |
| $C_1$ | $\frac{1}{\omega_s^2 L_1} = 12$ | nF |
| $C_2$ | $\frac{1}{\omega_s^2 L_2} = 17.6$ | nF |
| $R_1$ | 0.1 | Ω |
| $R_2$ | 0.7 | Ω |
| $R_L$ | 8.6 | Ω |

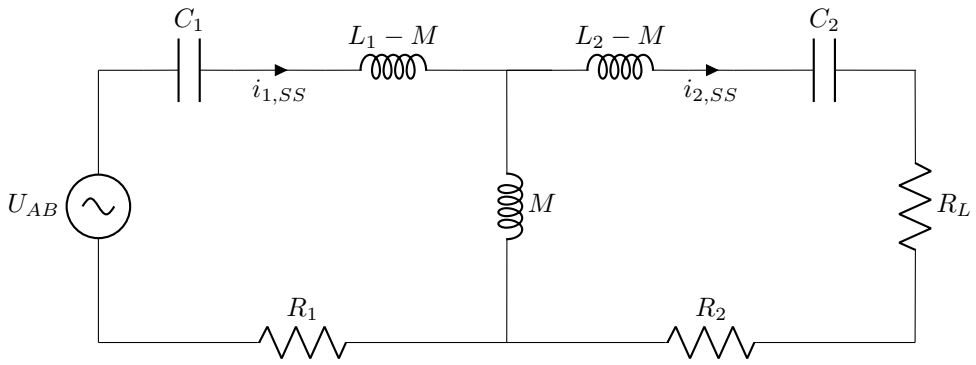


**Figure 6.1:** SS compensation circuit constructed in Simulink.

After constructing the model in Simulink, a simulation was run to analyze the behavior of the SS compensation circuit. The values for the primary winding current($I_1$) and secondary winding current($I_2$), which the latter is also the output current, were extracted from the Simulink model by using the "To Workspace" block from the Simulink library. These data were processed and plotted in MATLAB script. The plots are shown in Figure 6.2.

These graphs indicate that the peak value of $I_1$ and the peak value of $I_2$ is around 87 A and 86 A, respectively. To validate these results and eventually the constructed SS compensation circuit, the value of $I_1$ and $I_2$, readout from the graph, are compared with analytically derived values of $I_1$ and $I_2$, which are computed to be 87.1 A and 86.1 A, respectively. This validation step confirms that the SS compensation circuit model constructed in Simulink is correct.

The MATLAB code used to generate the plots are provided in Appendix A.1. To analytically determine $I_1$ and $I_2$, the final equations of Equation series 3.8 and 3.9, were used. These equations are also coded in MATLAB script. The relevant code is included in Appendix A.2.

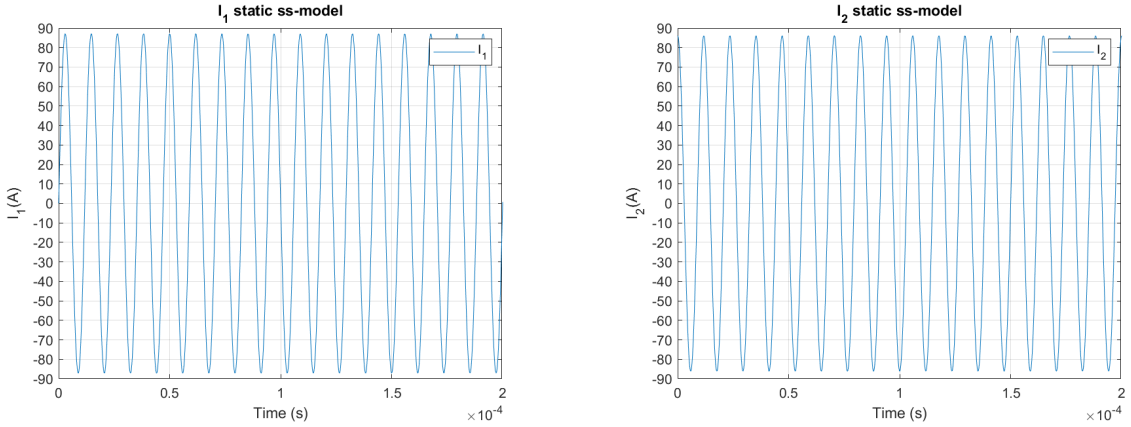


**(a)** $I_1$ from static SS compensation circuit.

**(b)** $I_2$ from static SS compensation circuit.

**Figure 6.2:** $I_1$ and $I_2$ from Simulink SS compensation circuit model.

## 6.2 DLCC Compensation Circuit: Static Model

In this section, the DLCC compensation circuit is constructed in Simulink and then in order to verify the correctness of it, the results obtained from the simulation are compared to the analytically computed values.

The values of the electrical components used for the DLCC compensation circuit are listed in Table 6.2. Like, the SS compensation circuit, the values are obtained from the book *Dynamic Wireless Charging of Electric Vehicles*[18].
The constructed DLCC compensation circuit is shown in Figure 6.3.

**Table 6.2:** Electrical component values used for DLCC compensation circuit.

| Parameter | Value | Unit |
|---|---|---|
| $U_{AB}$ | 800 | V |
| $f_s$ | 85 | kHz |
| $\omega_s$ | $2\pi f_s$=53 | rad/s |
| $L_1$ | 200.7 | µH |
| $L_2$ | 203.5 | µH |
| $M$ | 30 | µH |
| $L_{f1}$ | 66.39 | µH |
| $L_{f2}$ | 68.97 | µH |
| $C_{s1}$ | $\frac{1}{\omega_s^2(L_1-L_{f1})} = 26.10$ | nF |
| $C_{s2}$ | $\frac{1}{\omega_s^2(L_2-L_{f2})} = 21.06$ | nF |
| $C_{f1}$ | $\frac{1}{\omega_s^2 L_{f1}} = 52.8$ | nF |
| $C_{f2}$ | $\frac{1}{\omega_s^2 L_{f2}} = 50.8$ | nF |
| $R_L$ | 123 | Ω |

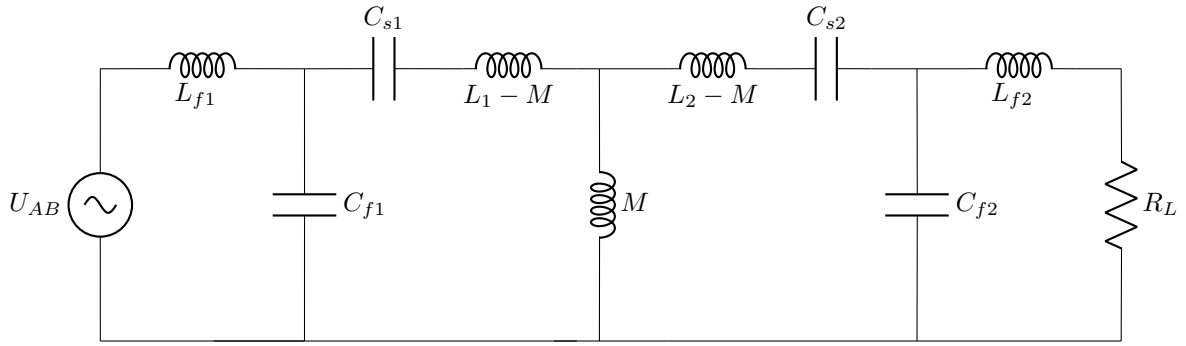


**Figure 6.3:** DLCC compensation circuit constructed in Simulink.

After the DLCC compensation circuit was constructed and simulated, the values of the primary winding current($I_{1,DLCC}$), the secondary winding current($I_{2,DLCC}$) and the output current($I_{out}$) were analyzed by making three individual plots for each of these currents. The plots are shown in Figure 6.4a, Figure 6.4b and Figure 6.5.

It can be observed from these graphs that $I_{1,DLCC}$, $I_{2,DLCC}$ and ($I_{out}$) reach their peak value around 22 A, 32 A and 9.8 A, respectively. To verify these results, these values were compared to those values that were obtained by analytical calculations. The analytical derived values for $I_{1,DLCC}$, the $I_{2,DLCC}$ and $I_{out}$ are 22.5 A, 32.7 A and 9.8 A, respectively. The closeness of the derived value by these two methods confirms that the DLCC compensation circuit in Simulink is correctly constructed.

The simulation data used to generate these current plots were exported from the Simulink model by using the "To Workspace" block. Then in MATLAB script the data were processed and the plots were generated. The MATLAB code to generate the plots can be found in Appendix A.3. To compute the analytical current values, Equation 3.14, Equation 3.17 and Equation 3.18 were used to determine $I_{out}$, $I_{2,DLCC}$ and $I_{1,DLCC}$, respectively. These equation were coded in MATLAB Script and can be found

in Appendix A.4.

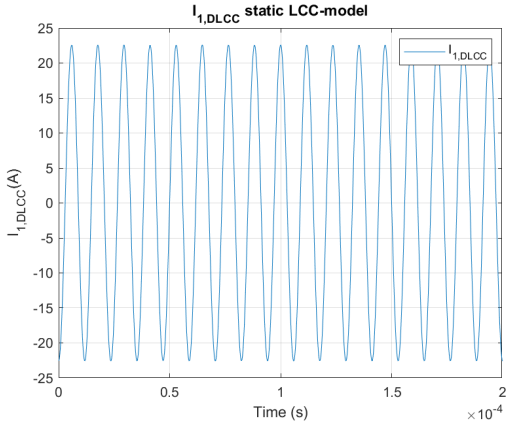


**(a)** $I_{1,DLCC}$ from static DLCC compensation circuit.

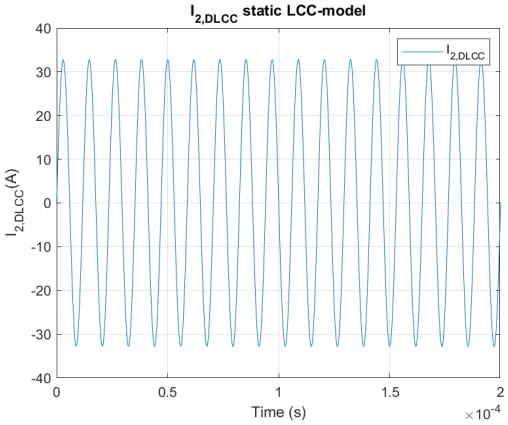


**(b)** $I_{2,DLCC}$ from static DLCC compensation circuit.

**Figure 6.4:** $I_{1,DLCC}$ and $I_{2,DLCC}$ from Simulink DLCC compensation circuit model.

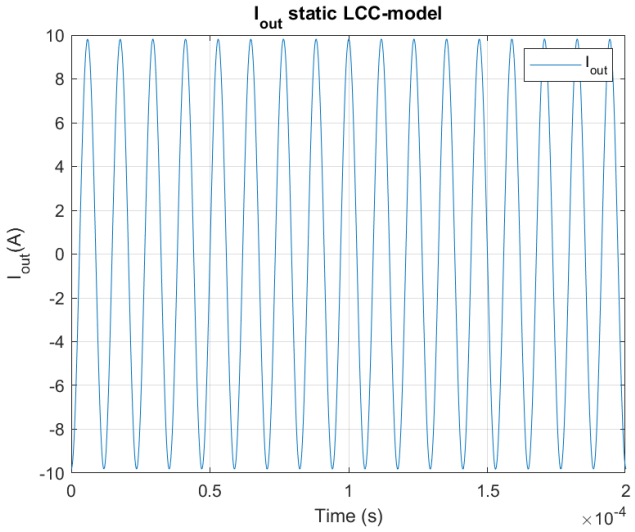


**Figure 6.5:** $I_{out}$ from Simulink DLCC compensation circuit model.

## 6.3 Comparison Between DLCC Compensation and SS Compensation Circuit

In this section, a comparison between DLCC compensation and SS compensation circuit is made to determine which topology is better suited for the implemention of DWPT. The objective is to select a topology that maintains stable performance despite the variation in mutual inductance during dynamic operation.

For the comparison between these two topologies, the equations that were derived for the primary winding current of both topologies, which are shown in Equations 6.1 and 6.2 are used. It can be observed that in the SS compensation topology, the primary winding current($I_{1,SS}$) is inversely proportional to the square of the mutual inductance. As a result, when the mutual inductance decreases to zero or approaches zero, the winding current will be enormous. Such a high current will cause damage to the inductor through which it flows. In DWPT the mutual inductance will vary due to the relative movement between the primary side and the secondary side sub-circuit. There will be moments in which the mutual inductance will approach zero. In contrast, the primary winding current of the DLCC compensation circuit is independent of the mutual inductance. Therefore, the DLCC compensation circuit is more suitable to be used in DWC systems. Hereby, the sub-research question which is "Which circuit, SS compensation or DLCC compensation circuit, should be used for DWPT" is answered.

$$I_{1,DLCC} = \frac{U_{AB}}{j\omega_s L_{f1}} \tag{6.1}$$

$$I_{1,SS} = \frac{U_{AB} R_L}{j\omega_s^2 M^2} \tag{6.2}$$

## 6.4 Dynamic DLCC Compensation

As discussed previously, during charging, the mutual inductance between the primary and secondary coils will not be constant when the vehicle is in motion. A dynamic mutual inductance has to be considered to account for the variations in the mutual inductance. In this section, the dynamic DLCC compensation circuit will be constructed in Simulink that considers the effects of the variations in coil alignment. To validate the correctness of the constructed model an analytical model is coded in MATLAB script in which the primary and secondary winding currents as well the output current are compared. This will ensure the correctness of the model constructed in Simulink.

As stated previously, due to the movement of the vehicle, the transmitting coil on the primary side and the receiving coil on the secondary side will not be optimally aligned during the entire journey. The magnitude of mutual inductance depends on the distance of the receiver coil with respect to the transmitting coil. When the distance of the vehicle with respect to the transmitting coil, embedded in the road, will decrease, the mutual inductance will decrease. Vice versa, when the vehicle approaches the next transmitting coil the absolute of the mutual inductance will increase. To model this dynamic nature in Simulink, the inductor M in Figure 6.3 was replaced by a variable inductor to represent the mutual inductance. The mutual inductance will be a sinusoid that will vary from zero to 30 µH in magnitude with a frequency of 10 Hz.

A comparative analysis was conducted between the simulation results and the analytically derived values for $I_{2,DLCC}$ and $I_{out}$ to evaluate the correctness of the dynamic DLCC compensation circuit constructed in Simulink. The values for $I_{2,DLCC}$ and $I_{out}$ were extracted from Simulink to MATLAB script by using the "To Workspace" block, and subsequently these currents were plotted. For the analytical comparison, Equation 3.14 and Equation 3.17 were adapted to account for the dynamic behavior of the mutual inductance. These equations were coded in MATLAB script and the results were plotted. The MATLAB code used for computing these currents and generating the plots of the analytical model is provided in Appendix A.5, and the code for plotting these currents from the Simulink model is given in Appendix A.6. In Figure 6.6, the plots obtained by the Simulink simulation are displayed and the plots obtained from the MATLAB simulation are shown in Figure 6.7. As can be observed, there is a high level of similarity in both the shape and the peak values. In Figure 6.6, the primary current,

$I_{1,DLCC}$, shows at the start higher values compared to the analytically derived $I_{1,DLCC}$. This is due to the transient of the circuit, after the transient duration it has the same value as the analytical one. This close alignment serves as a critical validation step indicating that the dynamic DLCC compensation circuits constructed in Simulink is implemented correctly.

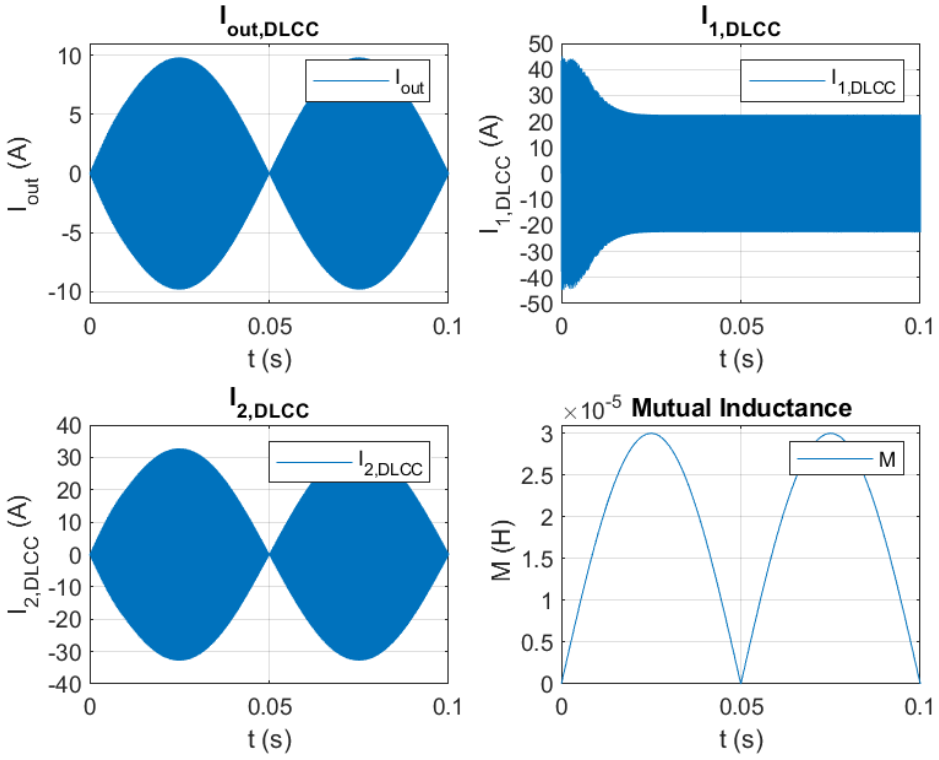


**Figure 6.6:** Plots of $I_{out}$, $I_{1,DLCC}$, $I_{2,DLCC}$ and M from the Simulink model.

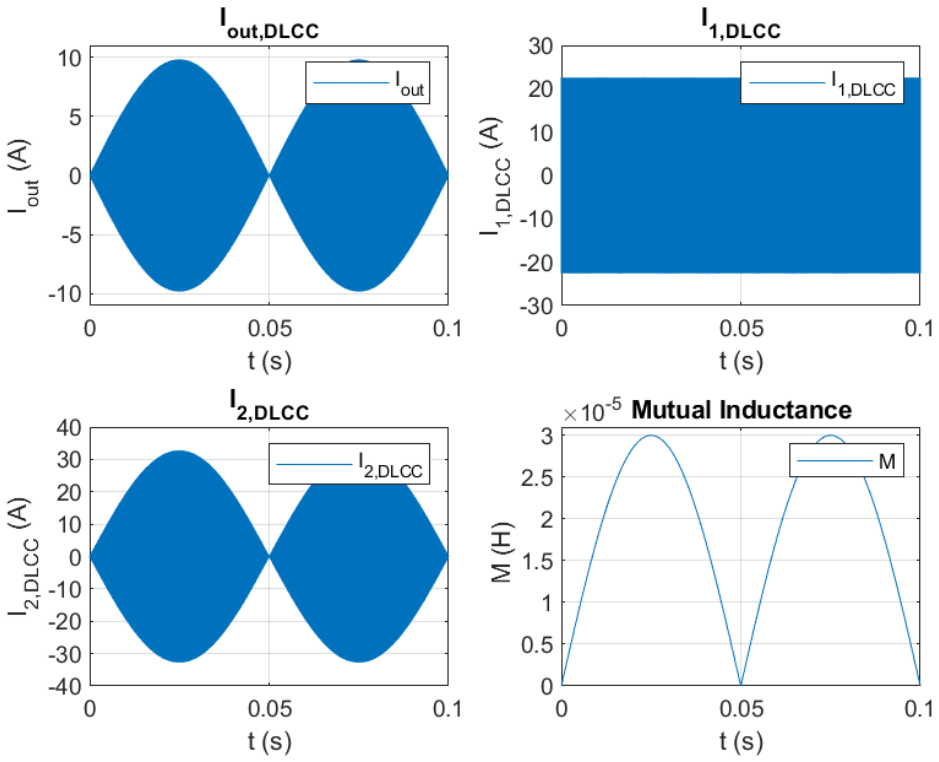


**Figure 6.7:** Plots of $I_{out}$, $I_{1,DLCC}$, $I_{2,DLCC}$ and M from the analytical model.

## 6.5 Rectifier

As previously stated in this report, in order to connect the DLCC compensation circuit with the buck converter, a rectifier has to be inserted between them. This is required because the buck converter needs a DC input voltage to operate while the output of the compensation circuit is an AC voltage. Furthermore, a rectifier is also necessary to convert the AC output voltage of the DLCC circuit to a DC output voltage in the DWC system that includes the inverter circuit. To convert AC to DC a full bridge rectifier is used. This rectifier is capable to convert both the positive and negative halves of the AC waveform into a suitable DC value. The schematic of the full bridge rectifier used is illustrated in Figure 6.8.

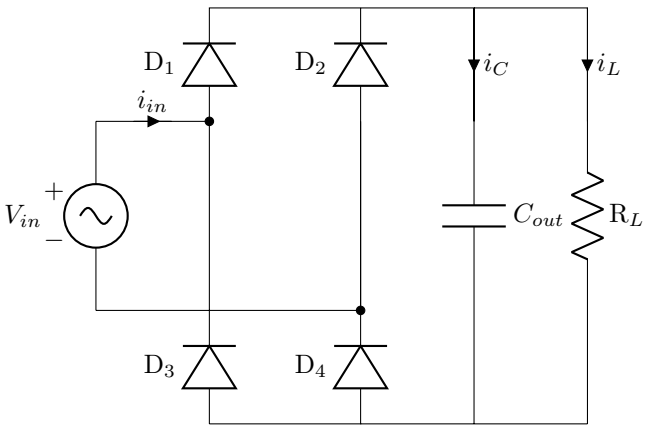


**Figure 6.8:** Schematic of full bridge rectifier.

Before running the simulation, it is necessary to determine the value of the DC-link capacitor($C_{out}$).

This capacitor is responsible for reducing the ripple voltage at the output of the rectifier to a predetermined percentage of the output voltage. The expression used to calculate the value of $C_{out}$ is shown in Equation 6.3. In this equation there are two unknown parameters, which are the output current($I_{out}$) and the allowable ripple voltage at the output($V_{out,ripple}$). The output current could be determined by applying Ohm's Law, $I_{out}$ =$V_{out}$·$R_L$ and an arbitrary output voltage of 100 V is selected to be the output voltage of interest.

Regarding the load of the rectifier($R_L$), the rectifier will eventually be connected to the buck converter which will behave as the load. For now, an arbitrary load value will be selected to make an initial estimation of the proper functioning of the rectifier. However, to stay close to the actual load value of the final system, and since the rectifier used in the inverter based DWC system will be connected to the load of the DWC system, the load value of the final DWC system will be used for $R_L$. Therefore, the value of $R_L$ will be 123 Ω.

Moreover, the expression in Equation 6.3 was simplified to the one shown in Equation 6.4. This simplification is carried out by substituting the expression for $V_{out,ripple}$, which is 0.01$V_{out}$, and Ohm's Law in Equation 6.3. $V_{out}$ will cancel out and as a result the expression shown in Equation 6.4 for $C_{out}$ is formed. Substituting the values in this equation, the capacitance of $C_{out}$ was calculated to be 4.78 µF. Typically, a voltage ripple is allowed that is 1% to 2% of the output voltage[39]. Since a ripple voltage is undesired, it should be as low as possible. Therefore, for the ripple voltage 1% was taken. Hence, 1% of 0.01 V was used in the calculation[40].

$$C_{out} = \frac{I_{out}}{2 \cdot f \cdot V_{ripple}} \tag{6.3}$$

Where:

- $f$ frequency of the voltage(85 kHz)
- $I_{out}$ is current at $R_L$
- $V_{ripple}$ is the ripple voltage

$$C_{out} = \frac{1}{2 \cdot f \cdot 0.01 \cdot R_L} \tag{6.4}$$

Where:

- $R_L$ is the load resistor

The simulation data corresponding to the output voltage of the rectifier was extracted from Simulink and plotted in MATLAB script. The code used for plotting the output voltage can be found in Appendix A.7.

For the input voltage of the rectifier, an arbitrary AC voltage of 100 V was selected. It is expected that a DC voltage of 100 V would be present at the output of the rectifier. However, due to the diode forward voltage, which is 0.8 V per diode, the output voltage would be less than 100 V. In a full bridge rectifier, two diodes are conducting in the same half cycle. Hence, there will be a voltage drop of 1.6 V. Therefore, theoretically speaking, the output voltage will oscillate around 98.4 V. In Figure 6.9, a magnified version of the output voltage is shown. It can be observed that the voltage is indeed a DC voltage, however, it is slightly lower than 98.4 V, namely 98.2 V. This minor deviation from the theoretical value is due to the on-resistance of the diodes and the switch. Nevertheless, the results are consistent with the theoretical expectations and therefore confirm the proper functioning of the full bridge rectifier.

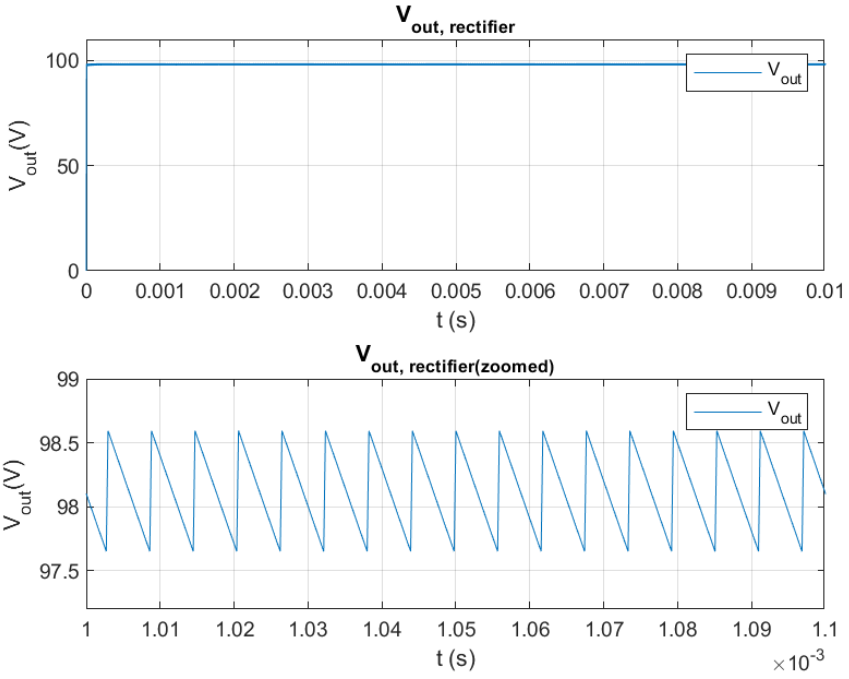


**Figure 6.9:** $V_{out}$ rectifier zoomed and non-zoomed version graphs.

## 6.6 Buck Converter Design

In this section, the buck converter is designed and tested. The test is carried out by extracting the simulation data from Simulink and plotting it in MATLAB script to inspect whether the buck converter functions as expected.

Since there are many unknown variables that have to be determined, Continuous Conduction Mode(CCM) will be used since the equations of this operating mode require less variables to determine the inductance and capacitance. The necessary equations to determine the inductance and capacitance are shown below:

$$
\begin{aligned}
D &= \frac{V_{\text{out}}}{V_{\text{in}}} \\
L &= \frac{(V_{\text{in}} - V_{\text{out}}) \cdot D \cdot T_s}{\Delta I_L} \\
C &= \frac{V_{\text{out}} \cdot (1 - D) \cdot T_s^2}{8 \cdot \Delta V_{\text{out}} \cdot L}
\end{aligned}
\tag{6.5}
$$

Where:

- $D$ is the duty cycle
- $T_s$ is the switching period ($T_s = 1/f_s$)
- $\Delta I_L$ is the inductor ripple current
- $\Delta V_{\text{out}}$ is the output voltage ripple

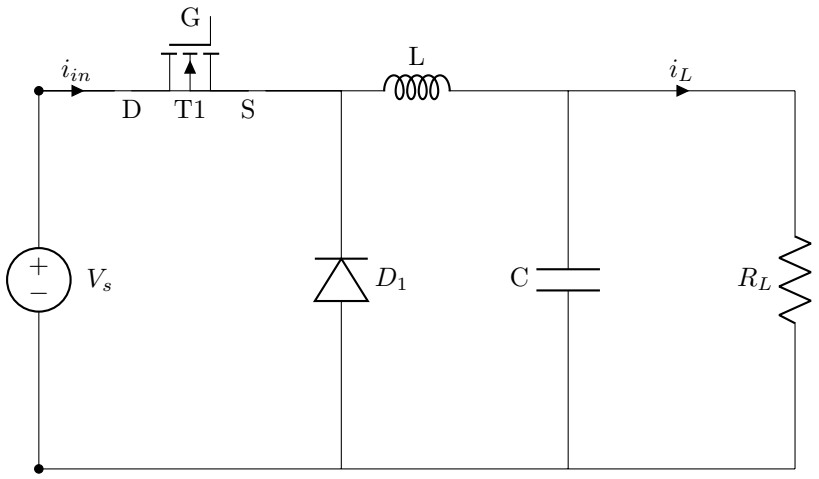


**Figure 6.10:** Schematic of the buck converter.

First, the duty cycle, D, is determined. For now, an arbitrary input and output voltage is selected to be 100 V and 50 V, respectively. This will result in a duty cycle of 0.5. To determine the inductance and capacitance the value of the ripple current and voltage are necessary. According to an application report of Texas instruments about a buck converter, the ripple current should be between 20% and 40%[41]. Like mentioned in Section 6.5, typically a voltage ripple that is 1% to 2% of the output voltage is allowed and it should be as low as possible[39]. Hence, for the ripple voltage 1% is taken and for the ripple current 20% of the output ripple current. To determine the output current, an arbitrary load resistance is taken of 123 Ω, which will also be the load value of the final DWC system at the end. An output voltage of 50 V was selected, by using Ohm's Law, V=I·R, the output current is determined to be 0.4065 A. Taking 20% of it results in a ripple current of 0.0813 A. Substituting all the values in Equation 6.5 results in a capacitance of 0.2033 µF and an inductance of 3.075 mH.

Before the control strategy is designed and implemented, the circuit was simulated to confirm that it functions correctly. Regarding the duty cycle, a PWM generator block is used to provide the duty cycle. This block generates a square wave in which the frequency and duty cycle can be set by the user. The buck converter is then simulated and the output voltage is plotted. It is expected that the output voltage is 50 V since the input is 100 V and the duty cycle is 50%. In Figure 6.11, the plot of the output voltage is shown. It can be observed that the voltage ripple is within 1% of the output voltage. Furthermore, the output voltage is slightly below 50 V namely around 49.6 V. This slight deviation from the expected value is due to the on-resistance of the diode and switch in the circuit. However, this slight deviation does not hold back that the circuit is not functioning properly. Hence, it is confirmed that the circuit is correct. For plotting the graphs, the same code was used as in Appendix A.7. Only the parameters were changed. A small but important note to take is, due to that the switching period was not a multiple of the fixed-step size, 0.1176 µs, an error was given by Simulink. To solve this issue the step size was decreased by a factor of 10 to 0.01176 µs.

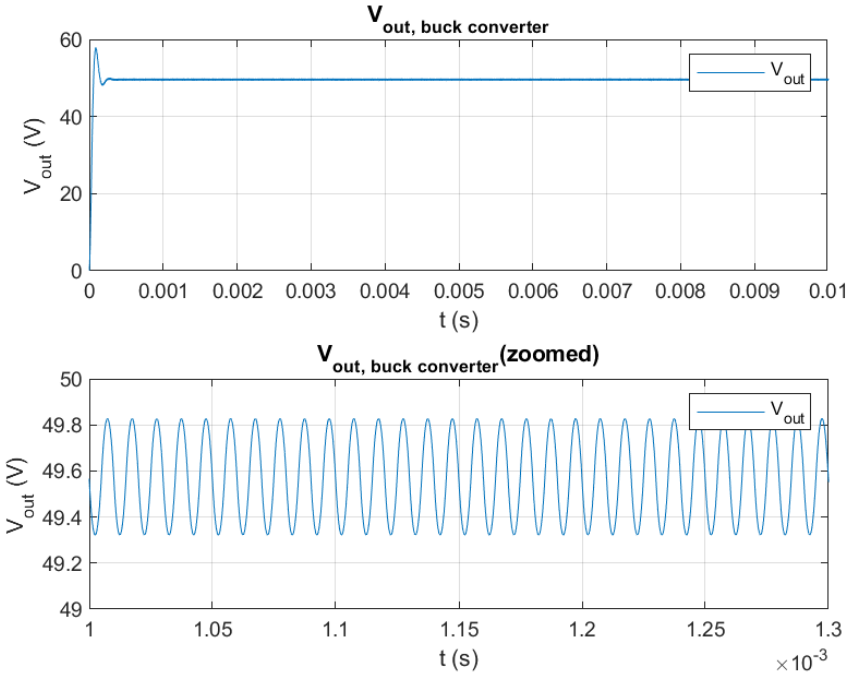


**Figure 6.11:** $V_{out}$ of the buck converter using fixed input and open loop feedback.

## 6.7 Control Design Buck Converter

The PI controller and modulation discussed in Section 5.2 is constructed in Simulink. After constructing it, it was integrated with the buck converter circuit. The block diagram of the buck converter with its control and modulation implemented in it is shown in Figure 6.12. To evaluate the functionality of the PI controller, the system was first tested by using a constant DC voltage source of 100 V as input with a reference voltage set at 50 V. After applying the tuning method described in Section 5.1, a stable output of around 50 V was achieved for Kp=1000 and Ki=1. As can be seen in Figure 6.13 the output voltage is 50 V and the ripple is less than 0.5 V which is lower than 1% of the desired output voltage. It is concluded that the buck converter with PI control functions properly.

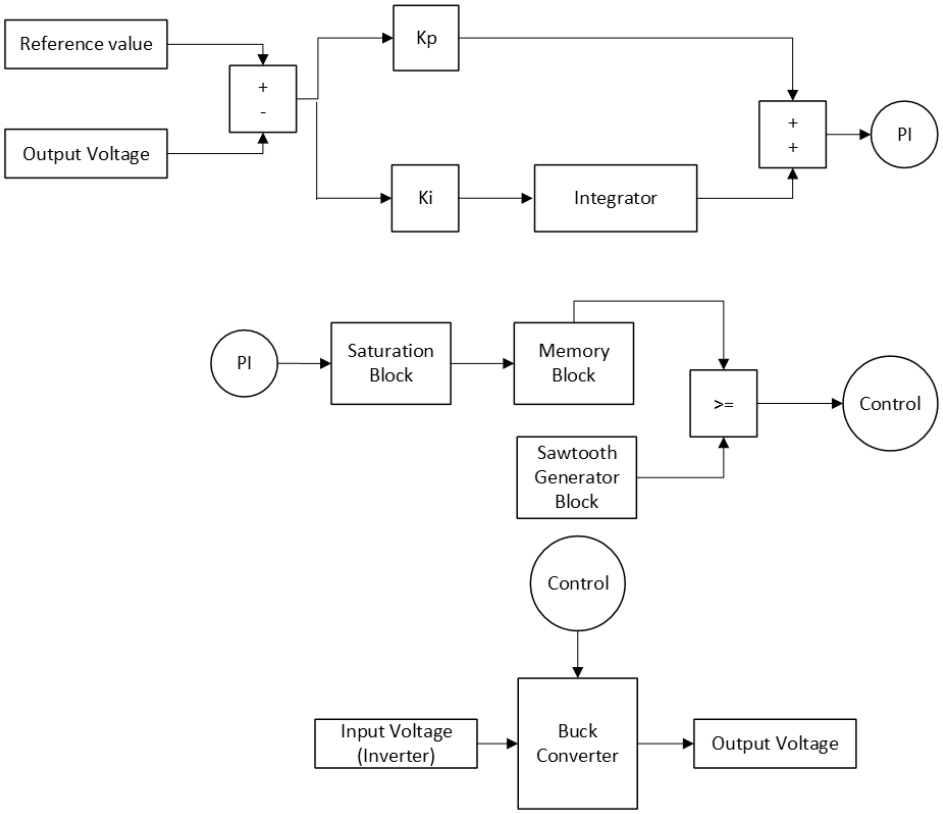


**Figure 6.12:** Block diagram of buck converter with its control and modulation.

The input voltage used is not dynamic. However, the circuit will be used in a dynamic environment and hence it is necessary to asses the performance of the PI control under dynamic conditions. To mimic a basic dynamic environment for the PI controller, the constant voltage reference was replaced by a step-function block. The functionality of this block is that it is given an initial and final value. After a pre-defined time, set by the user, the initial value will step up/down to the final value, thereby mimicking a changing system. The step-function for this test was configured to an initial value set to 40 V and the final value was set to 60 V. The controller's ability to cope with this dynamic reference was analyzed by inspecting the output voltage of the buck converter. As displayed in Figure 6.14, the PI controller managed to regulate the voltage as requested by the reference and the ripple voltage is within limits. The ripple voltage was less than 0.6 V when a reference of 60 V was used and less than 0.4 V when a reference of 40 V was used. These results provide an initial indication that the controller is capable of operating properly under dynamic conditions.

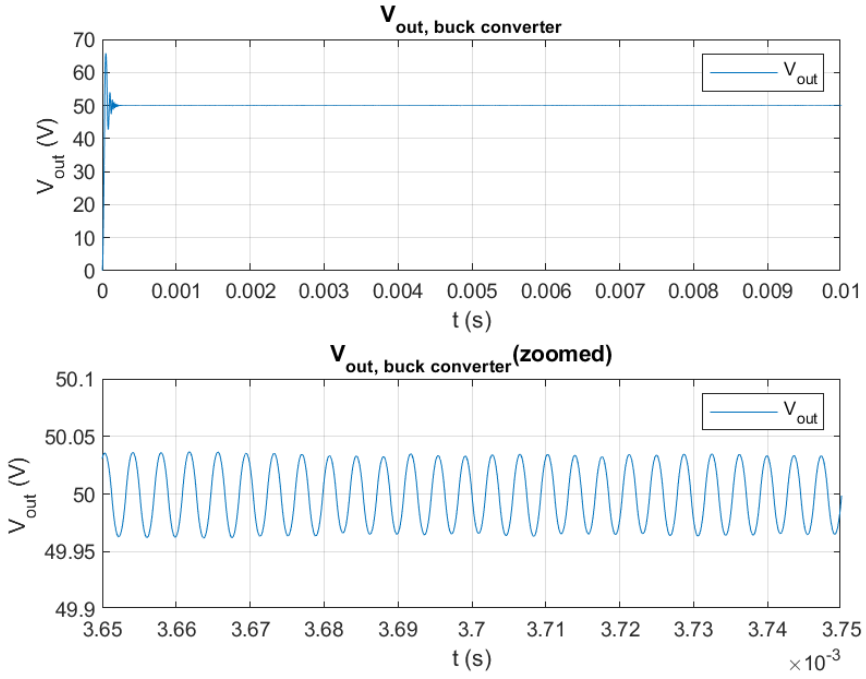


**Figure 6.13:** $V_{out}$ of the buck converter using a constant reference voltage.

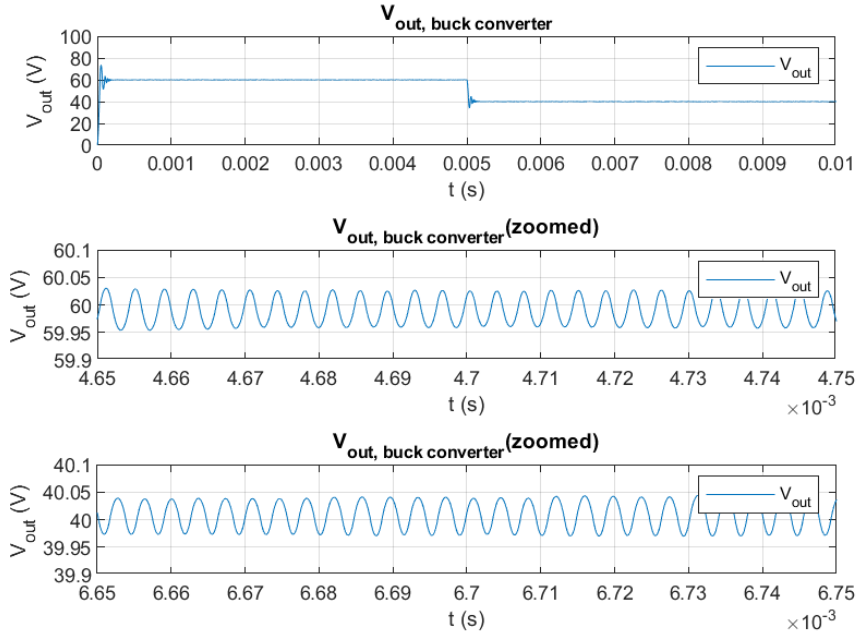


**Figure 6.14:** $V_{out}$ of the buck converter using a step reference.

## 6.8 Inverter Design

In this section the inverter is tested under open loop conditions. After successfully completing the test the inverter will be connected to the DLCC circuit and the buck converter. A diagram of the open loop control is shown in Figure 6.15. Label S1, S2, S3 and S4 represents the output that is connected to the

corresponding switch. Each switch gate is connected to a PWM signal with 50% duty cycle.

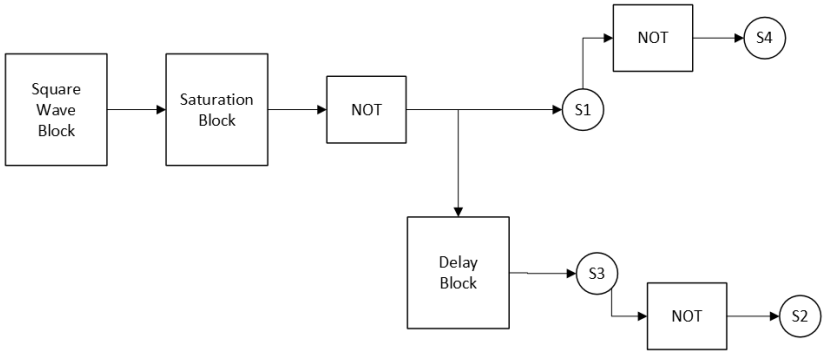


**Figure 6.15:** Block diagram of open loop control of the inverter.

Like mentioned in Section 5.4, a time delay block will be used to implement the phase shift. This block is connected to switch S3 of the inverter circuit illustrated in Figure 6.16.

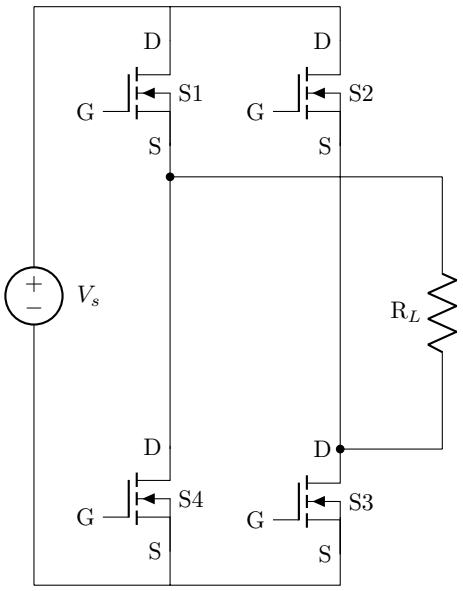


**Figure 6.16:** Schematic of the inverter.

To determine the time delay following equation is used:

$$\text{time delay} = \frac{0.5 \cdot PI}{T} \tag{6.6}$$

Where:

- $PI$ is the output of the PI controller.
- $T$ is the time period.

This expression is formed as follows: the time period has a magnitude of $10^{-6}$ while the output of the PI controller varies between 0 and 1. If the raw PI output is directly applied to the delay block, it will most likely cause the PWM signal of switch S3 to experience a delay for several time periods. To prevent this, the output of the PI controller is normalized by dividing it by the time period T. Furthermore, since the switches are intended to remain on for a maximum of half the time period, the PI output is multiplied by half.

For a PWM signal with 50% duty cycle it is expected that the output voltage would be a square wave in which, during the positive and negative half cycle, half of the duration the magnitude is zero and the other half is either positive one or negative one. In Figure 6.17, it is shown that this is indeed the case. This result verifies the correct functioning of the inverter circuit using open loop feedback.

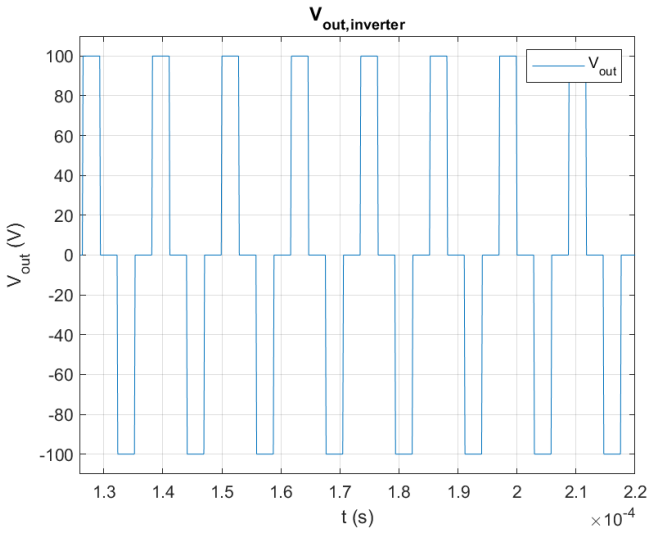


**Figure 6.17:** Output voltage of the inverter using open loop feedback.

The PI along its specific modulation will be implemented to apply closed loop feedback. The closed loop feedback is necessary to achieve a desired output voltage when the mutual inductance is dynamic. A diagram of the DWC system in which the inverter is used to stabilize the power is shown in Figure 6.18. The results of this system are discussed in the next chapter.

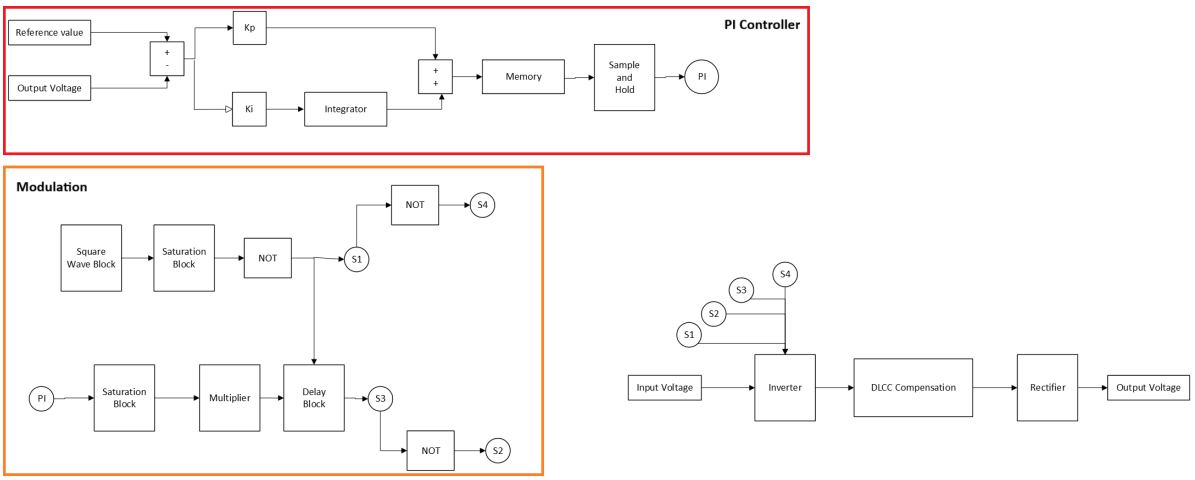


**Figure 6.18:** Block diagram of the DWC system using inverter.

## 6.9 Active Rectifier Design

Before connecting the active rectifier to the DLCC compensation circuit, preliminary testing is conducted to confirm that the active rectifier functions as expected. The block diagram of the active rectifier with its modulation and control is shown in Figure 6.19.

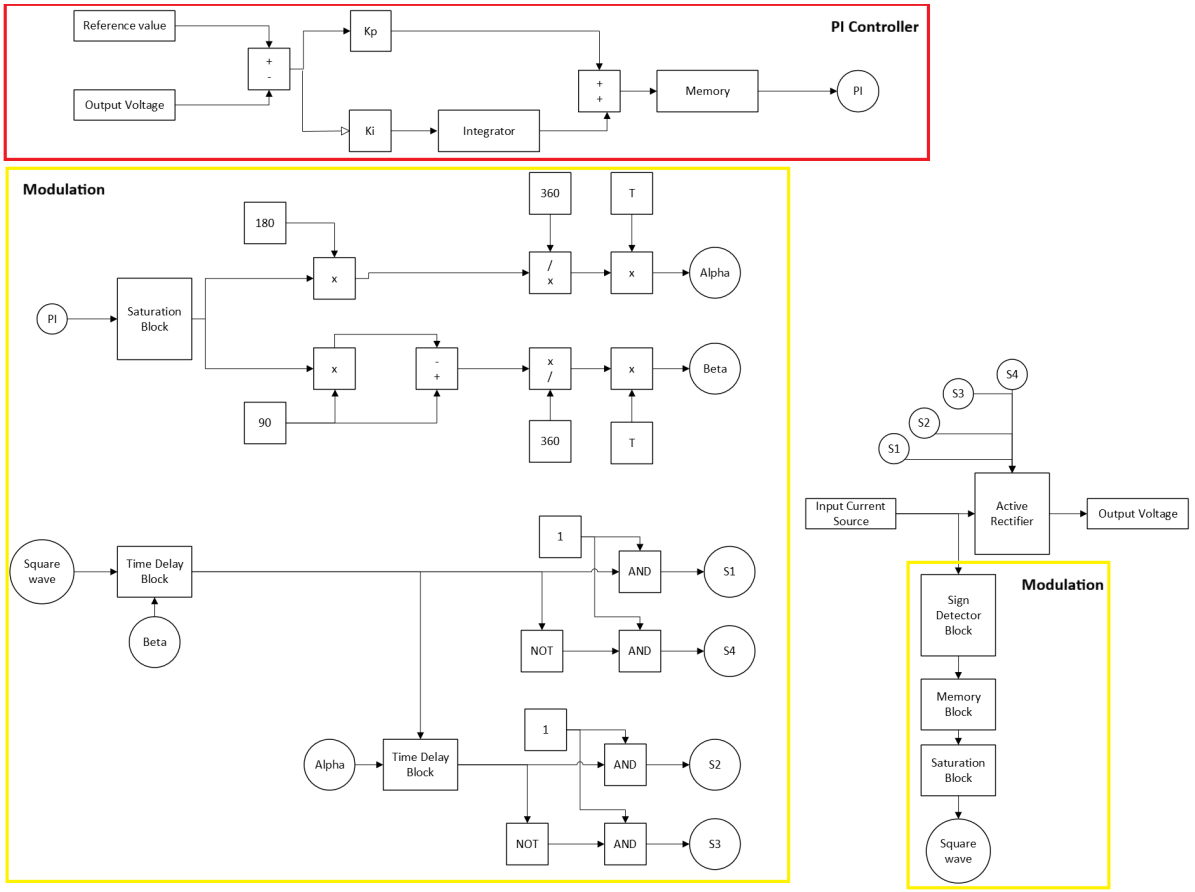


**Figure 6.19:** Block diagram of the active rectifier including its control and modulation.

Three things are checked, namely, correct working of the PSM, whether the input current and input voltage are in phase and the magnitude of the output voltage. Figure 6.20 shows that the output voltage is a constant 100 V DC value as expected. From Figure 6.21, it can be seen that the input voltage and input current are in phase. Regarding the PSM, from Figure 6.22, it is observed that all switching signals have a duty cycle of 50%, switches in the same leg are complement to each other and they have the fundamental frequency of 85 kHz. Hence, it is established that the active rectifier function as desired. The next step is to connect the DLCC compensation circuit to it.
The block diagram of the DWC system using the active rectifier is shown in Figure 6.23, the corresponding results are discussed in Chapter 7.

To have a fair comparison the same DLCC compensation circuit, rectifier, input voltage and load is used in all DWC systems. The output capacitance in all three cases are identical. The output capacitance of the active rectifier, buck converter and the diode rectifier is adjusted to 478 µF. This value was found to be most convenient for all three DWC systems. Furthermore, the input voltage and output voltage of buck converter is not the same as those used in Section 6.6. Therefore, the capacitance of the buck converter had to be adapted. The new value for the capacitance is 478 µF.

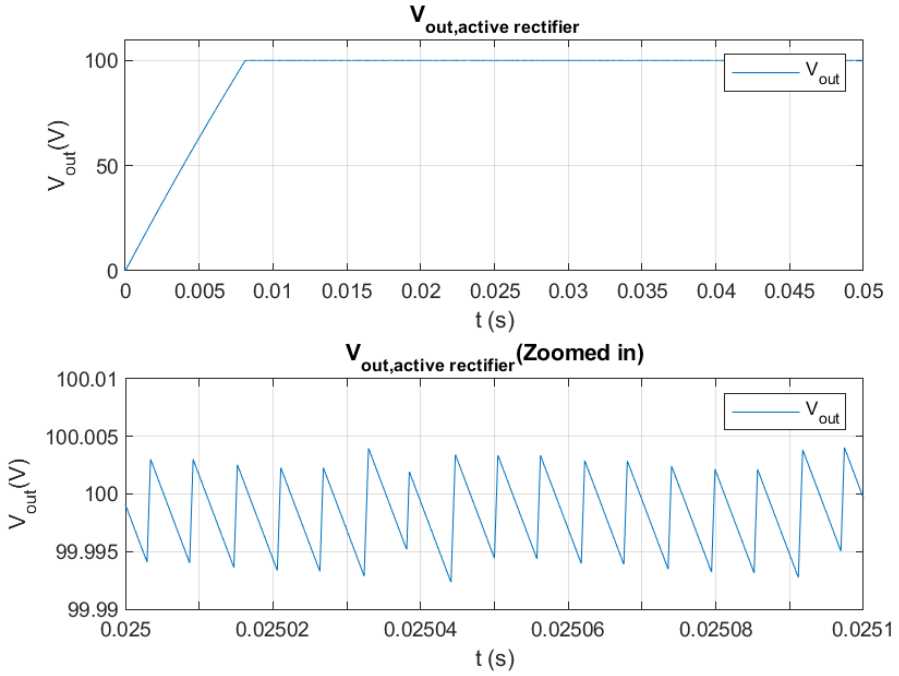


**Figure 6.20:** Output voltage of the active rectifier.

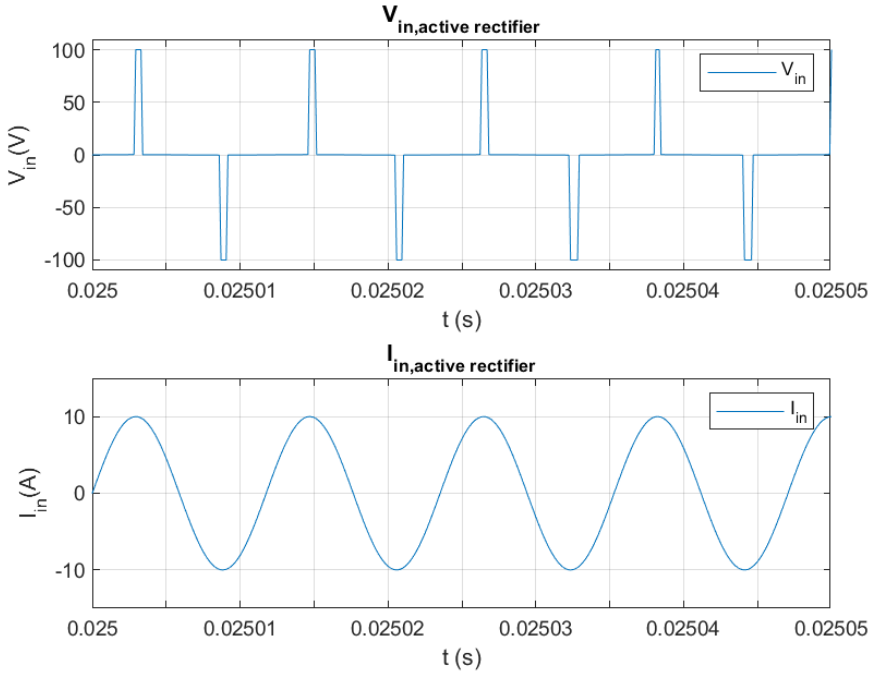


**Figure 6.21:** Input voltage and input current of the active rectifier.

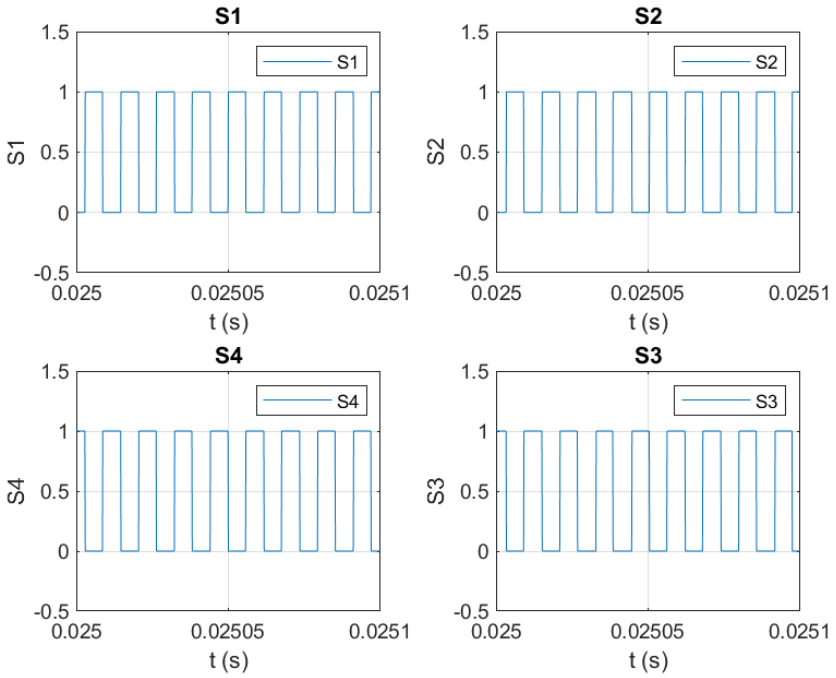


**Figure 6.22:** PWM signals used to control the active rectifier switches.

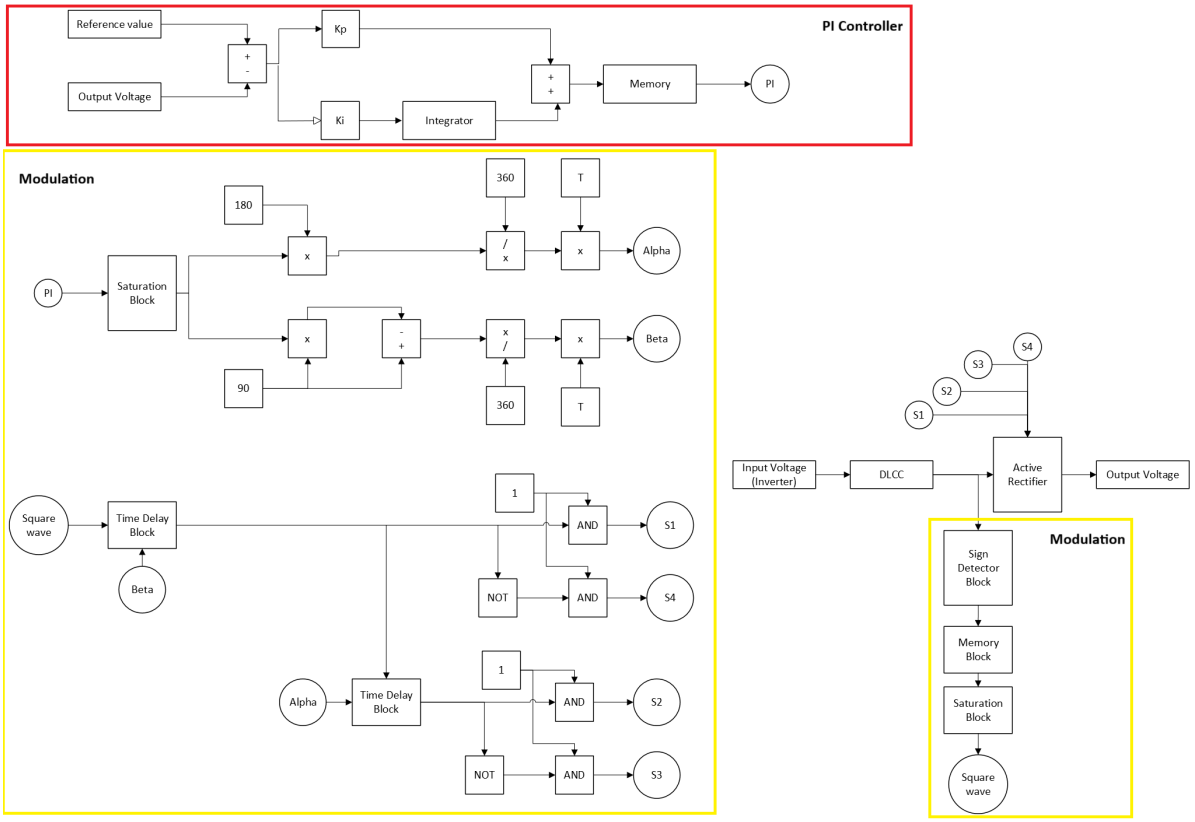


**Figure 6.23:** Diagram of the DWC system using active rectifier.

# 7

# Results

In this chapter, the results of the complete DWC systems will be presented and discussed, and a comparison between the power stabilization methods will be provided based on voltage ripple, start-up time, modulation complexity, space efficiency and voltage regulation.

## 7.1 Inverter

In the previous chapter it was confirmed that the inverter functions correctly. This circuit is connected to the DLCC circuit. When integrated in the DWC system, the PI controller had to be tuned. A stable output was achieved for $K_p$=1 and $K_i$=0.1. To validate the DWC system utilizing the inverter for power stabilization, three aspects are evaluated, the PSM, the output voltage of the inverter and the output voltage of the complete system. Beginning with evaluating the output voltage of the inverter, the input voltage of it is 800 V DC. It is expected that the output voltage is an AC voltage alternating between +800V, 0V and -800V. This is shown in Figure 7.2. This output behavior confirms that the inverter is capable of providing the necessary input for the DLCC compensation circuit. The functionality of the PSM is verified based on the following three criteria: each switching signal should have 50% duty cycle, each signal should have the fundamental frequency of 85 kHz and switches located on the same leg should be complementary. In the inverter circuit, as shown in Figure 4.8, switches S1 and S4 are located on the same leg and S2 and S3 are located on the other leg. Looking at the graphs provided in Figure 7.3, the three mentioned criteria of PSM are satisfied. Moving to the last aspect, Figure 7.1 shows that the output has a DC voltage of approximately 100 V with an average ripple voltage of 0.02 V, which is significantly lower than 1% of the output voltage. A small drop in voltage magnitude can be seen around t=0.05 s. This is due to that the mutual inductance decreases to zero at that time moment.
These results demonstrate that the DWC system that utilizes the inverter to stabilize the output power performs as expected.

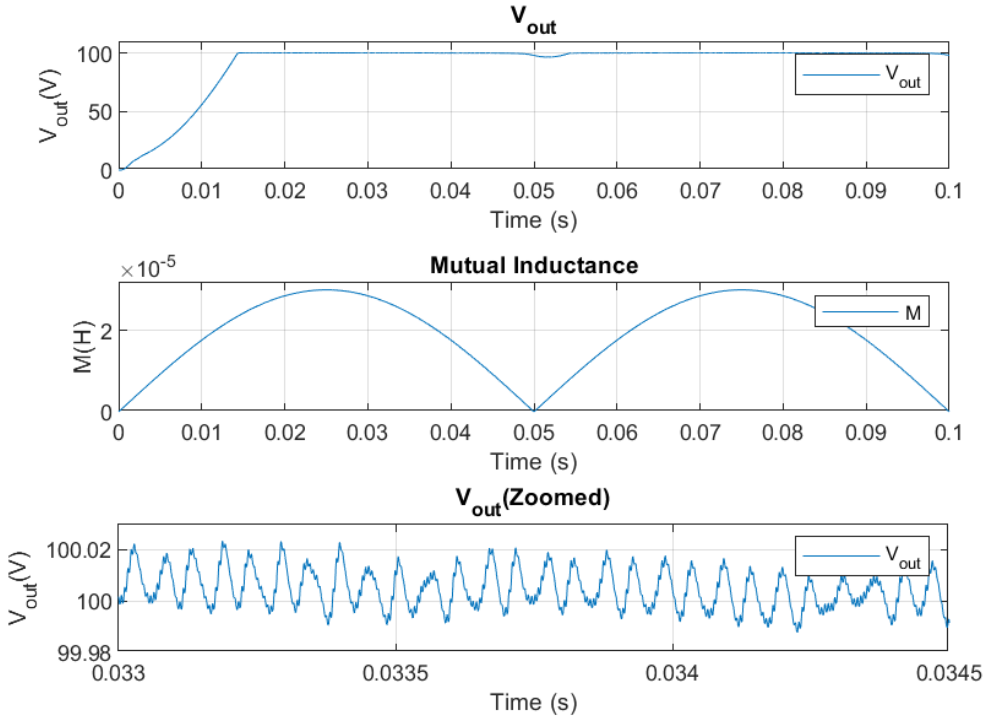


**Figure 7.1:** Output voltage of DWC system using inverter.

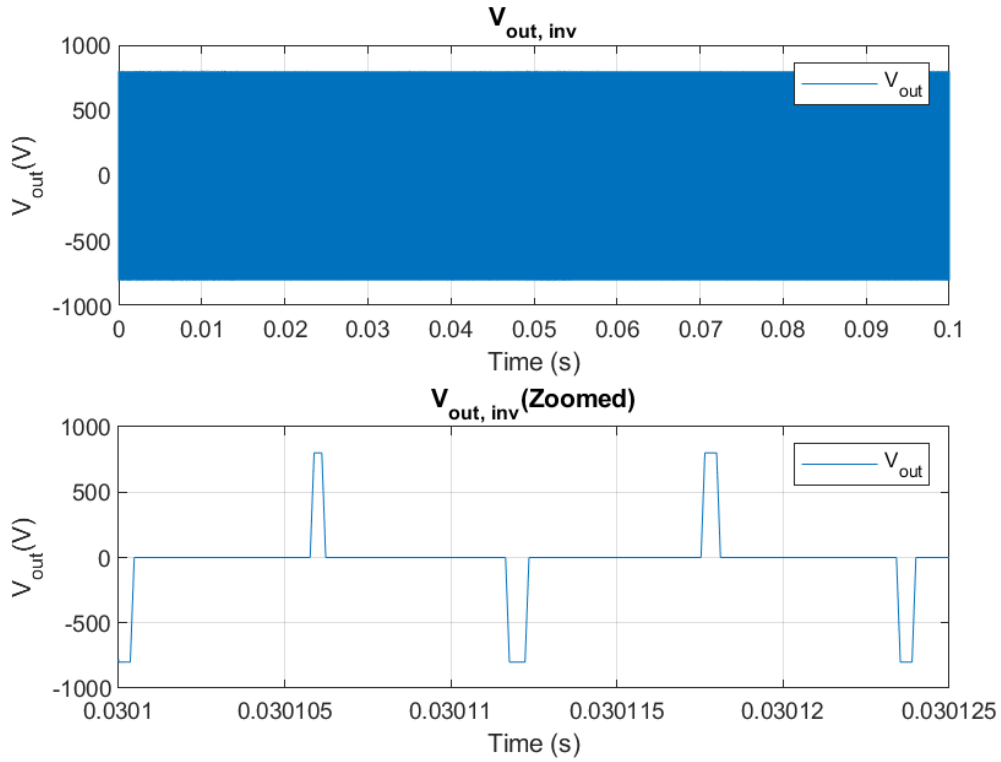


**Figure 7.2:** Output voltage of the inverter.

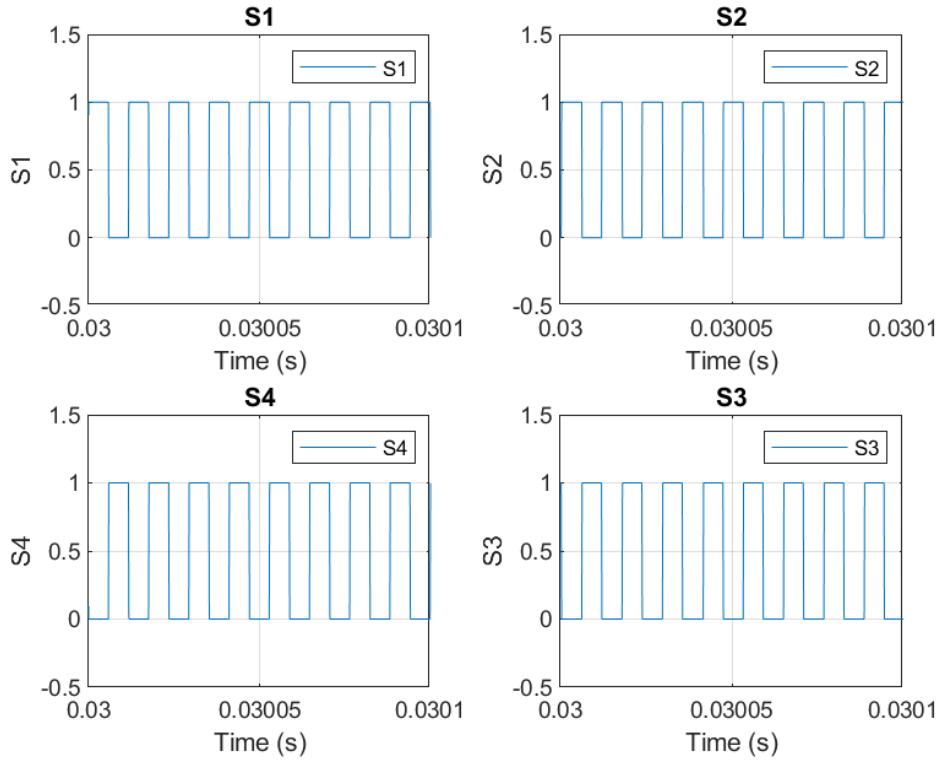


**Figure 7.3:** PWM signals used to control the inverter switches in the DWC system.

## 7.2 Active Rectifier

After confirming that the active rectifier functions properly, it was connected to the DLCC circuit. The PI controller had to be tuned. A stable output was achieved for $K_p$=1.5 and $K_i$=0.12. Three criteria of the active rectifier are examined to confirm its correct operation, namely, a stable output voltage, the PSM fulfilling its three criteria and zero phase difference between the input voltage and the input current of the active rectifier. Before proceeding with the analysis, note that switches S1 and S4 are positioned on the same leg, and S2 and S3 are located on another leg. In Figure 7.4, it is demonstrated that the output voltage is a stable value of 100V with a neglactable deviation of 0.025 V and a ripple voltage of 0.01 V which is 0.01% of the output voltage. Regarding the PSM, observing the graphs in Figure 7.5, all four switching signals operate with a duty cycle of 50%, the switches on the same leg are complementary, and their frequency is 85 kHz. Evaluating the input voltage and input current of the active rectifier, in Figure 7.6 it is shown that this voltage and current are in phase. In Figure 7.7, the non-magnified graphs of the input voltage and input current are shown. It can be observed that for the input current, at the beginning, a voltage spike is present. This is due to the transient. In addition, when the mutual inductance decreases to zero a small spike is shown again, however, as shown in Figure 7.4, it does not impact the stability of the output voltage. A decrease in output voltage is shown near 0.05 s, this is because the mutual inductance reaches zero at 0.05 s. More on this will be explained in Subsection 7.4.2. To conclude, these results confirm that the performance of the DWC system utilizing the active rectifier to stabilize the output power is as intended.

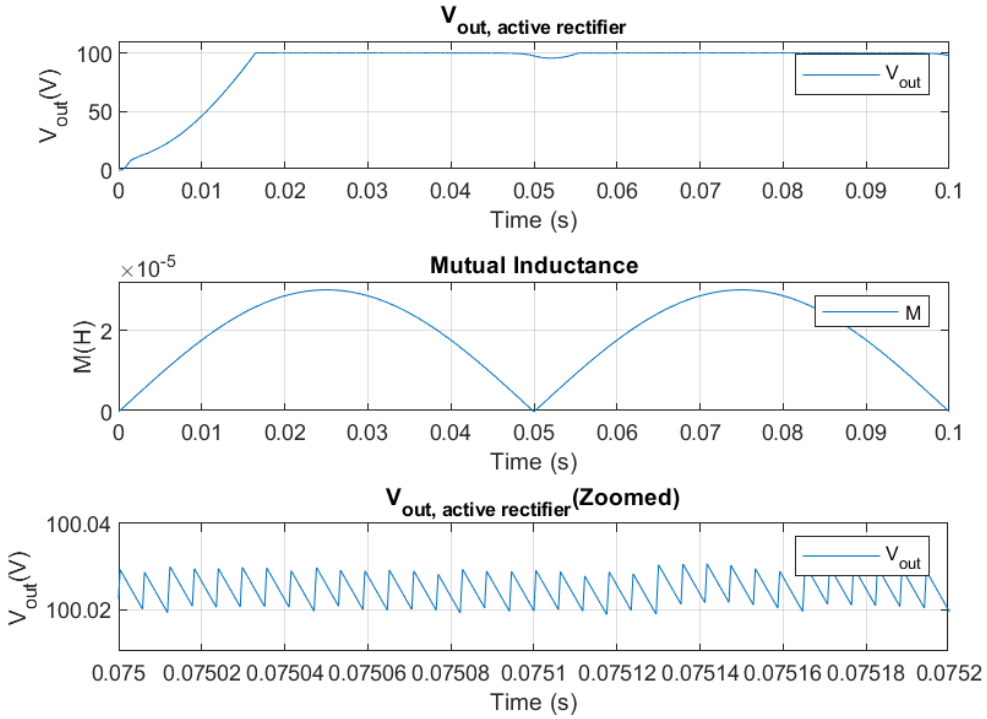


**Figure 7.4:** Output voltage of DWC system using active rectifier.

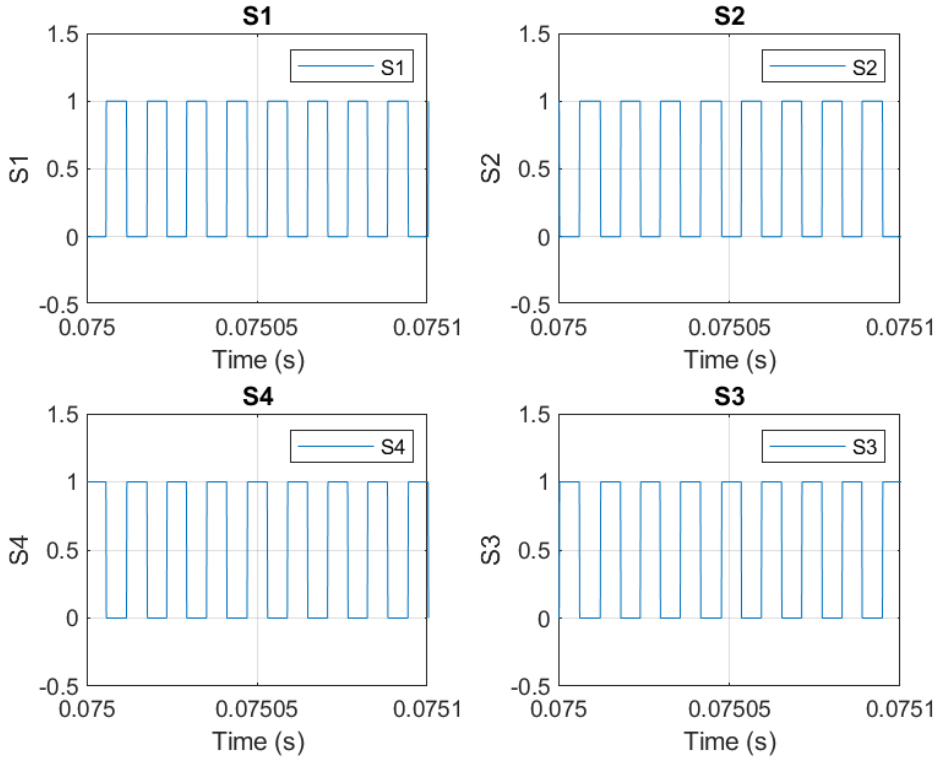


**Figure 7.5:** PWM signal used to control the active rectifier switches in DWC system.

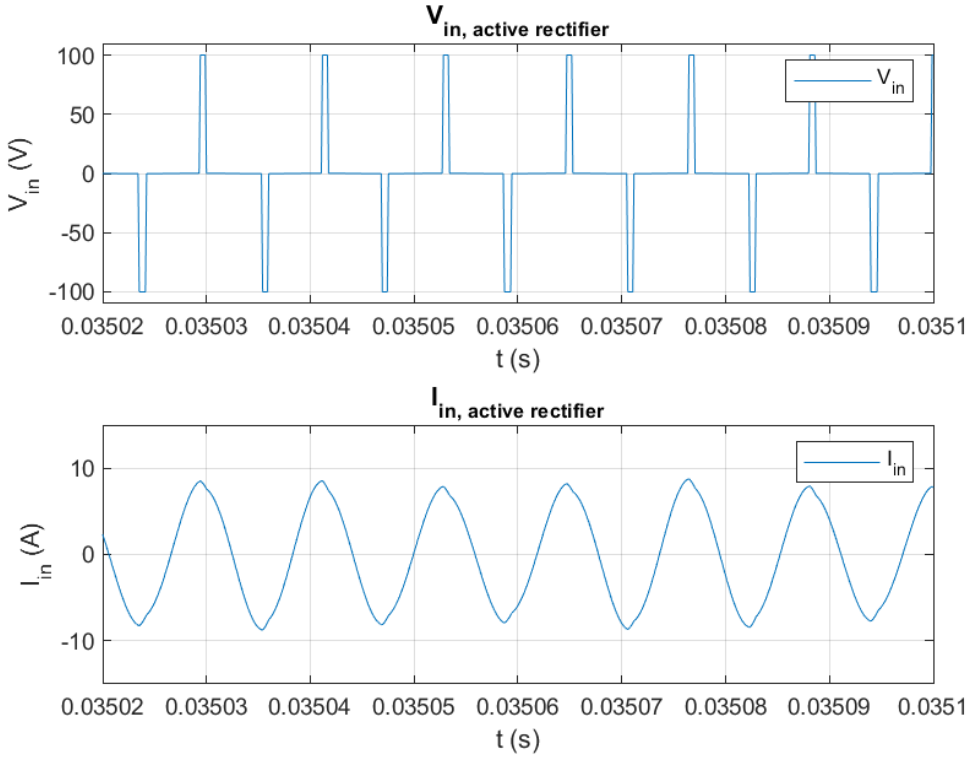


**Figure 7.6:** Input voltage and input current of the active rectifier in DWC system(magnified).

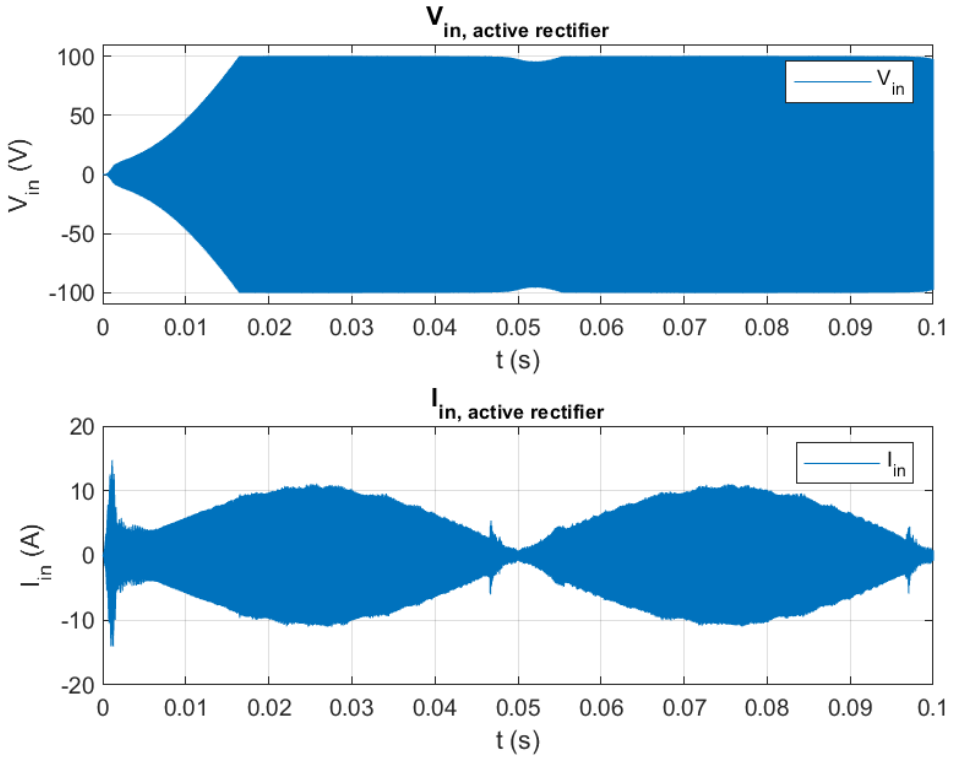


**Figure 7.7:** Input voltage and input current of the active rectifier in DWC system.

## 7.3 Buck Converter

In Chapter 6 it was confirmed that the buck converter functions as expected. This circuit was then connected to the rectifier to complete the DWC system in which the buck converter is used to stabilize the voltage. When integrated in the DWC system, the PI controller had to be tuned again. A stable output was achieved for $K_p$=10 and $K_i$=0.1.

In order to validate the functionality of the buck converter in the DWC system, the output voltage is examined based on two criteria. These criteria are voltage ripple and a stable output. In Figure 7.8, the output voltage of the DWC system is shown using a buck converter and a magnified version of the output to display the voltage ripple in detail. From these graphs, it is observed that the output is a stable 100 V DC voltage with a ripple of 0.06 V which is less than 1% of the output voltage. Furthermore, the drop in output voltage that the inverter and active rectifier based DWC system had, is not shown here. To conclude, the DWC system that utilizes the buck converter functions as intended.

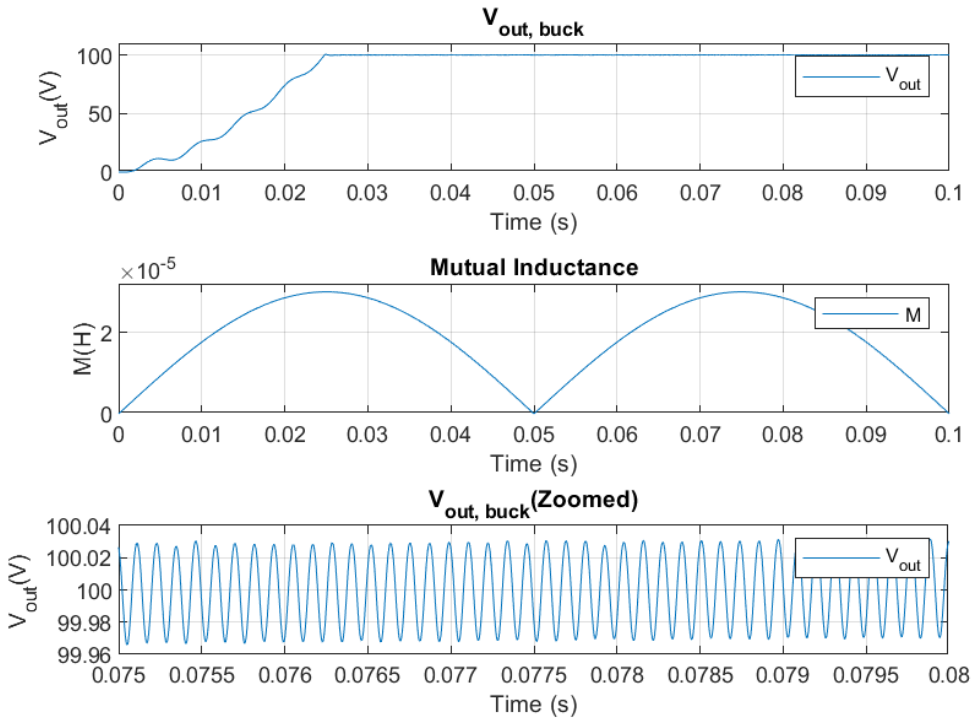


**Figure 7.8:** Output voltage of DWC system using buck converter.

## 7.4 Comparative Analysis

In this section, the comparative analysis is conducted. The three methods of power stabilization will be compared to each other based on the following metrics: voltage ripple, voltage regulation, start-up time, modulation complexity and space efficiency.

### 7.4.1 Voltage Ripple

First, the output voltage ripple of the three circuits used to stabilize the output power are compared to each other. Voltage ripple is an undesired phenomenon that usually appears after rectification. Voltage ripple can cause higher risks of degradation of electrical components, increase power losses and introduce thermal stress[42]. Therefore, it is crucial to minimize the voltage ripple to have a stable power output and to increase the overall lifetime of the components. Figure 7.9 shows the graph of the output voltage of the DWC system when the buck converter, inverter or active rectifier is used for purpose of stabilization of the output power. From the graphs it is determined that the output ripple

voltage of the buck converter is 0.06 V, 0.015 V to 0.030 V for the inverter and 0.01 V for the active rectifier. Hence, on the aspect of output voltage ripple, the active rectifier has the best performance out of the three.

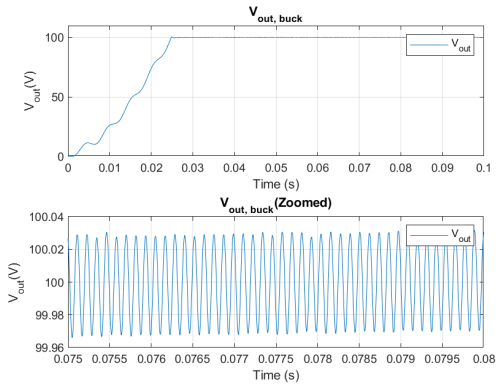


**(a)** Output voltage of DWC system using buck converter.

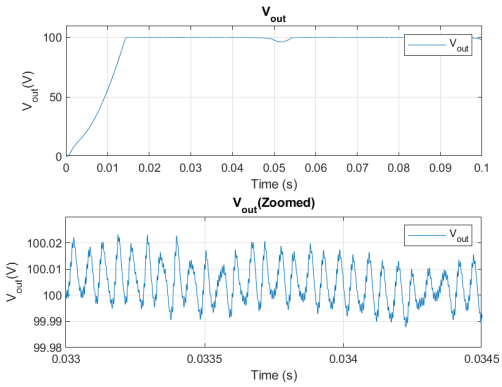


**(b)** Output voltage of DWC system using inverter.

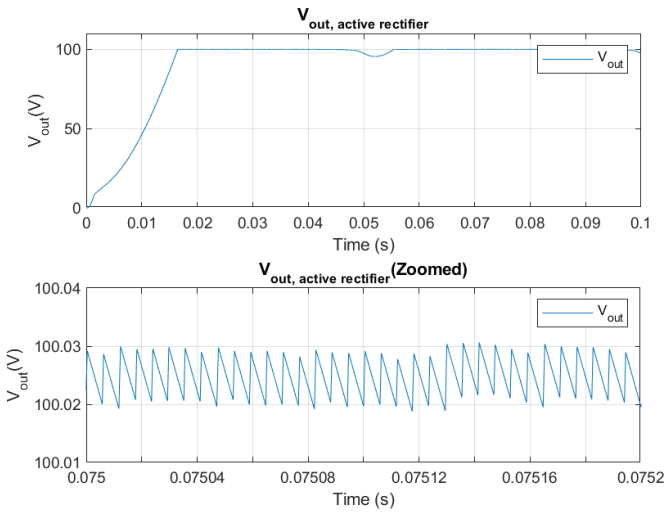


**(c)** Output voltage of DWC system using active rectifier.

**Figure 7.9:** Comparison of output voltages of the DWC system using (a) buck converter, (b) inverter, and (c) active rectifier.

### 7.4.2 Voltage Regulation

Examining the graphs in Figure 7.9, both the inverter and active rectifier based DWC system shows a momentary decrease in output voltage around t=0.05 s when the mutual inductance in the DLCC circuit reaches zero. This leads to a temporary absence of power transfer, and as a result to a temporary deviation in output voltage. In contrast, this is not the case for the buck converter. Indicating a more robust voltage regulation under varying mutual inductance. The reason for the absence of momentary decrease in output voltage in the buck converter based system is because the voltage across the capacitor used for the rectifier is large compared to the one in the inverter and active rectifier based system. Due to this large voltage, the circuit will have sufficient energy to provide in the momentary absence of power.

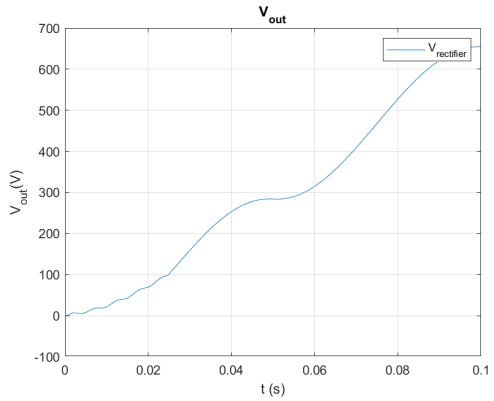


**(a)** Capacitor voltage of rectifier(buck converter).

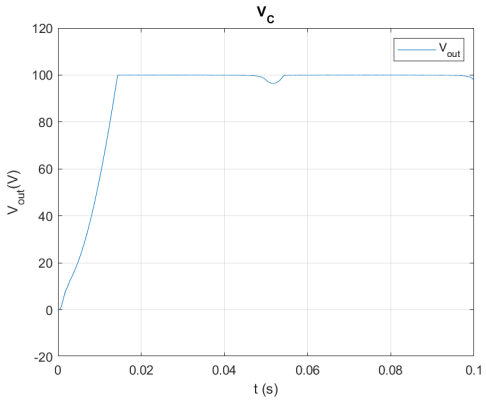


**(b)** Capacitor voltage of rectifier(inverter).

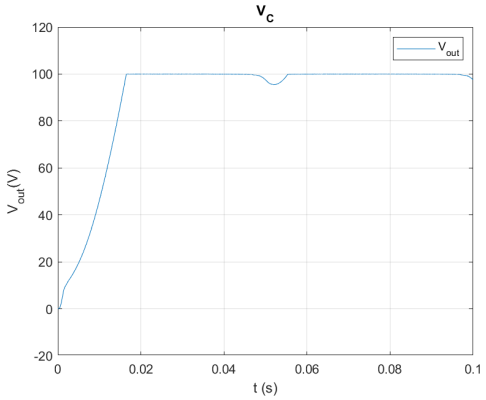


**(c)** Capacitor voltage of active rectifier.

**Figure 7.10:** Capacitor voltage of the (active)rectifier used in each DWC system model.

Furthermore, both the active rectifier and buck converter based DWC system shows stable oscillation between two voltage values, namely, 100.02 V and 100.03 V for the active rectifier and 99.97 V and 100.03 V for the buck converter. While in the inverter based DWC system, the fluctuation is not constant between two voltage values. For example, at t=0.033 s it is between 100 V and 100.02 V and around t=0.034 s it changes to 99.99 V to 100.01 V. This indicates that compared to the other two methods, the inverter is more sensitive to changes in the mutual inductance. Therefore, in terms of maintaining a constant stable output voltage, the buck converter outperforms the active rectifier and inverter.

### 7.4.3 Start-up Time

The start-up of a DWC system is a critical performance indicator, which demonstrates how fast the output voltage reaches steady state. A relatively slower start-up leads to less power delivery. Therefore, it is important that the system's output voltage stabilize as fast as possible. In Figure 7.9, the start-ups of the DWC systems utilizing either the buck converter, inverter or active rectifier are displayed. The buck converter shows the slowest start-up time compared to the active rectifier and the inverter. Both the inverter and the active rectifier based DWC system shows a faster transient response. Comparing these two, the inverter has a slightly shorter start-up duration compared to the active rectifier.

### 7.4.4 Modulation Complexity

Although all three methods uses the PI controller. Each of them has a unique modulation for their switching signals. The buck converter has the most simple modulation compared to the inverter and active rectifier since it needs to control only one switch. The active rectifier takes the most effort since it should not only stabilize the output voltage but also its input current and input voltage should have zero phase difference. To do so, two signals are modulated, namely, the square wave to drive the switches and the delay signal, as explained in Section 5.5. Regarding the inverter, PSM should be applied to

control the four switches such that the DWC system has the desired output voltage, and the output of the inverter should be an AC square wave as shown in Figure 7.2. This will take additional effort compared to the buck converter, however, unlike the active rectifier, only one signal is adjusted and that is the delay signal. Therefore, on the aspect of modulation complexity, the active rectifier is the most complex and the buck converter is the least complex.

### 7.4.5 Space Efficiency

Perhaps worth discussing is the amount of physical space each DWC system occupies. Referring to the DWC system that includes the buck converter, Figure 7.11, the active rectifier, Figure 7.12 and the inverter, Figure 7.13, all three contain the DLCC compensation circuit. However, the inverter and buck converter based DWC system contain an additional circuit, which is the full bridge rectifier, which is required to convert the AC output of the DLCC to a DC output. In contrast, this additional circuit is not necessary in the active rectifier based DWC system since it both rectifies and stabilize the voltage. Moreover, the active rectifier and buck converter based DWC system need an inverter at the input of the DWC system. Therefore, both the active rectifier and inverter based DWC system have three circuit blocks which are approximately similar in size. Hence, on the criteria of space efficiency, the active rectifier and inverter based DWC system occupies the least amount of space.

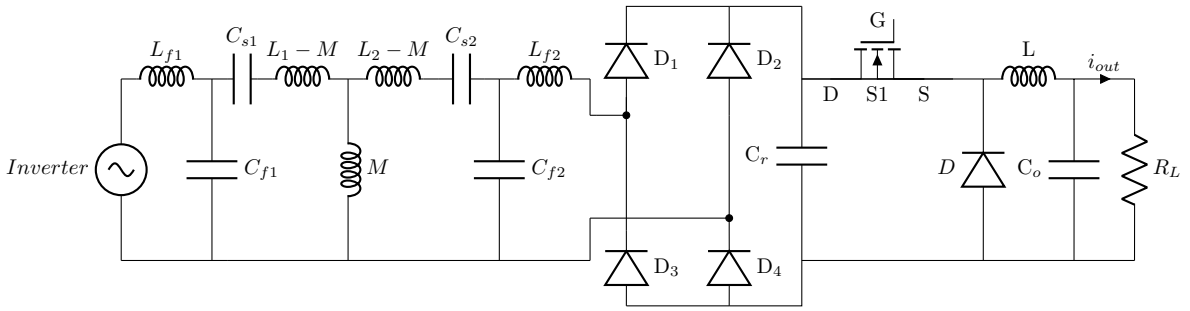


**Figure 7.11:** DWC system using the buck converter.

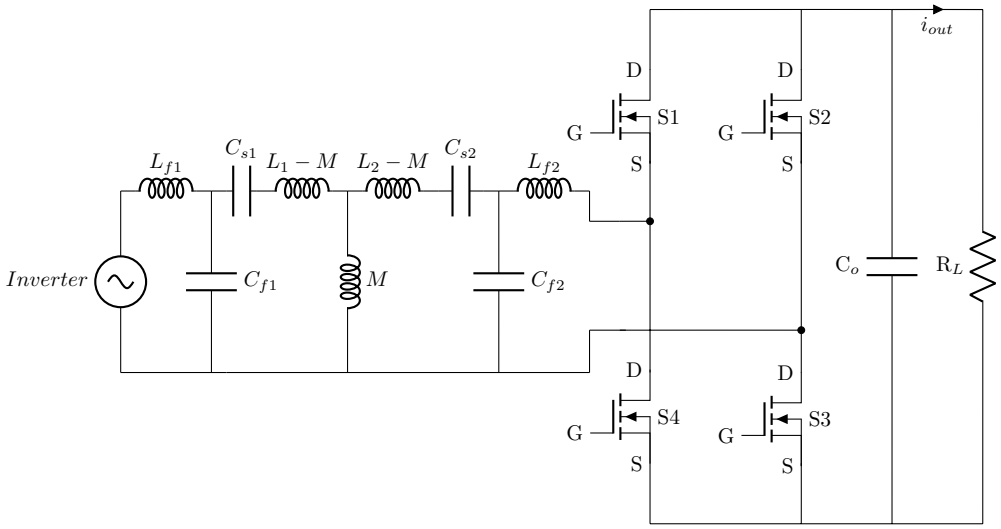


**Figure 7.12:** DWC system using the active rectifier.

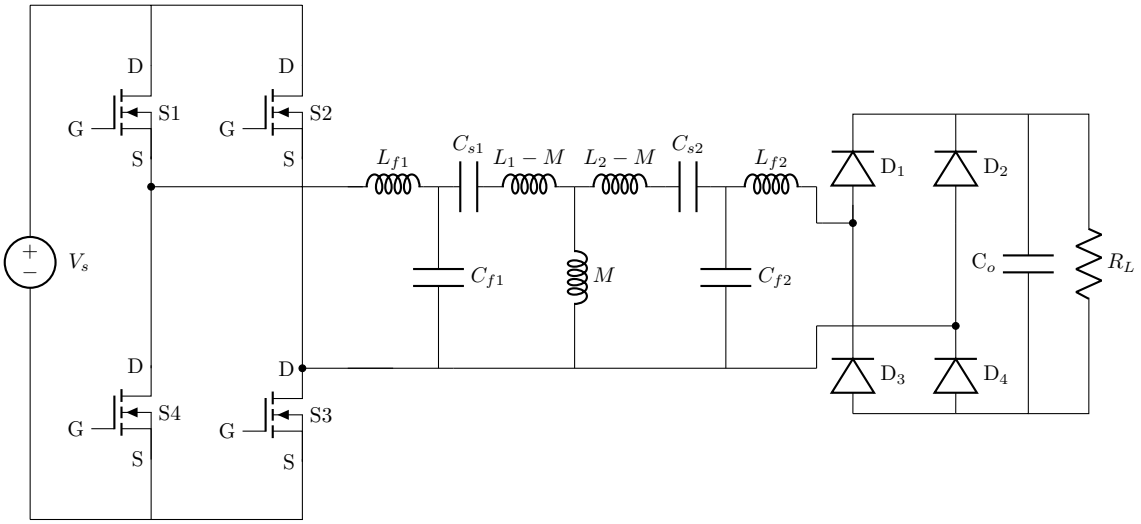


**Figure 7.13:** DWC system using the inverter.

In Table 7.1 the results are summarized. The indicators, high, moderate and low, assigned to each metric, serves as an indicator relative to the performance of one another.

**Table 7.1:** Results of the comparative analysis summarized.

| | Buck converter | Inverter | Active rectifier |
|---|---|---|---|
| Voltage ripple | High | Moderate | Low |
| Voltage regulation | Good | Bad | Moderate |
| Start-up time | Slow | Fast | Moderate |
| Modulation complexity | Low | Medium | High |
| Space efficiency | Low | High | High |

# 8

# Conclusion and Future Work

## 8.1 Conclusion

In this thesis, the ability of power stabilization carried out by a buck converter, inverter and active rectifier in dynamic wireless charging was evaluated. For this evaluation, a DWPT circuit was constructed in MATLAB Simulink. The DWPT was connected to either the buck converter, inverter or active rectifier along its necessary control and modulation. The design, modeling and a comparative analysis between these three methods of power stabilization are presented. The comparison was made based on five characteristics, namely, voltage ripple, voltage regulation, start-up time, modulation complexity and space efficiency. In addition to the comparative analysis, this thesis provides a detailed description of the design, control strategy and modulation of the dynamic wireless charging(DWC) system models constructed in Simulink, which lays the foundation to re-construct the Simulink model for a different purpose. Furthermore, the socio-economical impact of DWC was discussed in Chapter 2, emphasizing its potential contribution to a cleaner and more sustainable transport sector. The implementation of DWC for EVs, has the potential of encouraging more, and a broader range of people to switch from a traditional combustion engine car to an EV. This will lead to a decrease in greenhouse gas emission. This thesis contributes by providing a comparative analysis between three power stabilization methods to stabilize the power in order to improve DWC for EVs such that EVs are more convenient and an attractive alternative compared to a traditional combustion engine vehicle.

The results presented in Chapter 7 shows that all three methods are performing good in stabilizing the power. However, since one has to be selected, the active rectifier would be the most suitable circuit to select to achieve a stable power output in the DWC system. As summarized in Table 7.1, its main issue lies in its complexity in modulation. However, the modulation of it is explained in this thesis which makes it much less complex. Once that is completed, a circuit will be achieved that performs the best out of the three. It has the lowest ripple voltage, has a compact design and the start-up time is slightly longer compared to the inverter circuit. Overall, these findings demonstrate that the active rectifier offers the best solution for power stabilization of a DWC system. Hereby, the research question: *"Which method of power stabilization for dynamic wireless charging of electric vehicles is the most suitable in terms of voltage ripple, space efficiency, voltage regulation, modulation complexity and start-up time?"* is answered.

## 8.2 Future Work

- **Experimental evaluation:**
  The findings presented in this thesis are based on simulation results. The next step is to verify these results through experimental validation. To do so, the hardware should be made followed by an experimental evaluation. In addition to verifying the simulation results, the experimental evaluation will provide insight into real-world performance.

- **Cost analysis:**
  This thesis primarily focused on the technical aspects of DWC. To realize DWC, the necessary infrastructure is required such as embedding the primary side of the DLCC circuit in roads and providing a grid connection to power the DWC system. This implementation could be costly. Therefore, a cost-benefit analysis should be conducted to assess the economic feasibility and sustainability of DWC of EVs.
- **Power efficiency:**
  In this thesis, the power efficiency of the DWC system was not analyzed. The power efficiency plays a significant role in selecting a power stabilization method. To investigate the efficiency, the power losses of the MOSFET switches and diodes should be considered, and to obtain a more accurate estimation of the DWC system's power efficiency, the parasitic losses should be taken into account too.
- **Control:**
  In this thesis, a PI controller was implemented to regulate the output power. However, there are other control strategies, like Model Predictive Control(MPC). MPC has the potential to provide a faster response. For future research, exploring MPC may lead to enhanced overall performance of DWC.
- **Perfomance Under Higher Output Voltage:**
  An arbitrary output voltage of 100V was selected to conduct the comparative analysis. However, the question arises, is it possible to achieve similar results for higher output voltages like 400V. For future research, the analysis could be extended towards a higher output voltage target to determine the performances of the DWC systems under high output voltages.

# Bibliography


[1] United Nations. The paris agreement. Accessed: Mar. 20, 2025. [Online]. Available: https://unfccc.int/process-and-meetings/the-paris-agreement

[2] Statista. (2025) Annual greenhouse gas emissions in the European Union (EU-27) from 1990 to 2023, by sector. https://www.statista.com/statistics/1171183/ghg-emissions-sector-european-union-eu/. Accessed: Aug. 26, 2025.

[3] Ian Tiseo. (2025) Transportation GHG emissions in the European Union - Statistics Facts. https://www.statista.com/topics/7968/transportation-emissions-in-the-eu/. Accessed: Aug. 26, 2025.

[4] ANWB. Hoe lang duurt het opladen van een elektrische auto? Accessed: Sep. 30, 2025. [Online]. Available: https://www.anwb.nl/auto/elektrisch-rijden/opladen/hoe-lang-duurt-opladen-elektrische-auto

[5] Sarah Lozanova. (2025) Dynamic wireless charging for electric vehicles. GreenLancer. Accessed: Nov 21, 2025. [Online]. Available: https://www.greenlancer.com/post/dynamic-wireless-charging-electric-vehicles

[6] M. Choi, J. Cha, and J. Song, "Impact of lightweighting and driving conditions on electric vehicle energy consumption: In-depth analysis using real-world testing and simulation," *Energy*, vol. 323, 2025, doi: 10.1016/j.energy.2025.135746. [Online]. Available: https://www.sciencedirect.com/science/article/pii/S036054422501388X

[7] C. Poupinha and J. Dornoff. (2024, Apr.) The bigger the better? How battery size affects real-world energy consumption, cost of ownership, and life-cycle emissions of electric vehicles. https://theicct.org/publication/bev-battery-size-energy-consumption-cost-ownership-lca-ev-apr24/. Accessed: Aug. 27, 2025.

[8] Z. Bi, G. A. Keoleian, Z. Lin, M. R. Moore, K. Chen, L. Song, and Z. Zhao, "Life cycle assessment and tempo-spatial optimization of deploying dynamic wireless charging technology for electric cars," *Transportation Research Part C: Emerging Technologies*, vol. 100, pp. 53–67, 2019.

[9] Elektrische Voertuigen Database, "Accu capaciteit van elektrische auto's," https://ev-database.org/nl/cheatsheet/accu-capaciteit-elektrische-auto, accessed: 2025-11-18.

[10] EVBox, "The complete ev battery guide," https://evbox.com/en/complete-ev-battery-guide/#section-6, 2023, [Online; accessed Oct. 30, 2025].

[11] Battery Industry, "Ev batteries now cost 115 usd per kwh on average," https://batteryindustry.net/ev-batteries-now-cost-115-usd-per-kwh-on-average/, December 2024, accessed: 2025-11-18.

[12] W. C. Brown, "The history of wireless power transmission," *Solar Energy*, vol. 56, no. 1, pp. 3–21, 1996.

[13] Wikipedia. Wireless power transfer. Wikipedia. Accessed: aug. 4, 2025. [Online]. Available: https://en.wikipedia.org/wiki/Wireless_power_transfer

[14] C. K. Alexander and M. N. O. Sadiku, *Fundamentals of Electric Circuits*, 6th ed. McGraw-Hill Education, 2017.

[15] Wikipedia. Ampères circuital law. Accessed: May 19, 2025. [Online]. Available: https://en.wikipedia.org/wiki/Amp%C3%A8re%27s_circuital_law

[16] H. Dialani, "Highly Efficient Dual-Side Wireless Power Transfer: Implementation of Synchronization and Wireless Communication," Master's thesis, Delft University of Technology, Jul. 2023. [Online]. Available: https://repository.tudelft.nl/file/File_ae28eeb1-24af-4af0-9f4d-ef3b7c7d5020

[17] Khan Academy. Magnetic flux and faraday's law. Accessed: 14-11-2025. [Online]. Available: https://www.khanacademy.org/science/ap-physics-2/x0e2f5a2c:magnetism-and-electromagnetism/x0e2f5a2c:electromagnetic-induction/a/what-is-magnetic-flux

[18] W. Shi, *Dynamic Wireless Charging of Electric Vehicles*, Delft, Netherlands, November 2023. [Online]. Available: http://repository.tudelft.nl/

[19] J. Clayton Rawlins, "Resonance," in *Basic AC Circuits*. Elsevier, 2000, ch. 14, pp. 453–487.

[20] Q. Zhu, L. Wang, Y. Guo, C. Liao, and F. Li, "Applying lcc compensation network to dynamic wireless ev charging system," *IEEE Transactions on Industrial Electronics*, vol. 63, no. 10, pp. 6557–6567, October 2016.

[21] Learn about electronics. (2020) Buck Converters. https://learnabout-electronics.org/PSU/psu31.php. Accessed: Oct. 07, 2025.

[22] N. Mohan, T. M. Undeland, and W. P. Robbins, *Power Electronics: Converters, Applications, and Design*, 2nd ed., 1995.

[23] Sciamble. (2025, Sep.) Buck converter  Discontinuous conduction mode (DCM). https://sciamble.com/resources/pe-drives-lab/basic-pe/buck-converter-dcm. Accessed: Oct. 06, 2025.

[24] T. R. Rajeswari, C. Subramanian, and R. Manivannan, "Simulation of buck converter using simulink with pi controller," *International Journal for Scientific Research & Development (IJSRD)*, vol. 4, 2016, available at: https://ijsrd.com/articles/IJSRDV4I20376.pdf.

[25] A. Bhattacharya, S. Banerjee, S. Girotra, H. Shukla, G. Bhardwaj, and S. Talia, "Simulation and design of pi-controller for the control of buck converter," *Journal of Microelectronics and Solid State Devices*, vol. 7, 2020.

[26] B. Hauke, "Basic calculation of a buck converters power stage," https://www.ti.com/lit/an/slva477b/slva477b.pdf, Texas Instruments, Tech. Rep., 2015, rev. B (December 2011, revised August 2015), Accessed: Oct. 07, 2025.

[27] P. Evans. (2025) Power Inverters Explained. https://theengineeringmindset.com/power-inverters-explained/. Accessed: 2025-11-19.

[28] Electronics-Tutorials. Full wave rectifier. [Online]. Available: https://www.electronics-tutorials.ws/diode/diode_6.html

[29] CEHCO. Active switching rectifier. [Online]. Available: https://www.cehco.com/active-switching-rectifier/

[30] Y. Huangfu, B. Wang, R. Ma, and Y. Li. (2012) Comparison for buck converter with pi, sliding mode, dynamic sliding mode control. Available on IEEE Xplore: https://ieeexplore.ieee.org/document/6401927/figuresfigures.

[31] J. Pathan, "Model predictive control of dc-dc buck converter and its comparison with pid controller," *International Journal of Advanced Research in Engineering and Technology (IJARET)*, vol. 11, no. 9, pp. 362–367, Sep. 2020.

[32] K. J. Åström and T. Hägglund, *Advanced PID Control*, 2006.

[33] P. J. Woolf, "Pid tuning via classical methods," in *Chemical Process Dynamics and Controls*. University of Michigan Engineering Controls Group, 2009, ch. 9.3, accessed: 2025-11-02. [Online]. Available: https://eng.libretexts.org/Bookshelves/Industrial_and_Systems_Engineering/Chemical_Process_Dynamics_and_Controls_(Woolf)/09%3A_Proportional-Integral-Derivative_(PID)_Control/9.03%3A_PID_Tuning_via_Classical_Methods

[34] A. Bhattacharya, S. Banerjee, S. Girotra, H. Shukla, G. Bhardwaj, and S. Talia, "Simulation and design of pi-controller for the control of buck converter," *ResearchGate*, 2020. [Online].

Available: https://www.researchgate.net/publication/359831436_Simulation_and_Design_of_PI-Controller_for_the_Control_of_Buck_Converter

[35] C. Circuit, "Design of pi controller for buck converter in matlab simulink | automatic control | simulation," 2023, accessed: April 15, 2025. [Online]. Available: https://www.youtube.com/watch?v=6RC27OL73VM

[36] Wikipedia. Buck converter. Wikipedia. Accessed: Oct. 08, 2025. [Online]. Available: https://en.wikipedia.org/wiki/Buck_converter

[37] M. M. Rashid, M. N. M. Haque, M. S. Miah, and T. Akhtar, "Simulink model of controlling fuel cell powered direct current motor with comparative performance analysis," *ResearchGate*, 2019, accessed: April 14, 2025. [Online]. Available: https://www.researchgate.net/publication/339410456_Simulink_Model_of_Controlling_Fuel_Cell_Powered_Direct_Current_Motor_with_Comparative_Performance_Analysis

[38] Y. Li, J. Hu, F. Chen, Z. Li, Z. He, and R. Mai, "Dual-phase-shift control scheme with current-stress and efficiency optimization for wireless power transfer systems," *IEEE Transactions on Circuits and Systems I: Regular Papers*, vol. 65, no. 9, pp. 3110–3121, Sep. 2018.

[39] Texas Instruments, "Lm2596 simple switcher power converter 150-khz 3-a step-down voltage regulator," https://www.ti.com/lit/ds/symlink/lm2596.pdf, Nov. 1999, revision march 2023.

[40] Electronic Tutorials. Full wave rectifier. Accessed: Oct 13, 2025. [Online]. Available: https://www.electronics-tutorials.ws/diode/diode_6.html

[41] B. Hauke, "Basic calculation of a buck converter's power stage," Texas Instruments, Application Report SLVA477B, 2011, revised 2015.

[42] Wikipedia. (2025) Ripple (electrical). [Online; accessed 29-October-2025]. [Online]. Available: https://en.wikipedia.org/wiki/Ripple_(electrical)

# A

# Appendix

## A.1 MATLAB Code to Generate Plots of $I_{1,SS}$ and $I_{2,SS}$(Static)

```
%%I1
simout = out.I_in;

time = simout.Time;
data = simout.Data;

%plot I1
figure;
plot(time, data);
title('I_1 static ss-model');
xlabel('Time (s)');
ylabel('I_1(A)');
grid on;
legend('I_1');
grid on;
xlim([0 2e-4]); %Limit axis
ylim([-90 90]); %Limit axis
yticks(-90:10:90); %set intervals

saveas(gcf, 'I1_ss_static.png'); %save as pic

%%I2
simout = out.I_out;

time = simout.Time;
data = simout.Data;

%plot I2
figure;
plot(time, data);
title('I_2 static ss-model');
xlabel('Time (s)');
ylabel('I_2(A)');
grid on;
legend('I_2');
grid on;
xlim([0 2e-4]); %Limit axis
ylim([-90 90]); %Limit axis
```

```
yticks(-90:10:90); %intervals

saveas(gcf, 'figure.png'); %save as pic
```

## A.2 MATLAB Code for the Derivation of $I_{1,SS}$ and $I_{2,SS}$(Static)

```
I1_SS = ((R2 + RL) * U_AB) / (R1 * (R2 + RL) + omega_s^2 * M^2);
I2_SS = (omega_s * M * U_AB) / (R1 * (R2 + RL) + omega_s^2 * M^2);
```

## A.3 MATLAB Code to Generate Plots of $I_{1,DLCC}$, $I_{2,DLCC}$ and $I_{out}$(Static)

```
%%I_in
simout = out.I_in;

time = simout.Time;
data = simout.Data;

%plot I1
figure;
plot(time, data);
title('I_{1,DLCC} static LCC-model');
xlabel('Time (s)');
ylabel('I_{1,DLCC}(A)');
grid on;
legend('I_{1,DLCC}');
grid on;
xlim([0 2e-4]); %Limit axis

saveas(gcf, 'figure.png'); %save as pic

%%I_2
simout = out.I2;

time = simout.Time;
data = simout.Data;

%plot I2
figure;
plot(time, data);
title('I_{2,DLCC} static LCC-model');
xlabel('Time (s)');
ylabel('I_{2,DLCC}(A)');
grid on;
legend('I_{2,DLCC}');
grid on;
xlim([0 2e-4]); %Limit axis

saveas(gcf, 'I2_LCC_static.png'); %save as pic

%%I_out
simout = out.I_out;

time = simout.Time;
data = simout.Data;

%plot Iout
figure;
```

```
plot(time, data);
title('I_{out} static LCC-model');
xlabel('Time (s)');
ylabel('I_{out}(A)');
grid on;
legend('I_{out}');
grid on;
xlim([0 2e-4]); %Limit axis

saveas(gcf, 'figure.png'); %save as pic
```

## A.4 MATLAB Code for the Derivation of $I_{1,DLCC}$, $I_{2,DLCC}$ and $I_{out}$(Static)

```
I_out=(M*U_AB)/(omega_s*Lf2*Lf1);
I2_DLCC=(M*U_AB*RL)/(omega_s^2*Lf1*Lf2^2);
I1_DLCC=(U_AB)/(omega_s*Lf1);
```

## A.5 MATLAB Code Used to Verify the DLCC Compensation Simulink Model(Dynamic)

```
%values used for analytical verification
U_AB=800;
num_steps = 85e5;
f_=10;
t = linspace(0, 0.1, num_steps);

%DLCC circuit values
L1=200.7e-6;
L2=203.5e-6;
M=30e-6;
Lf1=66.39e-6;
Lf2=68.97e-6;

omega_s=2*pi*85000;

Cs1 = 1/(omega_s^2*(L1-Lf1));
Cs2 = 1/(omega_s^2*(L2-Lf2));
Cf1 = 1/(omega_s^2*Lf1);
Cf2 = 1/(omega_s^2*Lf2);
RL=123;

%used for analytical verification
for i = 1:num_steps
    M__(i) = M * sin(2 * pi * f_ * t(i)); % Mutual inductance sinusoidal
    M_(i)=abs(M__(i));
    U_AB_(i)= U_AB * sin(2 * pi * 85e3 * t(i));


    I_out(i)=(M_(i)*U_AB_(i))/(omega_s*Lf2*Lf1);
    I2_DLCC(i)=(M_(i)*U_AB_(i)*RL)/((omega_s^2)*Lf1*(Lf2^2));
    I1_DLCC(i)=(U_AB_(i))/(omega_s*Lf1);
end


%% plots for analytical check
figure %plot for I_out
subplot(2, 2, 1);
plot(t, I_out);
xlabel('t (s)');
ylabel('I_{out} (A)');
title('I_{out,DLCC}');
legend('I_{out}');
grid on;
ylim([-11 11]);
yticks(-10:5:10);

%plot for I1
subplot(2, 2, 2);
plot(t, I1_DLCC);
xlabel('t (s)');
ylabel('I_{1,DLCC} (A)');
```

```
title('I_{1,DLCC}');
legend('I_{1,DLCC}');
ylim([-30 30]);
yticks(-30:5:30);
grid on;

%plot for I2
subplot(2, 2, 3);
plot(t, I2_DLCC);
xlabel('t (s)');
ylabel('I_{2,DLCC} (A)');
title('I_{2,DLCC}');
legend('I_{2,DLCC}');
ylim([-40 40]);
yticks(-40:5:40);
grid on;

%plot for M
subplot(2, 2, 4);
plot(t, M_);
xlabel('t (s)');
ylabel(' M (H)');
title('Mutual Inductance');
legend('M');
ylim([0 3.1e-5]);
yticks(0:0.5e-5:3e-5);
grid on;

saveas(gcf, 'figure.png'); %save as pic
```

## A.6 MATLAB Code to Generate $I_{1,DLCC}$, $I_{2,DLCC}$ and $I_{out}$ Plots(Dynamic)

```
%%DLCC plots
figure %plot for I_out
subplot(2, 2, 1);
simout = out.DLCC_out;
time = simout.Time;
data = simout.Data;
plot(time, squeeze(data));
xlabel('t (s)');
ylabel('I_{out} (A)');
title('I_{out,DLCC}');
legend('I_{out}');
grid on;
ylim([-11 11]);
yticks(-10:5:10);

%plot for I1
subplot(2, 2, 2);
simout = out.DLCC_I1;
time = simout.Time;
data = simout.Data;
plot(time, squeeze(data));
xlabel('t (s)');
ylabel('I_{1,DLCC} (A)');
title('I_{1,DLCC}');
legend('I_{1,DLCC}');
ylim([-60 60]);
yticks(-60:5:60);
grid on;
```

```
%plot for I2
subplot(2, 2, 3);
simout = out.DLCC_I2;
time = simout.Time;
data = simout.Data;
plot(time, squeeze(data));
xlabel('t (s)');
ylabel('I_{2,DLCC} (A)');
title('I_{2,DLCC}');
legend('I_{2,DLCC}');
ylim([-40 40]);
yticks(-40:5:40);
grid on;

%plot for M
subplot(2, 2, 4);
simout = out.DLCC_M;
time = simout.Time;
data = simout.Data;
plot(time, squeeze(data));
xlabel('t (s)');
ylabel(' M (H)');
title('Mutual Inductance');
legend('M');
ylim([0 3.1e-5]);
yticks(0:0.5e-5:3e-5);
grid on;

saveas(gcf, 'figure.png'); %save as pic
```

## A.7 MATLAB Code to Generate Plot of the Rectifier

```
%Vout plot
simout = out.V_out;

time = simout.Time;
data = simout.Data;

figure;
plot(time, data);
title('V_{out} Rectifier');
xlabel('Time (s)');
ylabel('V_{out}(V)');
grid on;
legend('V_{out}');
grid on;

saveas(gcf, 'figure.png'); %save as pic
```

# B

# Derivations

## B.1 $Z_{in}$ Derivation

$$\begin{aligned} Z_{\text{in}} &= (Z_0 + jX) \,\|(-jX) + jX \\ Z_{\text{in}} &= \frac{(Z_0 + jX)(-jX)}{Z_0 + jX - jX} + jX \\ &= \frac{-Z_0 jX - jX^2}{Z_0} + jX \\ &= \frac{-Z_0 jX + X^2 + jXZ_0}{Z_0} \\ &= \frac{X^2}{Z_0} \\ \Rightarrow Z_{\text{in}} &= \frac{X^2}{Z_0} \end{aligned} \tag{B.1}$$

## B.2 $I_0$ Derivation

$$\begin{aligned} I_{\text{in}} &= \frac{U_{\text{in}}}{Z_{in}} \\ \Rightarrow I_0 &= \frac{U_{\text{in}}}{Z_{\text{in}}} \cdot \frac{(Z_0 + jX)(-jX)}{(Z_0 + jX) + (-jX)} \cdot \frac{1}{Z_0 + jX} \\ &= \frac{U_{in}}{\frac{X^2}{Z_0}} \cdot \frac{-jX}{Z_0 + jX - jX} \\ &= \frac{U_{in} \cdot Z_0}{X^2} \cdot \frac{-jX}{Z_0} \\ &= U_{\text{in}} \cdot \frac{-jX}{X^2} \\ &= U_{\text{in}} \cdot \frac{1}{jX} \\ &= \frac{U_{\text{in}}}{jX} \\ \Rightarrow I_0 &= \frac{U_{\text{in}}}{jX} \end{aligned} \tag{B.2}$$

## B.3 $I_{1,\,DLCC}$ Derivation

$$I_{1,DLCC} = \frac{U_{AB}}{j\omega_s L + \frac{1}{j\omega_s C_{S_1}}}$$

To achieve resonance state the following holds for $C_{s1} : C_{s1} = \frac{1}{\omega_s^2(L_1 - L_{f1})}$

$$\begin{aligned} &= \frac{U_{AB}}{j\omega_s L + \frac{1}{j\omega_s \frac{1}{\omega_s^2\left(L_1 - L_{f_1}\right)}}} \\ &= \frac{U_{AB}}{j\omega_s L_1 - j\omega_s \left(L_1 - L_{f_1}\right)} \\ &= \frac{U_{AB}}{j\omega_s L_1 - j\omega_s L_1 + j\omega_s L_{f_1}} \\ &= \frac{U_{AB}}{j\omega_s L_{f_1}} \end{aligned} \tag{B.3}$$